Abstract

Canonical and Non-canonical Functions of Dihydrouridine Synthases in Health and Disease

Austin Stratton Draycott

2023

Dihydrouridine is a universally conserved RNA modification which is installed by enzymes that are important for human health for reasons that are not yet clear. Here I investigate the functions of dihydrouridine (D) in RNA by developing methods to identify D sites in high-throughput and by characterizing the mechanisms by which dysregulation of dihydrouridine synthases (DUS) affects RNA metabolism and cellular physiology. D is universally present in tRNAs, where its unique nucleotide geometry permits proper folding of the tRNA D-loop. Recently, several studies demonstrated that multiple dihydrouridine synthases (DUS) cross link to mRNA in yeast and humans, suggesting they might modify mRNA. I developed dihydrouridine sequencing (D-seq) as a method for transcriptome-wide mapping of D with single-nucleotide resolution. Using D-seq, I discovered dihydrouridine in novel classes of RNA in yeast which include both mRNA and snoRNA. I find the novel D sites are concentrated in conserved stem-loop regions, suggesting a role for D in folding functional RNA structures. My work establishes D as a new functional component of the mRNA epitranscriptome and demonstrates its ability to broadly alter mRNA structure.

In humans, high expression of dihydrouridine synthase 2 (DUS2) predicts poor patient outcomes in non small cell lung cancer (NSCLC). I show in human cells that DUS2 suppresses ferroptosis, a metal-dependent non-apoptotic form of cell death that is emerging as a therapeutic target in lung cancer. In collaboration with Matthew Wang, I extend these results into a mouse xenograft model of NSCLC. Elevated DUS2 correlates with resistance to ferroptosis inducers and loss of DUS2 causes increased sensitivity with concomitant accumulation of toxic lipid peroxides. Because DUS2 is known to modify tRNAs at position 20 in yeast, I analyzed the tRNAome of DUS2 KO cells, and, surprisingly, identified a single family of tRNA isodecoders, CysGCA, as specifically depleted in the absence of DUS2. I tested the functional significance of the >40% decrease in charged CysGCA levels in DUS2 KO cells using multiple translational reporters and found that high cysteine content reporters produced ~50% less protein in the DUS2 KO cells, whereas low cysteine reporters were unaffected. I then performed quantitative proteomics to compare DUS2 KO and A549 cells and observed a significant reduction in endogenous cysteine-rich proteins in cells lacking DUS2. Notably, DUS2 KO cells cannot sustain normal levels of metallothioneins, a class of very cysteine rich proteins that serve as key regulators of both metal and redox homeostasis. Accordingly, DUS2 knockout cells are more susceptible to zinc intoxication and have lower levels of reduced glutathione, which partially explains their sensitivity to ferroptosis. My findings demonstrate that DUS2 is required to support tRNACys levels and fend off ferroptosis in lung cancer cells.

# Canonical and Non-canonical Functions of Dihydrouridine Synthases in Health and Disease

A Dissertation
Presented to the Faculty of the Graduate School
Of
Yale University
In Candidacy for the Degree of
Doctor of Philosophy

By
Austin Stratton Draycott

Dissertation Director: Wendy Victoria Gilbert

May 2023

## TABLE OF CONTENTS

# Acknowledgements

This work would not have been possible without the support and encouragement of many people. First and foremost, I want to thank my advisor, Wendy Gilbert for her support over the past six years. Wendy is an inimitable mentor to her “labbies”, and without her guidance and encouragement I would not be the person I am today.

The Gilbert lab has been a wonderful scientific home during my time in graduate school. Without its members this adventure would have been substantially less fun and probably unsuccessful. Cole Lewis joined the lab the same year as me and has been very generous with his time and advice since then. Cassandra Schaening-Burgos provided essential code, and invaluable advice. Rachel Niederer and Maria Rojas-Duran never tired of my endless questions about how to do simple things with yeast. Nicole Martinez, Erin Borchardt, Jiri Koubek, Julia Wang, Christian Fagre, Ritam Neupane, Kyrillos Abdallah, Danni Jin, and Shivani Bhandarkar, thank you for all of the enjoyable scientific and social interactions we’ve had. Leo Schärfen, thank you for the many good hours of scientific (and non-scientific) discussion and debate. I would also like to thank the Rocket household for their warmth and good company during the pandemic.

Finally, I would like to thank my family for their love and support: my mother Meredith Hamilton, my father Miles Draycott and my sisters Margot and Celia Draycott. I would not be here without you all.

# Prelude

When I started in Wendy's lab, I was certain I wanted to study "mRNA modifications" (even though I had only recently been introduced to the idea of a "mRNA modification"). However, after talking about projects with Wendy (which revealed how little I knew about "mRNA modifications"), we agreed that I would work on two projects in the lab: 1) characterizing the binding preferences of a core eukaryotic translation initiation factor (eIF4F) in yeast and 2) developing a high throughput sequencing method to identify dihydrouridine (D) residues in RNA, because there had been two recent publications that showed the dihydrouridine synthases (DUS) associated with polyA+ mRNA (Beckmann et al., 2015; Mitchell et al., 2013), which suggested to us that the DUS might be installing D in mRNA.

For the D project, I proposed to adapt D-specific chemistry from a low-throughput D-mapping method (Xing et al., 2004). This method relies upon the fact that dihydrouridine is susceptible to alkaline hydrolysis, which breaks the the 3-4 linkage in the dihydrouracil ring (Batt et al., 1954; Magrath and Shaw, 1967). The product of the ring-opening, β-ureidopropionic acid, no longer can participate in Watson-Crick base pairing, and blocks reverse transcription (Xing et al., 2004). The plan was to adapt an existing Gilbert lab high throughput reverse transcriptase stop mapping protocol (Carlile et al., 2015) to work for D by incorporating an alkaline hydrolysis step. I would then use this method to look for Ds in polyA+ RNA from a wild type yeast strain, and in RNA from a strain lacking all dihydrouridine synthase activity (Xing et al., 2004). However, when I incubated the polyA+ RNA in the basic conditions required for alkaline hydrolysis of the dihydrouracil ring, I realized the RNA was so badly degraded that it wasn't workable to

make a sequencing library after treatment. I then encountered a series of papers (Cerutti et al., 1968; Cerutti and Miller, 1967; Kaur et al., 2011; Pan et al., 2009) that showed D could be efficiently reduced by sodium borohydride ($NaBH_4$), and that the reduced D base had a damaged Watson-Crick face. I hypothesized that reduced D would block reverse transcription similarly to β-ureidopropionic acid.

As I describe in Chapter 1, reduced D does block reverse transcriptase, and $NaBH_4$ treatment does not significantly degrade RNA. Combining the $NaBH_4$ treatment with a pre-existing reverse transcriptase stop mapping protocol gave me a method to map Ds in high throughput (D-seq). Using D-seq, I mapped dihydrouridines transcriptome wide in budding yeast, and showed that D is installed at novel sites in both mRNAs and non-coding RNAs. Intriguingly, many of the novel D sites are located in conserved stem-loop regions. These compact stem-loops are structurally similar to the D loops of tRNAs, suggesting a role for D in promoting functional RNA folding. I used high-throughput chemical probing with DMS to profile RNA folding around the novel D sites, and identified D-dependent RNA structures in both mRNAs and ncRNAs. This work demonstrated that DUS install D in RNAs other than their canonical tRNA targets and highlighted the functional impact of this modification on folding of diverse classes of RNA.

After identifying Ds in mRNA in yeast, I then proposed to use D-seq to look for Ds in human mRNA. In humans, high expression of dihydrouridine synthase 2 (DUS2) in non-small cell lung cancers (NSCLC) leads to worse outcomes for NSCLC patients (Kato et al., 2005). I proposed to generate DUS2 knockouts in a model NSCLC cell line (A549). Using the DUS2 knockout cells and D-seq, I then planned to identify the cancer relevant

mRNA targets of DUS2 (this was not a well thought through experiment). However, as I describe in Chapter 2, when I measured tRNA expression in the DUS2 knockout cells (what I thought was a control experiment in preparation for human mRNA D-seq), I found that the DUS2 knockout cells had an approximately 40% decrease in the levels of a specific tRNA, tRNA cysGCA. I then uncovered that the NSCLC DUS2 knockout cells were more than twice as sensitive to ferroptosis, a metal-dependent non-apoptotic form of cell death that is emerging as a therapeutic target in lung cancer. I rationalized the ferroptosis sensitivity by showing that the DUS2 knockout cells have defects in the translation of cysteine codons which reduce steady state levels of many cysteine-rich proteins, including known anti-ferroptotic oncoproteins. In a mouse xenograft model of NSCLC, combinatorial induction of ferroptosis and inhibition of DUS2 in tumors significantly reduced tumor volume and extended mouse life span. My results highlight the potential of inhibiting tRNA-modifying enzymes as a therapeutic approach in cancer and emphasize the outsized roles that specific tRNA substrates play in the biological functions of tRNA-modifying enzymes.

# Chapter 1

# Transcriptome-wide mapping reveals a diverse dihydrouridine landscape including mRNA

## Abstract

Dihydrouridine is a modified nucleotide universally present in tRNAs, but the complete dihydrouridine landscape is unknown in any organism. I introduce dihydrouridine sequencing (D-seq) for transcriptome-wide mapping of D with single-nucleotide resolution and use it to uncover novel classes of dihydrouridine-containing RNA in yeast which include mRNA and snoRNA. The novel D sites are concentrated in conserved stem-loop regions consistent with a role for D in folding many functional RNA structures. I demonstrate the dihydrouridine synthase (DUS)-dependent changes in splicing of a D-containing pre-mRNA in cells and show that D-modified mRNAs can be efficiently translated by eukaryotic ribosomes in vitro. This work establishes D as a new functional component of the mRNA epitranscriptome and paves the way for identifying the RNA targets of multiple dihydrouridine synthase enzymes that are dysregulated in human disease.

## Introduction

Dihydrouridine (D) is a modified version of uridine that is installed by dihydrouridine synthase enzymes (DUS) in all domains of life. It is of great interest to determine the locations of D modifications because elevated expression of DUS and elevated D levels in tumors are associated with worse outcomes for patients in lung (Kato et al., 2005), liver (Kuchino and Borek, 1978) and kidney (Creighton et al., 2016, 2013) cancer. DUS target sites in tRNAs are best characterized in budding yeast (Xing et al., 2004, 2002) and include multiple positions within the eponymous D loops as well as sites in the variable loops of some tRNAs. D has also been detected in the genomic RNA of

Dengue, Zika, Hepatitis C and Polio viruses (McIntyre et al., 2018), but the specific locations are unknown. It is likely that DUS modify additional classes of cellular RNA as recently discovered for other tRNA modifying enzymes (Roundtree et al., 2017). Notably, DUS1 and DUS3 cross-link to mRNA in both yeast and human cells (Beckmann et al., 2015; Mitchell et al., 2013) suggesting their potential to modify mRNA target sites.

The D modification is a reduction of the C5-C6 double bond in uridine that has multiple effects on RNA structure. First, D subtly distorts the pyrimidine ring (Emerson and Sundaralingam, 1980) causing destacking of bases in oligonucleotides (Dalluge et al., 1996). D also disrupts the orientation of N3 and O4 in the pyrimidine ring, weakening Watson-Crick base pairing, which likely contributes to the 3-5°C reduction in melting temperature of RNA duplexes containing a D (Sipa et al., 2007). More significantly, D substantially destabilizes the typical C3′ endo conformation of the ribose thereby favoring the C2′ endo conformation in a D nucleotide by 5.3kcal/mol and in the nucleotide 5′ of D by 3.6kcal/mol (Dalluge et al., 1996). These changes to the RNA backbone conformation strongly disfavor RNA helical geometry (Westhof et al., 1988) and allow for greater flexibility in RNAs. NMR studies of modified and unmodified versions of the tRNA D loop illustrate the consequences of this effect for RNA folding: the unmodified D loop adopts several conformations that rapidly interconvert whereas the modified RNA folds into a hairpin with a stable stem and the D in a flexible loop region (Dyubankova et al., 2015). Thus, dihydrouridylation of RNA is expected to have large effects on RNA structure.

Profound alteration of RNA conformation and structure by D would be expected to affect multiple steps in mRNA metabolism depending on the location of the D nucleotide. For example, D antagonizes formation of RNA duplexes (Sipa et al., 2007; Westhof et al., 1988), which are required for pre-mRNA splicing (due to base-pairing between splice sites and U1, U2 and U6 snRNAs) and for regulation by micro RNAs (due to base-pairing between target mRNA and miRNA). Intramolecular RNA secondary structures have been found to affect the efficiency and regulation of translation initiation, alternative splicing, RNA localization and RNA stability (reviewed in (Kwok et al., 2015; Lu and Chang, 2016)). D is also expected to stabilize binding of numerous regulatory RNA binding proteins by favoring the C2′ endo conformation that is preferentially bound by K homology (KH) domains and RNA recognition motifs (RRM) (Kligun and Mandel-Gutfreund, 2015). KH and RRM domains are responsible for sequence-specific binding by proteins that regulate all aspects of mRNA processing and function.

In this chapter, I report the development of a novel method to map D residues in RNA in high-throughput. My method takes advantage of known D-selective chemistry(Cerutti et al., 1968; Kaur et al., 2011; Pan et al., 2009; Wintermeyer and Zachau, 1979) to reduce D and induce reverse transcriptase (RT) stops 1nt 3′ of Ds. I combine this D-selective chemistry with next-generation sequencing to determine the location of Ds across the yeast transcriptome. D-seq identifies known tRNA D sites and uncovers novel D sites in snoRNA and mRNA. These novel D sites occur in conserved stem-loop regions of mRNAs and snoRNAs—and are consistent with a broad function for D in folding

functional RNA structures. In support of the potential for dihydrouridine to affect mRNA biogenesis, I demonstrate DUS-dependent changes in splicing of a naturally dihydrouridylated pre-mRNA in cells. My results establish dihydrouridine (D) as a new component of the mRNA epitranscriptome and show that the D-seq method is broadly applicable to identifying and studying the functions of D.

**Results and Discussion**

In light of previous work showing that DUS1 and DUS3 cross-link to mRNA in both yeast and human cells (Beckmann et al., 2015; Mitchell et al., 2013) I collaborated with Loren Wilson and Sigrid Nachtergaele to perform bulk nucleotide analysis on RNA from budding yeast. I purified polyA+ mRNA from a *dus1Δ dus2Δ dus3Δ dus4Δ* quadruple mutant strain lacking all DUS activity (Xing et al., 2004), and a matched wild type (WT) strain. Loren detected D in the polyA+ mRNA fraction from WT but not DUS KO (Fig. 1a), confirming the hypothesis that DUS enzymes install D in mRNA. I therefore developed a method to map D at single nucleotide resolution by identifying chemical treatments that stall reverse transcriptase (RT) at D.

To identify RT stopping conditions for D, I tested different chemistries for selective RT stopping at D compared to U. Strong $OH^-$ treatment conditions used previously to map D in tRNA by primer extension (Xing et al., 2004) proved too harsh to use for mRNA due to substantial RNA degradation (Fig. S1a). In contrast, milder sodium borohydride

treatment conditions do not damage mRNA-like molecules (Fig. S1a). D is selectively reduced to tetrahydrouridine by sodium borohydride to remove a hydrogen bond donor on the Watson-Crick face (Fig. 1b) (Kaur et al., 2011). I prepared 194-nt synthetic RNAs with 4 Us or Ds positioned at ~20nt intervals for easy characterization by primer extension (Methods). Using these RNAs, I found that reduced dihydrouridine blocks several reverse transcriptase enzymes one nucleotide 3′ to the D site while having no effect on RT processivity on an identical U-containing template (Fig. 1c, S1b). I note that other non-U modified nucleosides (such as 7-methylguanosine) can react with sodium borohydride (Behm-Ansmant et al., 2011). I combined this D-specific chemistry with strand-specific cDNA sequencing to map the locations of D transcriptome-wide using high-throughput sequencing (Fig. 1d).

In collaboration with Wendy Gilbert and Maria Rojas-Duran, I tested the D-seq approach in budding yeast where positive control D sites in cytoplasmic tRNAs have been extensively although not exhaustively characterized (Xing et al., 2004, 2002). I observed strong DUS-dependent pileups of cDNA ends 1nt 3′ of many known tRNA D sites (Fig. 2a and Table 1). Given these encouraging findings, Cassandra Schaening-Burgos developed a quantitative approach to evaluate D-seq signal by calculating a modified Z score (MAD score) as a measure of the strength of the RT stop signal at every nucleotide. I used the difference between the distributions of MAD scores at known tRNA D sites (based on previous analysis by micro array and primer extension(Xing et al., 2004)) in WT and DUS KO libraries (Fig. S2a) to set cutoffs for defining a D site in abundant RNAs (Methods). Using these cutoffs, I identified

previously reported target sites of 3 of the 4 DUS as well as previously unannotated D sites in 9 tRNAs at positions in the D loop that are known to be modified by DUS1 and DUS4 in other tRNAs (Fig. 2a, b, S2b and Table 1, which compares these sites to previous annotations). I identified a single unanticipated site, at U32 in tRNA IleAAT (Table 1).

As implemented here, D-seq has specific 'blind spots' in tRNAs. First, the cDNA size selection step precluded detection of DUS3-dependent Ds at position 47 because they are too close to the 3′ end of the transcript. In addition, several known target sites of DUS1, DUS2 and DUS4 were not detected because they are shadowed by another D 3′ of them (Fig. S2b and Table 1). Other known tRNA D sites that were not visible occur 3′ of a penetrant RT-stop at position 26 in some tRNAs (Fig. S2c and Table 1). We suspect this RT stop is caused by N2,N2-dimethylguanosine ($m^{2,2}G$) (Ellis et al., 1986). Pre-treatment of RNA samples with AlkB demethylases to remove $m^{2,2}G$ as well as 1-methyladnosine ($m^1A$) and 7-methylguanosine ($m^7G$) (Cozen et al., 2015; Dai et al., 2017; Zheng et al., 2015) should overcome this limitation. Advantages of the D-seq method are that it inherently offers single-nucleotide resolution and can, in principle, be used to detect D sites in any type of RNA present in the sample.

I then examined other classes of non-coding RNAs (ncRNAs) with sufficient coverage (Methods). I identified 48 novel D sites in 23 different small nucleolar RNAs (snoRNAs), uncovering snoRNAs as a substantial new class of RNA targeted by DUS enzymes (Figure 2c and Table 2). I considered the possibility that DUS might modify ribosomal

RNA given that dihydrouridine has been reported in the bacterial ribosome at U2449 of the large subunit RNA (Kowalak et al., 1995). However, inspection of the cytoplasmic rRNAs did not reveal any DUS-dependent modification at the orthologous position (Fig. S2d).

Like tRNAs, snoRNAs must fold to perform their cellular function( Khanna et al., 2006; Watkins et al., 2002). Given the importance of D for tRNA folding (Dalluge et al., 1996; Dyubankova et al., 2015), Leonard Schärfen and I analyzed chemical probing data to determine if D occurs within structurally stereotyped regions in snoRNAs. Dimethyl sulfate (DMS) methylates the Watson-Crick face of unpaired As and Cs, which can be detected as sites of misincorporation by RT. The observed mutation rate at each A and C indicates the extent of pairing (Zubradt et al., 2017), with paired nucleotides having low DMS reactivity and low mutation rates and unpaired loop regions having high reactivity and high mutation rates. Comparing snoRNA D sites with DMS probing data from WT yeast cells (Zubradt et al., 2017) revealed a propensity for D to occur in unpaired regions (Fig. 2d). Intriguingly, most of the 48 snoRNA D sites are located in 4-8bp stem-loop regions (schematized in Fig. 2e). These compact stem-loops are structurally similar to the D loops of tRNAs, suggesting a common mechanism of recognition by DUS and/or a similar role for D within the loop region to promote stable folding of the adjacent stem by causing changes to the RNA backbone conformation (Dalluge et al., 1996; Dyubankova et al., 2015). My results establish that DUS modify additional ncRNAs beyond tRNAs and suggest a broad role for DUS in the biogenesis and function of many structured RNAs.

I next analyzed yeast mRNA for D. With help from Cassandra, I used a simple statistical metric, a modified Z score, to distinguish robust DUS-dependent RT stops from noise in these less abundant RNAs. (See Methods for the advantages and limitations of the MAD score and Z score metrics). As for tRNAs, I defined empirical thresholds for site calling based on differences in the distributions of scores in WT and DUS KO samples (Fig. S3a). Applying conservative cutoffs to the mRNA mapping reads (Methods), I identified 130 high-confidence D sites in mRNAs (Table 2). To estimate the number of false positives, I inverted the analysis (required high Z scores in the DUS KO replicates and low Z scores in WT replicates), which identified five false positives for an estimated false discovery rate for D sites in mRNA of 3.8%. Two false positives are understandable as 'shadow' peaks downstream of a D (Fig. S3b). To roughly estimate the stoichiometry of the mRNA Ds, I calculated the fraction of reads that traverse a D vs. terminate at a D. For the D site in the ALD6 coding sequence, approximately 13.5% of the reads terminate at the D. For the D site in the SEC63 coding sequence, the fraction of reads terminating at the D is approximately 5.7%. Given that on a synthetic RNA with 100% D occupancy RT terminates at a D only ~20% of the time (Fig. S1b), I estimate the ALD6 site at ~75% occupancy and the SEC63 site at ~25%. The number of D sites I identified (130) represents a lower bound for the total number of D sites in yeast mRNA as I surveilled only 1% of the yeast transcriptome that met the coverage threshold in all 6 libraries. These results show that interactions between DUS and mRNA (Beckmann et al., 2015; Mitchell et al., 2013) result in substantial modification and uncover dihydrouridine as a component of the mRNA epitranscriptome.

The 130 D sites were distributed throughout mRNA features including the 5′-UTR, CDS, introns and 3′-UTR (Fig. 3a-b and Table 2). The prevalence of D in coding sequences, including of essential genes, raised the question of how the presence of D in mRNA impacts translation. I generated model mRNAs encoding a short (12kD) protein, Top7 (Kuhlman et al., 2003), that can be produced with few uridines: 2 or 3, including the start/AUG, stop/UAG and an internal test codon (Fig. 3c). Wendy synthesized mRNAs with no internal U/D test codon, or one of three different internal codons that I detected as frequently D-modified in endogenous yeast mRNAs, ADC, AGD and GAD. Wendy translated the D or U versions of these mRNAs in rabbit reticulocyte lysate (RRL) and quantified protein production by measuring $^{35}$S-Met incorporation into full-length Top7 protein by SDS-PAGE and autoradiography (Fig. 3c and S3c). All 8 mRNAs were efficiently translated in RRL with no significant differences in the amount of protein produced from any D or U containing mRNA (n=6 replicates, Fig. 3c and S3c). Thus, eukaryotic ribosomes can efficiently traverse D sites in mRNAs. While Wendy's results show that the translational output is not impaired by these D-containing codons, other codons may behave differently. It is also possible that D could impact translational fidelity, as has been reported for pseudouridine (Eyler et al., 2019).

In light of the impacts of D on RNA structure (Dalluge et al., 1996; Dyubankova et al., 2015; Sipa et al., 2007), the location of D in the intron of RPL30 (Fig. 3d) is notable; this intronic D is adjacent to an RNA structure that is important for the auto-regulation of pre-mRNA splicing by free Rpl30 protein (White et al., 2004). To investigate the potential

consequences of this D site for splicing, I performed RNA-seq on WT and DUS KO. The absence of DUS activity caused a reproducible accumulation of introns in DUS KO cells that is consistent with a positive effect of D on splicing of this pre-mRNA (Fig. 3e). Other D-containing introns (RPL16B and COF1) were not affected indicating that splicing is not generally impaired in the absence of DUS activity (Fig. S3d).

It is interesting that several additional mRNA D sites occur in regions where secondary structure potential is evolutionarily conserved (Rouskin et al., 2014) suggesting biological function for these structures. Although the predicted structures of D sites in mRNA are more diverse than in snoRNAs, 19 of the 130 identified mRNA D sites occurred in structures very similar to the tRNA D-loop, which is consistent with modification of mRNAs at structurally stereotyped positions analogous to previously known D sites in tRNAs. Globally, Leonard Schärfen's analysis of DMS structure-probing data (Zubradt et al., 2017) found that mRNA regions flanking D sites were significantly likelier to be unpaired in cells than a background set of sites ($p<.05$, Fig. 3f). This might be a consequence of modification because D antagonizes RNA duplex formation, and promotes the formation of stem loop structures (Dalluge et al., 1996; Dyubankova et al., 2015; Sipa et al., 2007) (Fig. 3g). Alternatively, accessibility could be important for modification by DUS.

While the manuscript this chapter is based on was in review, Finet et al (Finet et al., 2021), reported the development of a method similar to D-seq, Rho-seq (so named for the coupling of rhodamine to reduced dihydrouridine). They identified sparse D

modification of mRNAs from human cells and Schizosaccharomyces pombe similar to the frequency of mRNA D sites that I uncovered in Saccharomyces cerevisiae. One notable difference between the studies is that Finet et al. report modest reductions in translation of D-containing mRNAs in vitro for several D-containing codons, including GAD. Wendy's results do not confirm this reported translational defect (Fig. 3c). Conceivably the source of translation components (rabbit reticulocytes vs wheat germ) and/or differences in the mRNA context, including sequences flanking the GAD codons, affect the amount of protein produced.

My results establish D-seq as a high-throughput method to map dihydrouridine sites with single-nucleotide resolution and reveal new classes of RNA targets for conserved DUS enzymes, which I now show include mRNA. The discovery of D in mRNA validates the function of DUS-mRNA interactions that have been observed from yeast to human cells (Beckmann et al., 2015; Mitchell et al., 2013). The D-seq method is broadly applicable to reveal the specific locations of D, including in pathogenic RNA viruses where dihydrouridine has been detected by mass spectrometry (McIntyre et al., 2018) and in tumors where elevated DUS expression is linked to worse patient outcomes (Creighton et al., 2016, 2013; Kato et al., 2005; Kuchino and Borek, 1978)

## Methods

### Synthetic RNAs for RNA degradation and RT stop testing

Synthetic 100% uridine or dihydrouridine containing RNA (5′-ggaacagaaacagagaaaggaacagagaaagacaU/DaaacagaaagagacaagaacagagacaagaacagU/DggcaggaacagagacaaacagagacaggaacaaU/DgacaggaacagaaagaaacagagacaagcacU/Dcgggcaccaaggacacgaaccggaacgcggaaccaaacgggcaacggaccggac-3′) was generated by run off transcription with T7 RNA polymerase and gel purified on an 8% urea-TBE polyacrylamide gel electrophoresis (PAGE) gel. To compare the harshness of the different D modifying treatments, a synthetic RNA was incubated either under published D mapping conditions(Xing et al., 2004), under published D reduction conditions(Kaur et al., 2011; Pan et al., 2009) or similar D reduction conditions with $NaBH_3CN$ substituted for $NaBH_4$. To measure RT at reduced dihydrouridine, we reverse transcribed reduced U or D RNA with Superscript III RT, using manufacturer conditions. Samples were prepared and run on sequencing gels as in(Smola et al., 2015).

**Strain construction**

Quadruple Dus mutant strain was generated by mating double knockout strains FX-34 (*dus1Δ dus2Δ)* and FX-42(*dus4Δ dus3Δ),* followed by sporulation on SD media and subsequent tetrad dissection. Genotyping was confirmed by PCR using the following oligos:

| | |
|---|---|
| oAD56_DUS1kanR_F | GCAAGGTGATCGTCAAACTGCACT |
| oAD57_DUS1kanR_R | ATGGAGACGGAGTTGAACATTTTCT |
| oAD58_DUS2kanR_F | TAGAGACGTAGTTATCCATTCGTCC |
| oAD59_DUS2kanR_R | CTTTGGACGATAAACTAAAGGGTTT |
| oAD60_DUS3kanR_F | GGTAATAGTACACGGGATGAAGAGA |

| | |
|---|---|
| oAD61_DUS3kanR_R | TATTTTGATTTTCTTGGAACCCATA |
| oAD62_DUS4kanR_F | ACTGCATTCATTTTTGTTAGAAAGG |
| oAD63_DUS4kanR_R | CAAGCTATCTGGAAAAGAGGTGTTA |

**RNA isolation and Poly-A selection**

Yeast total RNA was isolated by hot acid phenol extraction from 750mL OD 6 culture, followed by isopropanol precipitation. Poly-A RNA was isolated from 8 mg total RNA using oligo dT cellulose beads (NEB), as described(Carlile et al., 2015). Two sequential rounds of poly-A selection were performed. For analysis of mRNA by LC-MS/MS, residual tRNAs were removed by size selection (>200t nt) on a zymo RNA Clean & Concentrator column according to manufacturer instructions. Removal of small RNA and ribosomal RNA contamination was verified by bioanalyzer analysis using Agilent RNA 6000 Pico chips.

**D-seq Library preparation**

Yeast RNA was fragmented in 10 mM ZnCl2 at 94°C for 1min and precipitated. $BH_4$ treatment of RNA was as follows: Poly-A+ mRNA was resuspended in 18 µL ddH2O, and treated 2 µL of 10mg/mL $NaBH_4$ in 500mM Tris pH 7.5 at 0°C for 1hr. The $BH_4$ treatment was quenched with 4uL of 6N $CH_3COOH$ and precipitated. RNA fragments were dephosphorylated and end repaired with CIP (NEB) and PNK (NEB), followed by size selection of RNA fragments (70-80nt) on an 8% urea-TBE PAGE gel. RNA fragments were eluted from gel slices overnight at 4°C with gentle rocking in 400µL RNA elution buffer (300 mM NaOAc pH 5.5, 1 mM EDTA, 100 U/ml RNasin (Promega)

followed by precipitation. Ligation of a pre-adenylated adaptor (IDT) was carried out with T4 RNA ligase (NEB) in buffer without ATP (50mM Tris-HCl pH 7.8, 10 mM MgCl2, 10 mM DTT) at 22°C for 2.5 h, followed by precipitation. Adapter ligated RNA fragments were reverse transcribed with SuperScript III reverse transcriptase (Thermo). RNA and primer were denatured and annealed at 95°C for 5 min then placed on ice for 5 min. After annealing, 1µL 10mM dNTPs, 1µL 0.1M DTT, 1µL RNAsin (Promega), 3µL 5X First Strand Buffer (Thermo), 1µL SSIII RT were added, and reverse transcription was carried out at 50°C for 1 h. Truncated cDNAs were size-selected (50-80nt) and purified on an 8% urea-TBE PAGE gel, followed by precipitation. cDNAs were eluted from gel slices overnight at room temperature with gentle rocking in 400µl DNA elution buffer (300 mM NaCl, 10 mM Tris, pH 8.0). A 5′ adapter was ligated on to the cDNA using T4 RNA ligase. 0.8uL 80uM linker (IDT) was mixed with 1µL DMSO, 5µL of eluted cDNA, incubated at 75°C for 2 min and immediate placed on ice for 2min. After cooling, 2uL RNA Ligase buffer (NEB), 0.2 µL.1M ATP (NEB), 6.5 µL PEG-8000 (NEB), 3.6 µL ddH2o and 0.5 µL T4 RNA ligase 2 were added to the cDNA/linker mix. The ligation was incubated overnight at 22°C . The ligation was cleaned up with Dynabead MyOne Silane magnetic beads (Thermo) according to the manufacturer's instructions. Sequencing libraries were amplified from 5′ and 3′ linker ligated cDNA using Phusion DNA polymerase (NEB). PCR products were gel-purified, precipitated, pooled and sequenced on an Illumina HiSeq 2500.

**RNA-seq Library preparation**

RNA seq libraries were generated in parallel with D-seq libraries by omitting the $NaBH_4$ treatment and selecting for full length (90-100nt) RT products.

**Sequencing Data Analysis**

Demultiplexed reads were adapter trimmed using BBTools(Bushnell, n.d.; Bushnell et al., 2017) bbduk.sh . Adapter trimmed reads were then PCR-duplicated collapsed based on unique molecular identifier (UMI) using dedupe.sh. The UMI was then force trimmed with a second round of trimming. Adapter trimmed and duplicate collapsed reads were then aligned to the sacCer3 genome using bbmap.sh. For the tRNA mapping D analysis, we aligned the trimmed and PCR-duplicate collapsed reads to a pseudo-genome containing 1 copy of each unique tRNA sequence. Uniquely mapping strand specific read end position was obtained using bedtools(Quinlan and Hall, 2010). We generated wig files and visualized the read end positions using mochiview(Homann and Johnson, 2010). D peaks were annotated using the sacCer3 features file and bedtools.

**mRNA D-seq peak calling**

D-sites were identified as statistical outliers in position-specific accumulation of D-seq reads. We required at least 50 reads in the 100nt window surrounding the test position and quantified and compared sites using a modified Z-score, in which the position of interest is excluded when calculating the mean and standard deviation. For all of the test positions that met the read cutoff, we calculated a Z score of read ends based on the distribution of read ends in the 100nt window centered on the test position.

$$Z_{pos} = \frac{ends_{pos} - mean(ends_{window})}{stdev(ends_{window})}$$

**tRNA and snRNA D-seq peak calling**

In the highly structured and heavily modified tRNAs and snRNAs, we identified D sites by analyzing the absolute deviation around the median (MAD), which scores sites relative to the median rather than the mean. See below regarding the choice of metric for different classes of RNA. We considered every position in the test transcriptome where there were more than 50 reads in the 100nt window surrounding the test position and additionally required that the window median was greater than zero. For all test positions that met the read cutoff, we calculated a MAD score of read ends based on the distribution of read ends in the 100nt window centered on the test position.

$$M_{pos} = \frac{ends_{pos} - median(ends_{window})}{MAD(ends_{window})}$$

And:

$$MAD = median(|ends_{pos} - median(ends_{window}|)$$

**Selection of D-seq signal scoring metrics**

Two different scoring approaches were necessary for unbiased identification of D sites in different classes of RNA due to large differences in the distributions of strong RT stops as well as RNA abundance. The presence of multiple RT stops in close proximity, which is common in tRNA due to pervasive RNA modification and strong secondary structure, precludes use of the intuitive and statistically principled Z-score which we use

for less structured mRNAs. The Z-score cannot identify RT stop signals in windows with multiple strong signals because these background RT stops in ncRNA dampen the signal at the position of interest(Leys et al., 2013) (Fig. S2e). We therefore analyzed non-coding RNAs using the absolute deviation around the median (MAD), which scores sites relative to the median rather than the mean. The MAD score requires much higher coverage than the Z-score because, for the denominator to be non-zero, more than half the positions in the window surrounding a site must have 5′ ends mapped to them. In mRNA, it is rare for a 100-nt window to contain more than one strong RT stop and the modified Z-score is preferred to quantify and compare sites.

**D-seq peak thresholding**

For each set of peaks (tRNA, snRNA, mRNA), we defined library cutoffs for peak score by plotting the distribution of peak scores in each library as an inverse CDF. We set cutoffs for D peaks by requiring D site scores be substantially greater than the score at which the distributions of WT and DUS KO diverge in 3 out of 3 WT replicates, and less than the score at which the distributions diverge in the quad KO. For tRNA, MAD score cutoffs were $MAD_{wt} > 40$ and $MAD_{dus} < 40$. For snRNA, MAD score cutoffs were $MAD_{wt} > 12$ and $MAD_{dus} < 8$. For mRNA, the Z-score cutoffs were $Z_{wt} > 10$, and $Z_{dus} < 7$.

**DMS reactivity near D sites**

A previously published DMS-MaPseq(Zubradt et al., 2017) data set for *S. cerevisiae* was downloaded from GEO (accession number GSE84537). Raw reads were preprocessed and aligned according to the original publication, and DMS reactivities

were calculated as the ratio of mutations to coverage. Reactivities around called D sites in mRNAs or snRNAs were pooled for each nucleotide position relative to the respective D coordinate. Values were included in the analysis only if the coverage was larger than 350 and the nucleotide identity in the transcript was A or C. To visualize background reactivities and control for nucleotide bias, 70 samples matching the size of called D sites were randomly drawn from a population of background sites that fell below the Z score cutoffs in wildtype and quad KO. Significance testing was done using two-sided Mann Whitney U tests between reactivities around the full set of background positions and the called D sites.

**Detecting dihydrouridine by LC-MS/MS**

For each sample, duplicate digestions of 50ng and 750ng for each sample were digested with 5 U/uL Benzonase (Sigma, #E8263), 0.1 U/uL phosphodiesterase (Sigma #P3243), 1 U/uL alkaline phosphatase (Sigma #P5521) in 500mM Tris-HCl pH 8.0, 10mM $MgCl_2$ in a final reaction volume of 50µL for 6 hours at 37ºC. An equal volume of water was then added to each sample before filtration through a 0.2µm PVDF filter (0.2µm pore size, 0.4mm diameter, Millipore). 10µL of each sample was separated by reverse phase ultra-performance liquid chromatography on a Shim-pack GIST C18 2µm, 2.1 x 50mm column (Shimadzu, #227-30001-02) on a Nexera LC-40D XS liquid chromatography system using a gradient of 5mM ammonium acetate pH 5.3 and acetonitrile. After separation, samples were analyzed by mass spectrometry on a Shimadzu LCMS-8060 Triple Quadrupole Liquid Chromatograph Mass Spectrometer (Shimadzu). Nucleosides were quantified using the following nucleoside-to-base

transitions: 267.966>136.000 (A), 284.004>152.100 (G), 245.30>113.10 (U), and 247.20>115.15 (D). Mixes of nucleoside standards were injected alongside the samples in the same run to generate standard curves, from which concentrations of each nucleoside in each sample were calculated. The percentages of modified to unmodified nucleoside in each sample were calculated based on calibrated concentrations. These conditions were adapted from reference (Finet et al., 2021).

**Synthesis of U and D substituted mRNAs**

mRNAs were designed based on the coding sequence of Top7(Kuhlman et al., 2003) by replacing all but three uridine-containing codons: start, stop and a single test codon. The UTRs also lacked U. RNA was synthesized with T7 by run-off transcription of linearized plasmid templates with either 100% UTP or 100% DTP (Trilink Biotechnologies) and purified on 6% denaturing Urea-PAGE gels. Samples of purified mRNAs were denatured with glyoxal at 50°C for 30 minutes and analyzed for integrity by separation on 1% agarose gels in BPTE buffer (100mM PIPES, 300mM Bis-Tris, 10mM EDTA, pH 6.5) and imaging (Bio-Rad ChemiDoc). Bands were quantified using GelAnalyzer 19.1 (www.gelanalyzer.com).

**In vitro translation of U and D substituted mRNAs**

Uncapped Top7 mRNAs were translated in nuclease-treated rabbit reticulocyte lysate (Promega). 500ng mRNA was incubated in 8.4 µL rabbit reticulocyte lysate, 0.24 µL 1mM amino acid mixture minus methionine, 0.48 µL $^{35}$S methionine, 0.24 µL RNasin, and dd$H_2O$ to 20 µL. Translation reactions were incubated at 30°C for 90 minutes and

quenched with 20 µL 2X SDS sample buffer. Translation reactions were then incubated at 60°C for 20 minutes and resolved on a 14-20% SDS-PAGE gel. Gels were fixed in 30% methanol 10% acetic acid, incubated in Amplify solution (GE Healthcare) and dried on a vacuum drier. Dried gels were exposed for a minimum of 12 hours on a storage phosphor screen (GE), scanned (Bio-Rad) and quantified using GelAnalyzer 19.1 (www.gelanalyzer.com).

## Figures

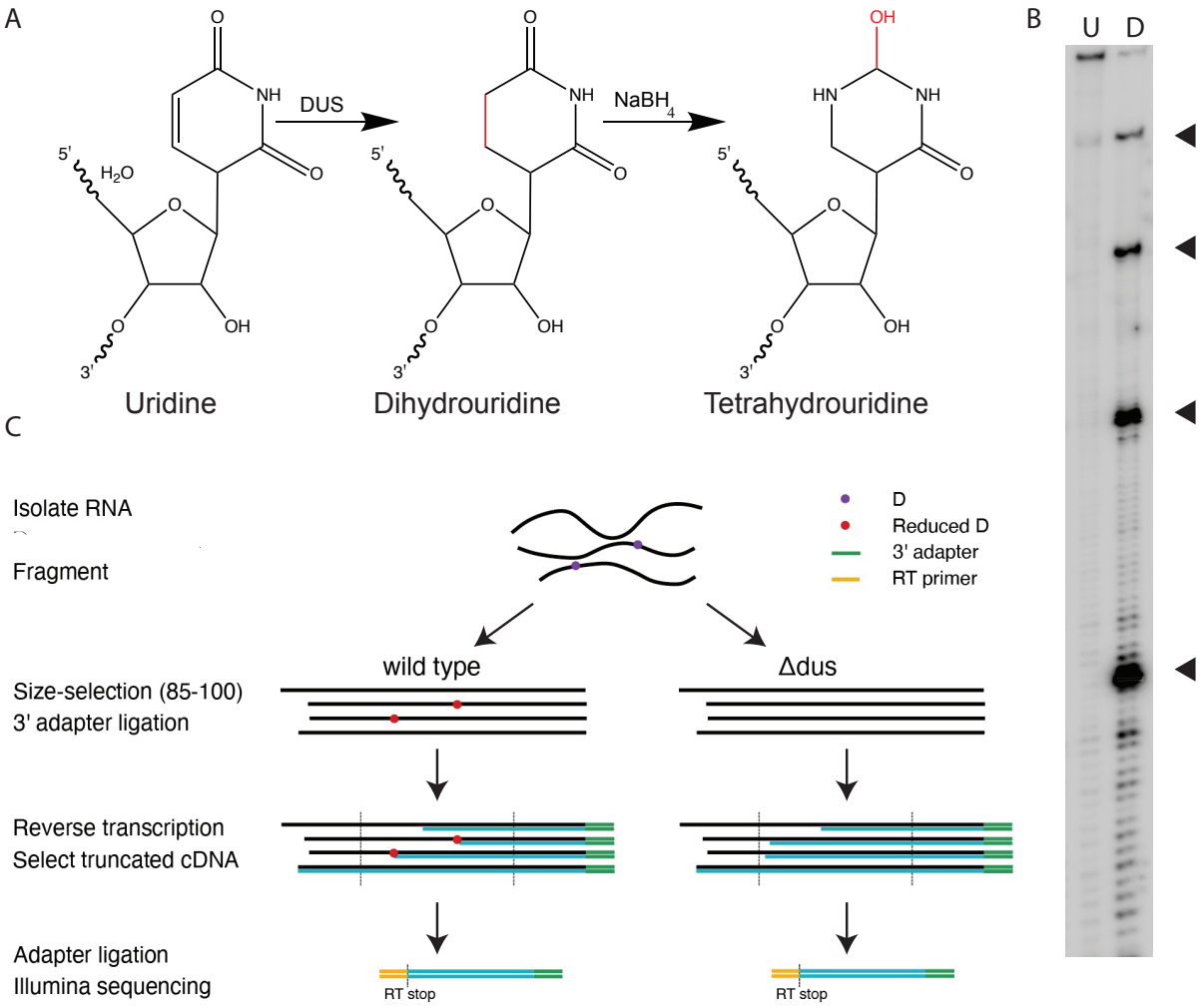
A
DUS
NaBH4
Uridine
Dihydrouridine
Tetrahydrouridine
B
U
D
C
Isolate RNA
Fragment
D
Reduced D
3' adapter
RT primer
wild type
Δdus
Size-selection (85-100)
3' adapter ligation
Reverse transcription
Select truncated cDNA
Adapter ligation
Illumina sequencing
RT stop
RT stop

**Figure 1 Dihydrouridine-specific chemistry to map dihydrouridine sites in RNA with single-nucleotide resolution**

a. Bulk nucleoside analysis of detects D in mRNA from WT but not DUS KO yeast. mRNA was purified by selecting for poly(A)+ and tRNAs were removed by size selection.
b. Structures of uridine, dihydrouridine and tetrahydrouridine.
c. Primer extension analysis of synthetic 4D and 4U RNAs treated with $NaBH_4$ and reverse transcribed with Super Script III RT. D-dependent RT stop positions are highlighted.

d. Schematic of D-seq library preparation.

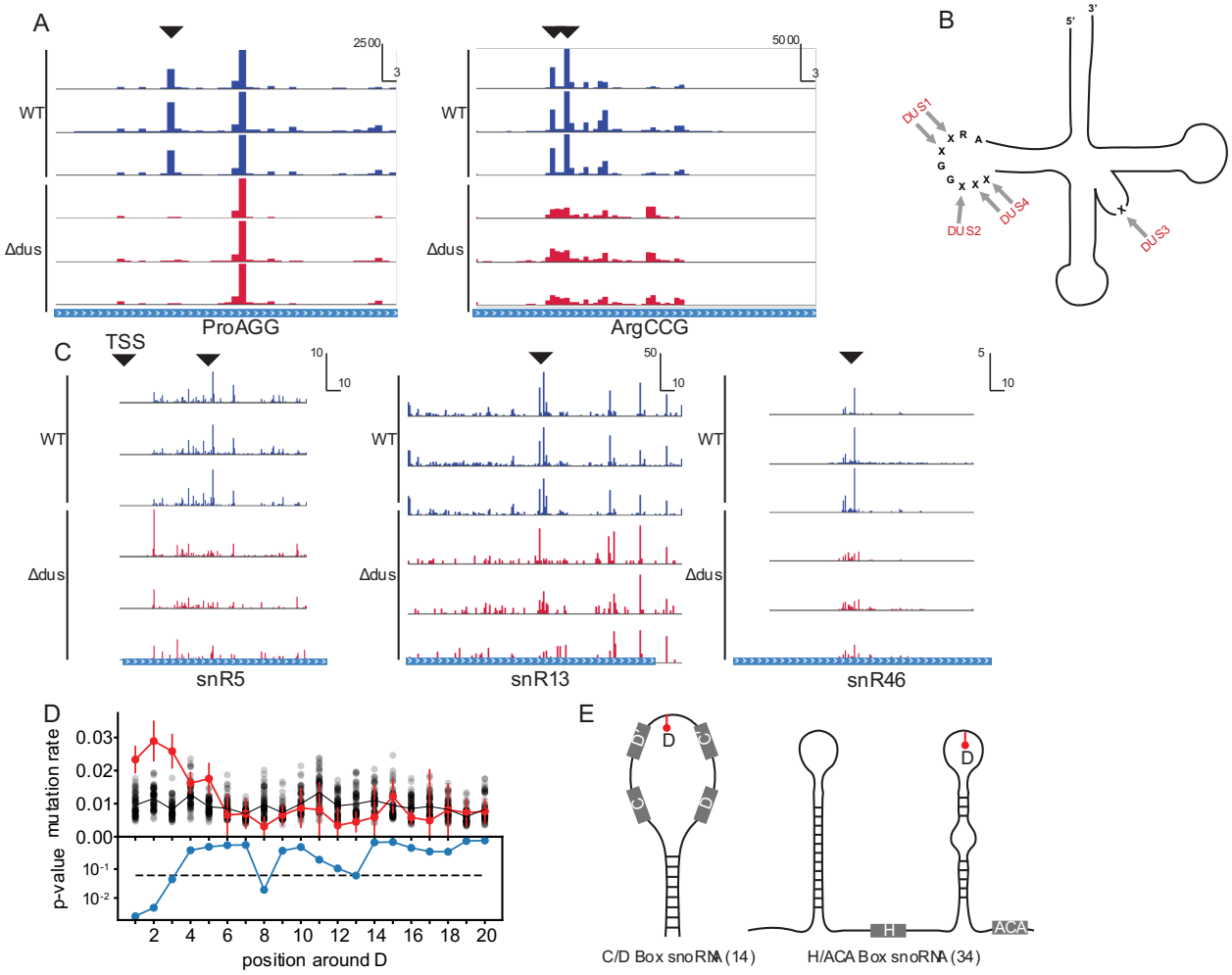
A
WT
Δdus
ProAGG
ArgCCG
B
5'
3'
DUS1
DUS2
DUS4
DUS3
C
TSS
snR5
snR13
snR46
D
p-value
mutation rate
position around D
E
C/D Box snoRNA (14)
H/ACA Box snoRNA (34)

**Figure 2 D-seq identifies known and novel dihydrouridine sites in structured ncRNAs**

a. Plots of cDNA end positions in Dus2 target tRNA ProAGG, and Dus2, Dus4 target tRNA ArgCCG. D Peaks are highlighted. X scale in RPM and Y scale in bp.
b. Summary of known tRNA D positions and corresponding DUS.
c. Plots of cDNA end positions in snR5, snR13, and snR46 snoRNAs. D peaks and are highlighted. TSS, transcription start site of snR5. X scale in RPM and Y scale in bp.
d. snoRNA Ds occur primarily in stem loop structures that resemble tRNA D loops. Plot of median DMS induced mutation rate in 25nt window flanking D site. Red trace is median DMS reactivity flanking D positions. Black dots are median DMS reactivity for randomly selected set of background positions. Blue trace is p-value for difference in DMS reactivity for sequences flanking D or background sites.
e. D sites occur in stem-loop structures of 16 H/ACA and 7 C/D box snoRNAs.

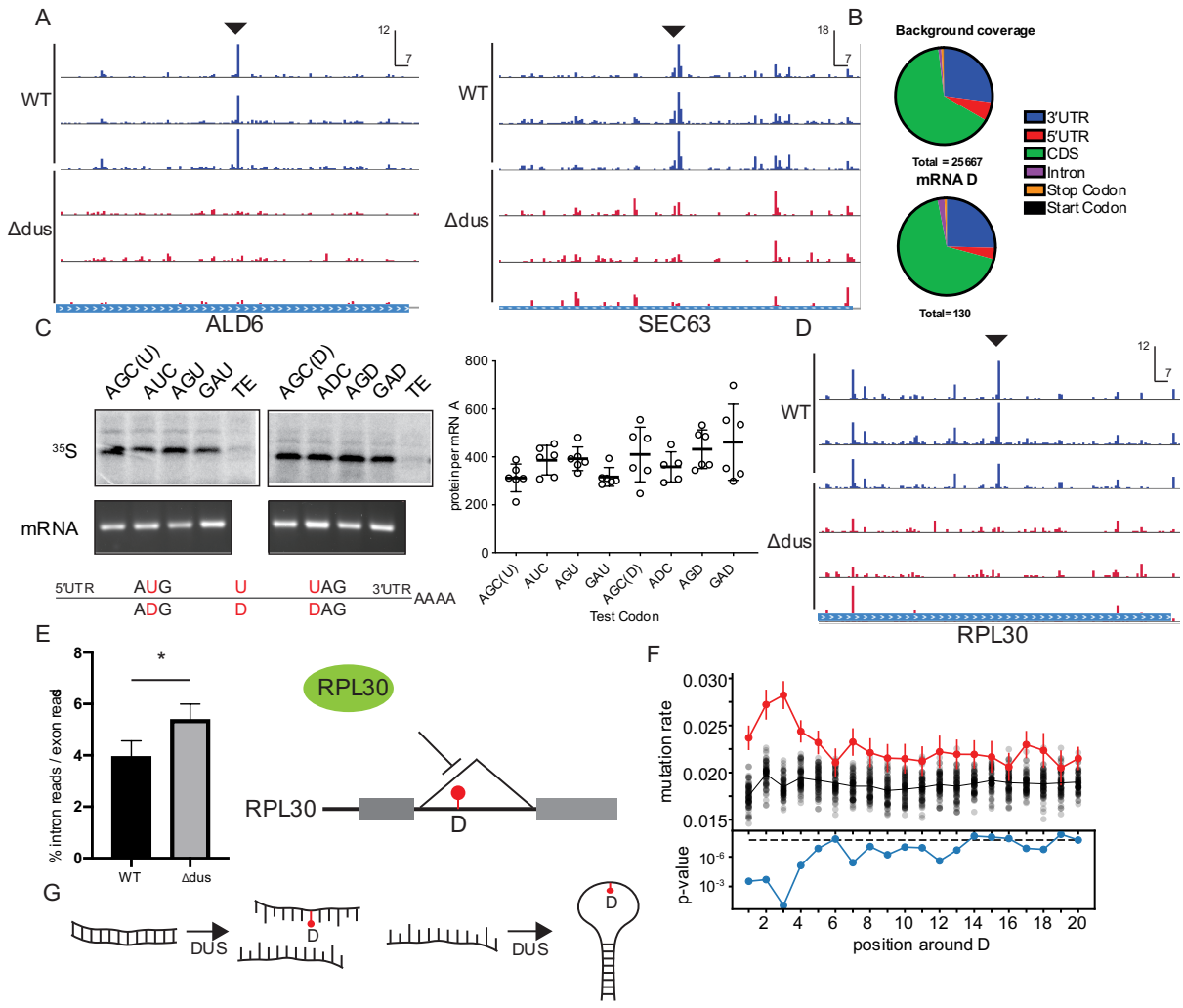
A
WT
Δdus
ALD6
B
SEC63
Background coverage
Total = 25667
mRNA D
Total=130
3'UTR
5'UTR
CDS
Intron
Stop Codon
Start Codon
C
AGC(U)
AUC
AGU
GAU
TE
AGC(D)
ADC
AGD
GAD
35S
mRNA
5'UTR AUG U UAG 3'UTR AAAA
ADG D DAG
protein per mRNA A
Test Codon
D
RPL30
E
% intron reads / exon reads
RPL30
D
F
mutation rate
p-value
position around D
G
DUS

**Figure 3 D-seq identifies dihydrouridine sites in mRNAs**

a. Plots of cDNA end positions in ALD6 and SEC63 mRNAs. D peaks are highlighted. Scale in RPM and bp.
b. Distribution of D sites among mRNA features, and background distribution of features for all sites interrogated for D.
c. SDS-PAGE gels showing Top7protein produced from U and D containing mRNAs with 4 different test codons. Denaturing glyoxal agarose gel showing mRNA integrity. All 4 test constructs showed no significant difference in protein produced per mRNA +/- D. Schematic of U/D mRNAs with U/D positions highlighted in red
d. Plots of cDNA end positions for intronic D in RPL30 mRNA. D peak is highlighted. Scale in RPM and bp.
e. DUS KO strain has increased ratio of RPL30 intron mapping reads to exon mapping reads ($p < .05$, students t-test). Model of regulation of RPL30 pre-mRNA splicing by RPL30 protein.
f. mRNA sequences flanking Ds have higher DMS reactivity indicating greater flexibility. Plot of median DMS induced mutation rate in 25nt window flanking D site. Red trace is median DMS reactivity surrounding D positions. Black dots are median DMS reactivity for randomly selected set of background positions. Blue is p-value for difference in DMS reactivity for sequences flanking D or background sites.
g. D has multiple impacts on RNA structure. D both promotes loop formation and antagonizes duplex formation.

## Supplementary Figures

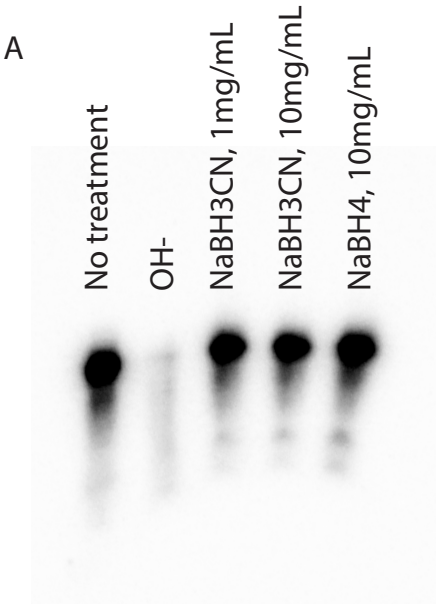


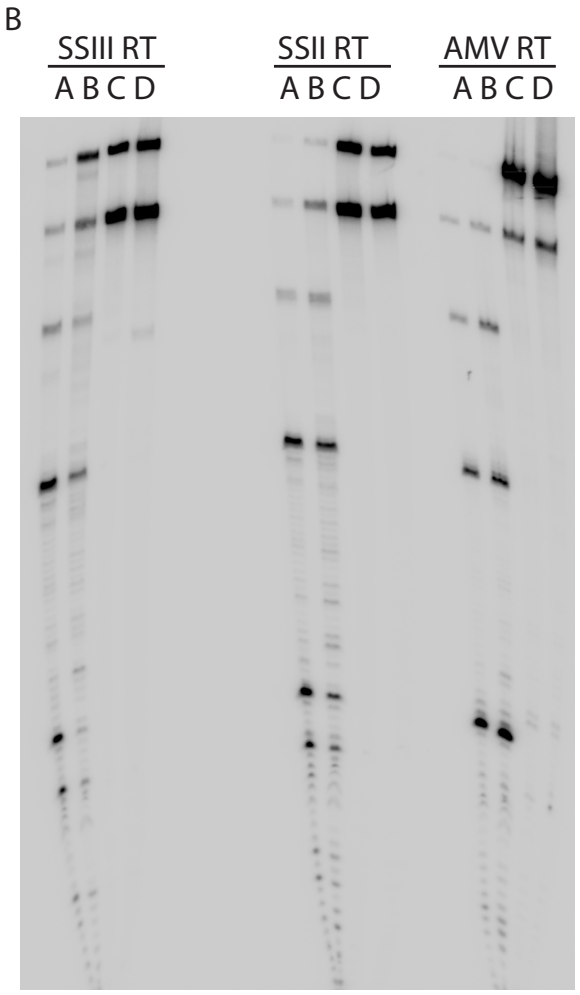

**Figure S1 Testing RNA treatment and RT conditions for D-seq**

a. Unmodified 194nt RNA was treated with strong base (OH-), $NaBH_3CN$ or $NaBH_4$, precipitated and run on an 8% urea-PAGE gel.
b. Multiple RTs stall at reduced D. 1: 4D RNA treated with borohydride and benzyhydrazide, 1: 4D RNA treated with borohydride 3: 4U RNA 4: 4D RNA
c. Bioanalyzer analysis of total RNA and PolyA+ mRNA for mass spectrometry.

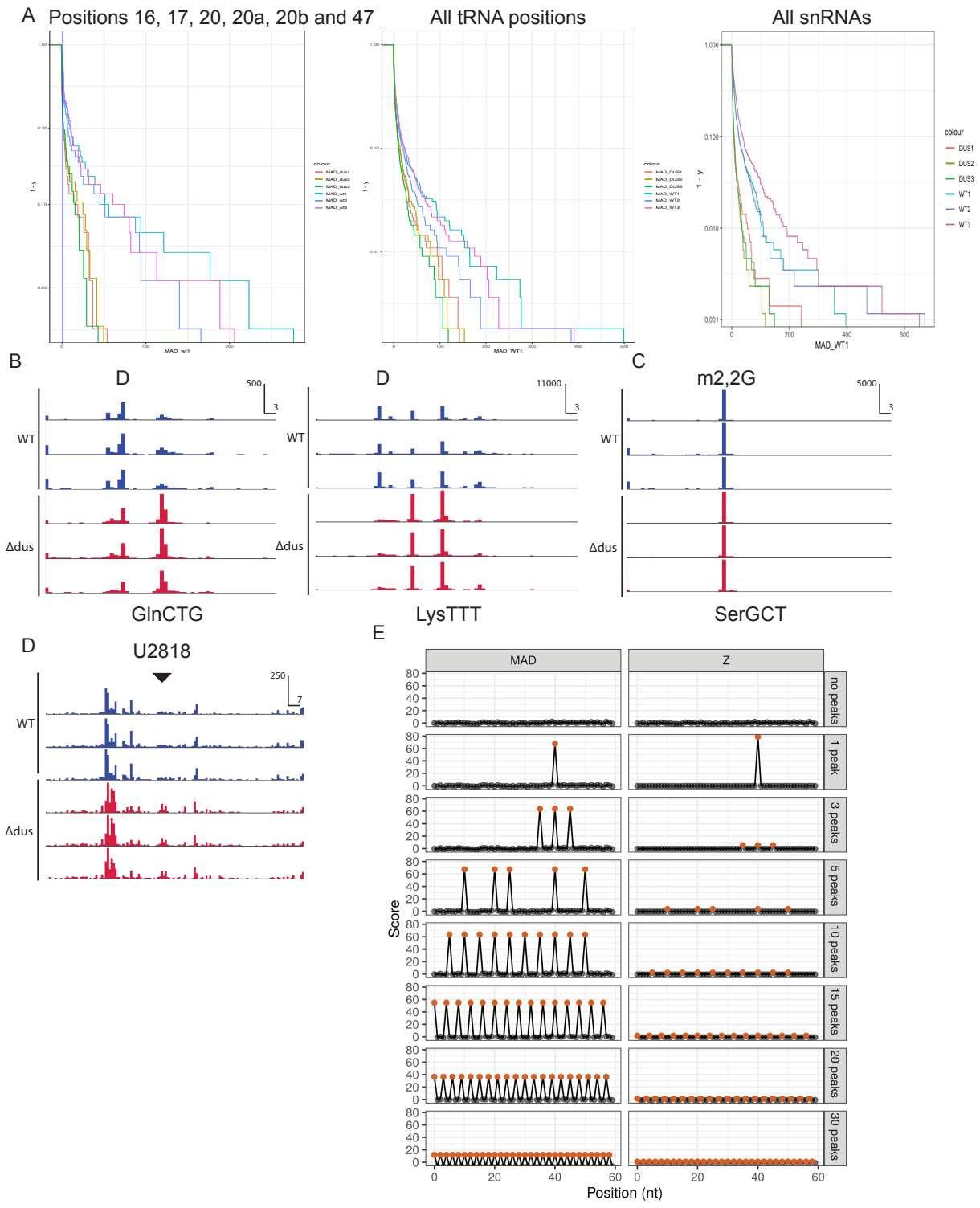
A
Positions 16, 17, 20, 20a, 20b and 47
All tRNA positions
All snRNAs
colour
DUS1
DUS2
DUS3
WT1
WT2
WT3
MAD_WT1
B
D
WT
Δdus
GlnCTG
C
m2,2G
SerGCT
LysTTT
D
U2818
E
MAD
Z
no peaks
1 peak
3 peaks
5 peaks
10 peaks
15 peaks
20 peaks
30 peaks
Score
Position (nt)

**Figure S2**

a. Inverse CDF plots of MAD score for possible D positions (16,17, 20, 20a, 20b and 47) in tRNAs, MAD score for all tRNA U positions, and all snRNA U positions.
b. Plots of cDNA end positions in tRNA GlnCTG and tRNA LysTTT containing multiple Ds. 3′ most D peak is highlighted.
c. Plots of cDNA end positions in SerGCT where D signal is blocked by $m^{2,2}G$. $m^{2,2}G$ position is highlighted.
d. Plots of cDNA end positions in cytoplasmic 25S rRNA at the position orthologous to E. coli position 2449.

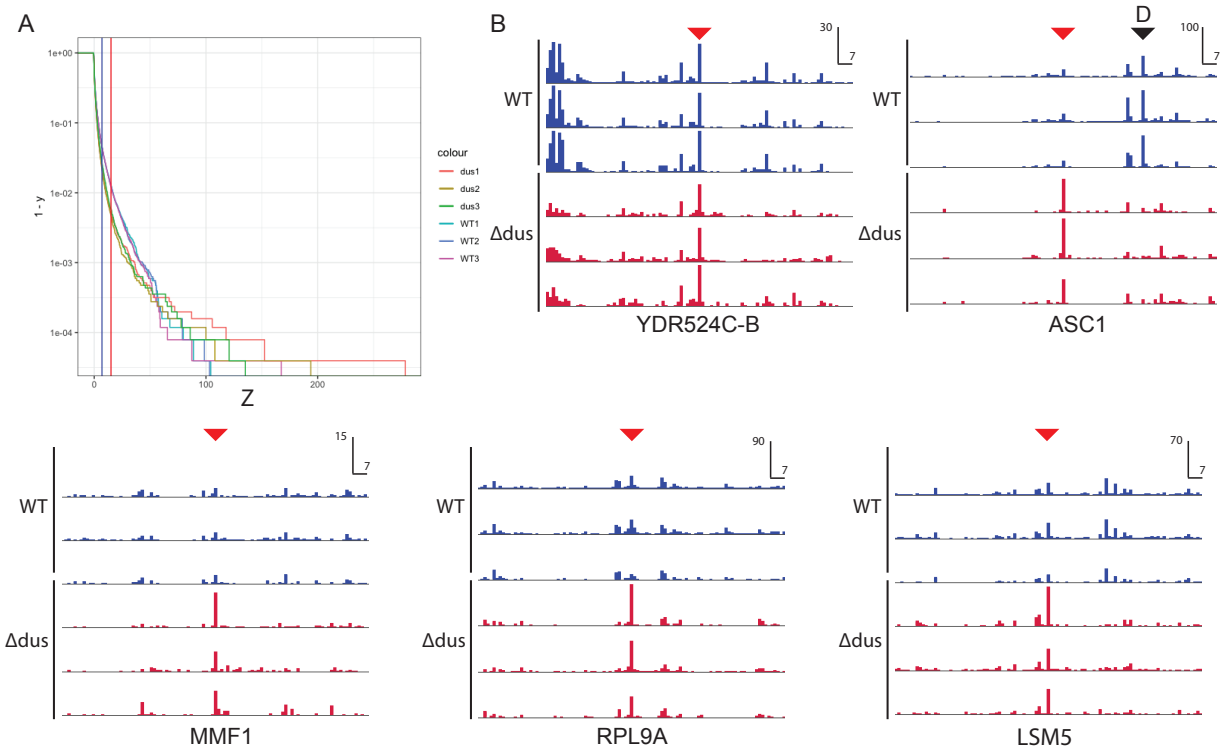
A
1e+00
1e-01
1e-02
1e-03
1e-04
1 - y
0
100
200
Z
colour
dus1
dus2
dus3
WT1
WT2
WT3
B
30
7
WT
Δdus
YDR524C-B
D
100
7
WT
Δdus
ASC1
15
7
WT
Δdus
MMF1
90
7
WT
Δdus
RPL9A
70
7
WT
Δdus
LSM5

**Figure S3**

a. Inverse CDF plots of Z score for mRNA mapping reads. Blue line is $Z_{dus}$ cutoff and red line is $Z_{wt}$ cutoff
b. Plots of cDNA end positions for 5 false positive sites in mRNAs. Shadowing D peaks are highlighted in black. False positive sites are highlighted in red.
c. Uncropped Top7 $^{35}S$ SDS-PAGE and mRNA 1% BP-TE agarose gels from Fig 3c.
d. DUS KO strain does not have a change in ratio of intron mapping reads to exon mapping reads for COF1 or RPL16b.

## Tables

| | Called in Xing 2004? | Known position? | Postion | Strand |
|---|---|---|---|---|
| tRNA-Val-CAC-1-1.21.+ | No | Yes | 21 | + |
| tRNA-Gln-TTG-1-1.21.+ | No | Yes | 21 | + |
| tRNA-Gly-TCC-1-1.21.+ | No | Yes | 21 | + |
| tRNA-Gln-CTG-1-1.21.+ | Yes | Yes | 21 | + |
| tRNA-His-GTG-1-1.21.+ | Yes | Yes | 21 | + |
| tRNA-Arg-CCG-1-1.17.+ | No | Yes | 17 | + |
| tRNA-Arg-CCG-1-1.20.+ | No | Yes | 20 | + |
| tRNA-Asp-GTC-1-1.17.+ | Yes | Yes | 17 | + |
| tRNA-Gln-TTG-3-1.17.+ | No | Yes | 17 | + |
| tRNA-Gln-TTG-3-1.20.+ | No | Yes | 20 | + |
| tRNA-Leu-GAG-1-1.17.+ | No | Yes | 17 | + |
| tRNA-Ile-TAT-1-1.35.+ | No | No | 35 | + |
| tRNA-Pro-AGG-1-1.20.+ | Yes | Yes | 20 | + |
| tRNA-Pro-TGG-1-1.17.+ | Yes | Yes | 17 | + |
| tRNA-Trp-CCA-1-1.17.+ | No | Yes | 17 | + |
| tRNA-Cys-GCA-1-1.17.+ | Yes | Yes | 17 | + |

**Table 1** Detection of D sites in tRNAs

| snR name | Chromosome | Class | Position | Strand |
|---|---|---|---|---|
| snR46 | chrVII | H/ACA | 545462 | + |
| snR10 | chrVII | H/ACA | 346182 | + |
| snR10 | chrVII | H/ACA | 346123 | + |
| snR10 | chrVII | H/ACA | 346095 | + |
| snR10 | chrVII | H/ACA | 346022 | + |
| snR10 | chrVII | H/ACA | 346017 | + |
| snR82 | chrVII | H/ACA | 316834 | + |
| snR32 | chrVIII | H/ACA | 381681 | + |
| snR32 | chrVIII | H/ACA | 381653 | + |
| snR3 | chrX | H/ACA | 663871 | + |
| snR44 | chrXII | H/ACA | 856828 | + |
| snR30 | chrXII | H/ACA | 199241 | + |
| snR30 | chrXII | H/ACA | 199090 | + |
| snR30 | chrXII | H/ACA | 198986 | + |
| snR30 | chrXII | H/ACA | 198814 | + |

| | | | | |
|---|---|---|---|---|
| snR30 | chrXII | H/ACA | 198812 | + |
| snr11 | chrXIII | H/ACA | 652470 | + |
| snR11 | chrXIII | H/ACA | 652409 | + |
| snR11 | chrXIII | H/ACA | 652351 | + |
| snR11 | chrXIII | H/ACA | 652288 | + |
| snR49 | chrXIV | H/ACA | 716267 | + |
| snR5 | chrXV | H/ACA | 842466 | + |
| snR31 | chrXV | H/ACA | 842135 | - |
| snR8 | chrXV | H/ACA | 832441 | + |
| snR8 | chrXV | H/ACA | 832438 | + |
| snR8 | chrXV | H/ACA | 832382 | + |
| snR35 | chrXV | H/ACA | 759456 | - |
| snR35 | chrXV | H/ACA | 759397 | - |
| snR9 | chrXV | H/ACA | 408123 | - |
| snR9 | chrXV | H/ACA | 408106 | - |
| snR9 | chrXV | H/ACA | 408038 | - |
| snR81 | chrXV | H/ACA | 234503 | + |
| snR81 | chrXV | H/ACA | 234457 | + |
| snR81 | chrXV | H/ACA | 234397 | + |
| snR13 | chrIV | C/D | 1402965 | + |
| snR13 | chrIV | C/D | 1402945 | + |
| snR68 | chrIX | C/D | 97140 | + |
| snR68 | chrIX | C/D | 97128 | + |
| snR4 | chrV | C/D | 424796 | + |
| snR4 | chrV | C/D | 424702 | + |
| snR64 | chrXI | C/D | 38880 | + |
| snR77 | chrXIII | C/D | 297561 | + |
| snR77 | chrXIII | C/D | 297559 | + |
| snR40 | chrXIV | C/D | 89212 | + |
| snR45 | chrXVI | C/D | 821816 | + |
| snR45 | chrXVI | C/D | 821766 | + |
| snR45 | chrXVI | C/D | 821758 | + |
| snR45 | chrXVI | C/D | 821749 | + |

**Table 2** Detection of D sites in snRNAs

| Gene ID | Gene Name | Chromosome | Position | Strand | Feature type |
|---|---|---|---|---|---|
| YJR009C | TDH2 | chrX | 453577 | - | 3UTR |

| | | | | | |
|---|---|---|---|---|---|
| YCR031C | RPS14A | chrIII | 177432 | - | 3UTR |
| YHL001W | RPL14B | chrVIII | 105123 | + | 3UTR |
| YBR189W | RPS9B | chrII | 605545 | + | 3UTR |
| YGL123W | RPS2 | chrVII | 278393 | + | 3UTR |
| YDL061C | RPS29B | chrIV | 340517 | - | 3UTR |
| YNL067W | RPL9B | chrXIV | 500328 | + | 3UTR |
| YPL090C | RPS6A | chrXVI | 377241 | - | 3UTR |
| YLR264W | RPS38B | chrXII | 673486 | + | 3UTR |
| YOR122C | PFY1 | chrXV | 552259 | - | 3UTR |
| YHL001W | RPL14B | chrVIII | 105176 | + | 3UTR |
| YNL209W | SSB2 | chrXIV | 253948 | + | 3UTR |
| YEL046C | GLY1 | chrV | 67230 | - | 3UTR |
| YAR002C-A | ERP1 | chrI | 154020 | - | 3UTR |
| YNL135C | FPR1 | chrXIV | 371782 | - | 3UTR |
| YNL096C | RPS7B | chrXIV | 443312 | - | 3UTR |
| YKL182W | FAS1 | chrXI | 106851 | + | 3UTR |
| YNL104C | LEU4 | chrXIV | 424810 | - | 3UTR |
| YLR395C | COX8 | chrXII | 909694 | - | 3UTR |
| YHL011C | PRS3 | chrVIII | 80621 | - | 3UTR |
| YJL159W | HSP150 | chrX | 121868 | + | 3UTR |
| YDR211W | GCD6 | chrIV | 886918 | + | 3UTR |
| YBL028C | YBL028C | chrII | 167396 | - | 3UTR |
| YML001W | YPT7 | chrXIII | 267806 | + | 3UTR |
| YER025W | GCD11 | chrV | 206897 | + | 3UTR |
| YBR078W | ECM33 | chrII | 395191 | + | 3UTR |
| YKL210W | UBA1 | chrXI | 42303 | + | 3UTR |
| YCR004C | YCP4 | chrIII | 119541 | - | 3UTR |
| YJL138C | TIF2 | chrX | 153338 | - | 3UTR |
| YKL054C | DEF1 | chrXI | 336462 | - | 3UTR |
| YLR209C | PNP1 | chrXII | 560770 | - | 3UTR |
| YJL002C | OST1 | chrIV | 38679 | + | 3UTR |
| YKL125W | RRN3 | chrXI | 210188 | + | 3UTR |
| YDR524W | YDR524W | chrIV | 1489324 | - | 5UTR |
| YGR034W | RPL26B | chrVII | 555803 | + | 5UTR |
| YLR342W-A | YLR342W-A | chrXII | 815797 | + | 5UTR |
| YML006C | GIS4 | chrXIII | 258873 | - | 5UTR |
| YJL062W-A | COA3 | chrX | 316720 | + | 5UTR |
| YDL081C | RPP1A | chrIV | 310097 | - | CDS |
| YKL060C | FBA1 | chrXI | 326455 | - | CDS |

| | | | | | |
|---|---|---|---|---|---|
| YHR021C | RPS27B | chrVIII | 148058 | - | CDS |
| YBL087C | RPL23A | chrII | 60127 | - | CDS |
| YOR234C | RPL33B | chrXV | 778687 | - | CDS |
| YER117W | RPL23B | chrV | 397284 | + | CDS |
| YGR034W | RPL26B | chrVII | 556614 | + | CDS |
| YLR075W | RPL10 | chrXII | 283269 | + | CDS |
| YKL056C | TMA19 | chrXI | 334697 | - | CDS |
| YPL143W | RPL33A | chrXVI | 282838 | + | CDS |
| YGL147C | RPL9A | chrVII | 228073 | - | CDS |
| YKL060C | FBA1 | chrXI | 327468 | - | CDS |
| YML063W | RPS1B | chrXIII | 147205 | + | CDS |
| YDR050C | TPI1 | chrIV | 556061 | - | CDS |
| YLL050C | COF1 | chrXII | 39850 | - | CDS |
| YOL086C | ADH1 | chrXV | 159965 | - | CDS |
| YGR209C | TRX2 | chrVII | 913196 | - | CDS |
| YDR050C | TPI1 | chrIV | 556122 | - | CDS |
| YKL060C | FBA1 | chrXI | 326956 | - | CDS |
| YDR050C | TPI1 | chrIV | 556283 | - | CDS |
| YMR242C | RPL20A | chrXIII | 753590 | - | CDS |
| YDL130W | RPP1B | chrIV | 229980 | + | CDS |
| YDR225W | HTA1 | chrIV | 915651 | + | CDS |
| YPL079W | RPL21B | chrXVI | 407383 | + | CDS |
| YLR264W | RPS28B | chrXII | 673178 | + | CDS |
| YMR116C | ASC1 | chrXIII | 500571 | - | CDS |
| YOL086C | ADH1 | chrXV | 160476 | - | CDS |
| YLR155C | ASP3-1 | chrXII | 469375 | - | CDS |
| YHR203C | RPS4B | chrVIII | 504865 | - | CDS |
| YBR118W | TEF2 | chrII | 477756 | + | CDS |
| YIL069C | RPS24B | chrIX | 231818 | - | CDS |
| YGR148C | RPL24B | chrVII | 787413 | - | CDS |
| YHR203C | RPS4B | chrVIII | 504954 | - | CDS |
| YCR012W | PGK1 | chrIII | 138189 | + | CDS |
| YJR145C | RPS4A | chrX | 702777 | - | CDS |
| YDR139C | RUB1 | chrIV | 733916 | - | CDS |
| YCR031C | RPS14A | chrIII | 177778 | - | CDS |
| YGR063C | SPT4 | chrVII | 617665 | - | CDS |
| YMR242C | RPL20A | chrXIII | 753323 | - | CDS |
| YMR242C | RPL20A | chrXIII | 753732 | - | CDS |
| YCL043C | PDI1 | chrIII | 48741 | - | CDS |

| | | | | | |
|---|---|---|---|---|---|
| YER009W | NTF2 | chrV | 172164 | + | CDS |
| YLR044C | PDC1 | chrXII | 233955 | - | CDS |
| YFR031C-A | RPL2A | chrVI | 220998 | - | CDS |
| YML073C | RPL6A | chrXIII | 123610 | - | CDS |
| YDL082W | RPL13A | chrIV | 309054 | + | CDS |
| YJL052W | TDH1 | chrX | 338772 | + | CDS |
| YGL245W | GUS1 | chrVII | 41052 | + | CDS |
| YLR150W | STM1 | chrXII | 441061 | + | CDS |
| YBL002W | HTB2 | chrII | 236876 | + | CDS |
| YLR150W | STM1 | chrXII | 440987 | + | CDS |
| YAR002C-A | ERP1 | chrI | 154502 | - | CDS |
| YDR115W | MRX14 | chrIV | 682373 | + | CDS |
| YNL030W | HHF2 | chrXIV | 576814 | + | CDS |
| YDL055C | PSA1 | chrIV | 356523 | - | CDS |
| YDR134C | CCW22 | chrIV | 721486 | - | CDS |
| YLR048W | RPS0B | chrXII | 242837 | + | CDS |
| YLR179C | protein_coding | chrXII | 514413 | - | CDS |
| YDR115W | MRX14 | chrIV | 682205 | + | CDS |
| YPL225W | protein_coding | chrXVI | 126354 | + | CDS |
| YDL084W | SUB2 | chrIV | 306440 | + | CDS |
| YNL071W | LAT1 | chrXIV | 492888 | + | CDS |
| YKL058W | TOA2 | chrXI | 330199 | + | CDS |
| YPR080W | TEF1 | chrXVI | 701422 | + | CDS |
| YJR143C | PMT4 | chrX | 698471 | - | CDS |
| YPL061W | ALD6 | chrXVI | 433969 | + | CDS |
| YOR254C | SEC63 | chrXV | 805085 | - | CDS |
| YOL139C | CDC33 | chrXV | 60623 | - | CDS |
| YDL072C | YET3 | chrIV | 330084 | - | CDS |
| YMR074C | SDD2 | chrXIII | 413309 | - | CDS |
| YOR187W | TUF1 | chrXV | 685212 | + | CDS |
| YPL225W | protein_coding | chrXVI | 126301 | + | CDS |
| YGL191W | COX13 | chrVII | 144814 | + | CDS |
| YGR106C | VOA1 | chrVII | 699643 | - | CDS |
| YDL185W | VMA1 | chrIV | 129970 | + | CDS |
| YML001W | YPT7 | chrXIII | 267409 | + | CDS |
| YPR074C | TKL1 | chrXVI | 692962 | - | CDS |
| YAL046C | AIM1 | chrI | 57064 | - | CDS |
| YCL033C | MXR2 | chrIII | 63023 | - | CDS |
| YML106W | URA5 | chrXIII | 57156 | + | CDS |

| | | | | | |
|---|---|---|---|---|---|
| YGR159C | NSR1 | chrVII | 806414 | - | CDS |
| YJR139C | HOM6 | chrX | 689725 | - | CDS |
| YMR217W | GUA1 | chrXIII | 703186 | + | CDS |
| YDL116W | NUP84 | chrIV | 253697 | + | CDS |
| YDL143W | CCT4 | chrIV | 201505 | + | CDS |
| Q0105 | COB | chrM | 43479 | + | CDS |
| YNL069C | RPL16B | chrXIV | 494532 | - | intron |
| YLL050C | COF1 | chrXII | 40229 | - | intron |
| YGL030W | RPL30 | chrVII | 439186 | + | Intron |
| YPR132W | RPS23B | chrXVI | 795766 | + | STOP CODON |
| YLL024C | SSA2 | chrXII | 95568 | - | STOP CODON ADJ |
| YPL189C-A | COA2 | chrXVI | 188309 | - | STOP CODON ADJ |

**Table 3** Detection of D sites in mRNAs

# Chapter 2

# Dihydrouridine synthase 2 sustains levels of tRNACys and prevents ferroptosis in lung cancer

**ABSTRACT**

Dihydrouridine is a universally conserved tRNA modification installed by enzymes that are important for human health for reasons that are yet unclear. High expression of dihydrouridine synthase 2 (DUS2) predicts poor patient outcomes in lung adenocarcinoma (Kato et al., 2005). Here, I show in human cells that DUS2 suppresses ferroptosis, a metal-dependent non-apoptotic form of cell death to which many lung cancers are unusually sensitive (Xiong et al., 2021), which is emerging as a therapeutic target in lung cancer. Consistent with a positive role for DUS2 in lung adenocarcinoma growth and metastasis, high expression of DUS2 correlates with increased resistance to ferroptosis inducers. In collaboration with Matthew Wang and Luisa Escobar-Hoyos, I extend these results to a mouse xenograft model of lung adenocarcinoma. Loss of DUS2 causes increased sensitivity with concomitant accumulation of toxic lipid peroxides, a hallmark of ferroptotic cell death. Mechanistically, DUS2 is required to maintain tRNA CysGCA levels and support translation of cysteine-rich proteins including metallothioneins that serve as key regulators of both metal and redox homeostasis. Metallothionein deficiency in DUS2 knockout cells leads to increased susceptibility to zinc intoxication and lower levels of reduced glutathione, which partially explains their sensitivity to ferroptosis. My results reveal a tRNA-specific vulnerability and demonstrate the therapeutic potential of targeting DUS2.

## MAIN

Many cancers display resistance to canonical apoptotic cell death pathways (Hanahan and Weinberg, 2000). Non small cell lung cancers (NSCLC) use a number mechanisms to avoid apoptosis including loss of expression of the pro-apoptotic gene Bcl-2-like protein (BIM) (Ng et al., 2012) and amplification of an anti-apoptotic gene, induced myeloid leukemia cell differentiation protein (MCL1) (Beroukhim et al., 2010). Recently, several novel cell death mechanisms have been described. One of these, ferroptosis, is a form of non-apoptotic cell death that is emerging as a therapeutic target in lung cancer (Bebber et al., 2021).

### DUS2 is overexpressed in lung cancer and loss of DUS2 sensitizes cells to ferroptosis

Hallmarks of ferroptotic cell death include dependence on redox active iron and accumulation of toxic lipid peroxides (Dixon and Stockwell, 2019). Several compounds have been described to induce ferroptosis, including class I ferroptosis inducers that inhibit import of cystine (erastin) and class II ferroptosis inducers which inhibit activity of the phospholipid hydroperoxidase GPX4 ((1*S*,3*R*)-RSL3, M162, and ML210) (Fig. 1a). Several studies have demonstrated that NSCLC cell lines are sensitive to chemical ferroptosis inducers, both in vitro and in vivo (Alvarez et al., 2017; Wohlhieter et al., 2020), and development of ferroptosis modulating drugs is an active area of research (Hadian and Stockwell, 2021). Intriguingly, resistance to treatment with several class II ferroptosis inducers (RSL3, ML162 and ML210) correlates with expression of the tRNA

modifying enzyme dihydrouridine synthase 2 (DUS2) in a panel of 860 cancer cell lines (Basu et al., 2013; Rees et al., 2016; Seashore-Ludlow et al., 2015) (Fig. 1b).

Dihydrouridine synthases (DUS) install a modified form of uridine in RNA (Fig 1c). Dihydrouridine (D) is the most common modified nucleotide in tRNA, and is found in tRNA from organisms from all branches of the tree of life (Xing et al., 2002). In tRNAs, D is thought to stabilize to the correct folding of the D-loop (Dyubankova et al., 2015). Eukaryotes including humans express four D synthases, and each DUS has unique target nucleotides in multiple individual tRNAs (Xing et al., 2004). Disturbance of D levels and/or DUS expression are implicated in lung, brain and kidney cancer (Kato et al., 2005; Kuchino and Borek, 1978). DUS2 is known to modify tRNAs at position 20 in the tRNA D-loop in yeast (Xing et al., 2004). DUS2 is frequently overexpressed in non-small cell lung cancer (NSCLC) tumors (Fig 1d), and NSCLC patients whose tumors express high levels of DUS2 have shorter survival time when compared to patients whose tumors do not express high levels of DUS2 (Kato et al., 2005) (Fig. 1e).

Here, I investigate the role that DUS2 plays in NSCLC disease progression. Using CRISPR/Cas9, I knock out DUS2 in a NSCLC cell line (A549) that expresses high levels of DUS2 (Kato et al., 2005) and show that loss of DUS2 leads to hypersensitivity to ferroptosis inducing compounds. Consistent with the in vitro sensitivity of the DUS2 KOs to ferroptosis, Matthew Wang and I show that DUS2 KO cells form smaller tumors in a mouse xenograft model and are more sensitive to systemic administration of a ferroptosis inducer. I probe the role of DUS2 in gene expression and find that loss of

DUS2 causes a ~40% decrease in the level of a single tRNA, CysGCA. This loss of tRNACysGCA reduces levels of cysteine rich proteins proteome wide, including decreasing synthesis of a family of small, highly conserved cysteine rich proteins called metallothioneins (MTs). MTs are known to inhibit ferroptosis(Sun et al., 2016), and play two critical roles in cells: first, MTs directly inhibit the formation of lipid peroxides (Hurnanen et al., 1997; Miura et al., 1997) and defend the cell against oxidative stress (Thornalley and Vašák, 1985). Second, MTs are major regulators of intracellular zinc levels (Krężel and Maret, 2017; Sutherland et al., 2012; Vallee, 1995). My results establish the loss of MT expression as the likely basis for increased ferroptosis in the absence of DUS2 and suggest therapeutic potential for targeting DUS2 in lung cancer.

To investigate the link between high DUS2 expression and poor patient prognosis in NSCLC, I used CRISPR/Cas9 to generate knockout (KO) cell lines in a common NSCLC model cell line (A549) that expresses high levels of DUS2 (Kato et al., 2005). Using two different lentiviral delivered guide RNAs targeting exons 3 and 4 of the DUS2 coding sequence, I recovered multiple independent clonal KO cell lines. As expected, the clonal DUS2 KO CRISPR lines did not have detectable DUS2 protein expression (Fig. 1f).

The correlation between DUS2 mRNA levels and resistance to known ferroptosis inducing compounds across a panel of 860 cell lines prompted me to test the sensitivity of DUS2 KO cells to ferroptosis. The DUS2 KO cells showed an approximately 2-fold increase in the fraction of dead cells after ferroptosis induction with the GPX4 inhibitor

RSL3 (Fig 1g). This sensitivity was reversed upon re-expression of DUS2 (Fig S1a), or by treatment with known ferroptosis inhibitors, trolox and ferrostatin (Fig S1a), but not by treatment with Z-FAD-FMK, an apoptosis inhibitor (Fig S1a). A key feature of ferroptotic cell death is a buildup of toxic lipid peroxides (Wiernicki et al., 2020). I measured the levels of lipid peroxidation after GPX4 inhibitor treatment using an oxidation-sensitive fluorescent lipid peroxidation probe, C11-BODIPY (Drummen et al., 2002). When compared to WT A549 cells, the DUS2 KO cells had 6-8 fold higher levels of lipid peroxides when treated with RSL3 (Fig 1h, 1i), or a second GPX4 inhibitor, ML162 (Fig S1b). Consistent with the higher levels of lipid peroxidation in the DUS2 KO cells, using a probe for cellular reactive oxygen species (ROS), 2',7'-dichlorodihydrofluorescein diacetate ($H_2$DCFDA), I observed higher cellular ROS levels in the DUS2 KOs when treated with RSL3 (Fig S1c).

**DUS2 is required to sustain levels of a specific tRNA, tRNACysGCA**

As DUS2 is known to modify tRNAs at position 20 in the tRNA D-loop in yeast (Xing et al., 2004)(Fig 2a), and D is known to stabilize tRNA folding (Alexandrov et al., 2006; Dyubankova et al., 2015) I next investigated if DUS2 is required to sustain tRNA expression or function in NSCLC cells. I performed tRNA sequencing using a combination of the ARM-seq and DM-TIGRT-seq protocols (Cozen et al., 2015; Zheng et al., 2015). The DUS2 KO cells showed no significant change in charging fraction of any tRNA (Table S1). As a positive control I detected a ~70% reduction of tRNAGln charging after starving cells of glutamine (Fig. 2b). Notably, both DUS2 KO cell lines showed a reproducible decrease in expression of nearly every tRNACysGCA

isodecoder expressed in A549 cells (Fig. 2c, 2d, Table S2). When tRNACysGCA levels are summed across all isodecoders, the DUS2 KO cells have a ~40% decrease in the total pool of tRNACysGCA (Fig S2a, Table S2).

I next re-analyzed small RNA seq data from TCGA lung adenocarcinoma (LUAD) samples for tRNA expression (Network et al., 2013). For tRNACysGCA, I found statistically significant increased levels in patient tumor samples as compared to non tumor samples (Fig. 2e). Levels of another U20 containing tRNA (tRNAGlnCTG) were not significantly different in tumor samples (Fig. 2e). Together, these results show that DUS2 is required to sustain levels of a specific tRNA, tRNACysGCA, in NSCLC cells and suggest a role for tRNACysGCA levels in lung cancer disease.

**Loss of DUS2 impairs translation of cysteine rich proteins, including known anti-ferroptotic oncoproteins**

To determine if the ~40% decrease in tRNACysGCA expression in the DUS2 KO cells has a functional impact on translation, I measured cysteine codon translation using luciferase reporters. An array of 15 cysteine codons was prepended to a P2A sequence followed by firefly luciferase as a proxy for production of the cysteine repeat peptide, with an IRES driven renilla luciferase as a normalization control (Fig. 3a). Because cysteine is encoded by two independent codons (UGU and UGC) that are decoded by the same pool of GCA anticodon tRNA, I generated versions of the cysteine repeat reporter with either UGU or UGC codons. When transfected into the DUS2 KO cells, these reporters showed a ~40% decrease in the ratio of firefly luciferase produced to renilla luciferase produced (Fig. 3b). This loss of efficient cysteine translation was

partially rescued by transfection of in vitro transcribed tRNACysGCA into the DUS2 KO cells (Fig. 3c). The observed cysteine translation defects did not affect bulk protein synthesis as determined by $^{35}S$ methionine incorporation (Fig. S3a).

I then used SILAC proteomics to measure changes in the levels of endogenous proteins in DUS2 KO cells. When analyzed by amino acid content, proteins with greater than 5% Cys content showed a significant decrease in abundance (Fig. 3d) consistent with deficient translation of cysteine codons in cells lacking DUS2. Due to the inherently limited coverage of shotgun proteomics and the fact that many cysteine rich proteins are secreted, the SILAC experiment detected only relatively abundant proteins with moderate cysteine content (Table S3). I did not observe any peptides corresponding to many cysteine rich proteins, including any of the metallothioneins. Metallothioneins (MTs) are a class of very cysteine rich proteins (~35% cysteine content) that have been linked to ferroptosis and cancer progression (Ryu et al., 2012; Sun et al., 2016). I therefore measured metallothionein translation in DUS2 KO cells using a dual luciferase reporter similar to the cysteine codon repeat reporter by replacing the arrays of cysteine codons with the coding sequences of MT 1A or MT 1G (Fig. 3e). Production of metallothionein proteins was impaired in the DUS 2 KO cells (Figs. 3g and 3h), demonstrating that loss of DUS2 activity leads to defects in production of an endogenously expressed cysteine rich oncoprotein known to inhibit ferroptosis and lipid peroxidation (Orct et al., 2015; Sun et al., 2016).

In parallel I measured steady state mRNA levels in the DUS2 KO cells by RNA seq. Among the hundreds of mRNAs that were differentially expressed in the DUS2 KO cells (Fig. S3b, Table S4), I noticed that mRNAs encoding cysteine rich proteins were decreased in the DUS2 KO cells (Fig. S3b). Slow translation elongation has been shown to trigger mRNA degradation downstream of surveillance by the ribosome quality control (RQC) pathway (Hickey et al., 2020; Juszkiewicz et al., 2018). I hypothesized that reduced tRNACysGCA levels, which impair cysteine translation in DUS2 KO cells, cause ribosomes to stall more frequently on cysteine codons, leading to RQC mediated degradation of cysteine rich mRNAs. Supporting this hypothesis, metallothionein mRNAs were decreased in abundance in the DUS2 KO cells and partially restored by knocking down the RQC factor GIGYF2 (Fig. S3c).

Metallothioneins utilize their high thiol content to play two interrelated roles in cells: first, through direct coordination of $Zn^{2+}$ and $Cu^{2+}$ ions, they are key regulators of cellular zinc and copper levels. Although ferroptosis was initially characterized as an iron-dependent form of cell death (Dixon et al., 2012), more recent studies show that defects in zinc homeostasis which elevate cytosolic zinc concentrations sensitize cells to ferroptosis (Chen et al., 2021). Given the established role of metallothioneins in regulating intracellular zinc levels(Krężel and Maret, 2017; Vallee, 1995), I explored the role of zinc in the ferroptosis sensitivity of cells lacking DUS2. DUS2 KO cells are more sensitive to $Zn^{2+}$ intoxication and $Zn^{2+}$-induced cell death (Fig. 3g). The second function of the MTs is to defend the cell from oxidative stress and directly inhibit the accumulation of lipid peroxides, which is a hallmark of ferroptosis (Orct et al., 2015; Schwarz et al., 1994; You et al., 2002). I hypothesized that because of the decreased MT levels in the DUS2

KOs there would be an increased demand for GPX4 mediated reduction of lipid peroxides, and lower cellular levels of reduced glutathione (GSH). Supporting this hypothesis, I found significantly lower GSH levels in the DUS2 KO cells (Fig. 3h). Together, these observations suggest that a major cause of ferroptosis sensitivity in the DUS2 KO cells is loss of MT synthesis, which in turn triggers defects in metal and redox homeostasis (Fig. 3i).

**Combined loss of DUS2 and ferroptosis induction extends lifespan in a mouse xenograft NSCLC model**

To characterize the impact of DUS2 on tumor growth and progression *in vivo*, Matthew Wang subcutaneously injected either A549 or DUS2 KO cells to develop xenograft tumors in nude mice. After injection, Matthew and I monitored tumor size and mouse survival. The tumors derived from DUS2 KO cells took 33% longer to establish and were notably smaller than tumors from A549 cells (Fig. 4a, 4b). Examining the DUS2 WT and KO tumors revealed modestly increased expression of the ferroptosis biomarker PTSG2 in the DUS2 KO tumors, suggesting endogenous induction of ferroptosis in the tumors (Fig. 4c) Ferroptosis inducers are a promising therapeutic approach for the treatment of some cancers (Hadian and Stockwell, 2021). My in vitro experiments indicate that ferroptosis induction might be a more effective strategy to treat NSCLC in combination with inhibition of DUS2. To determine if the ferroptosis sensitivity of the DUS2 KO cells could be exploited for therapeutic benefit, Matthew Wang induced ferroptosis in mice with established tumors by administration of a GPX4 inhibitor (Fig. 4d). Most GPX4 inhibitors (RSL3, ML162, ML210) suffer from poor

pharmacological properties and have limited utility in vivo. However, a new class of GPX4 inhibitors with improved physiochemical and pharmacokinetic properties was recently developed (Eaton et al., 2020, 2019). I first tested if oral administration of one of these compounds (JKE-1674) could induce ferroptosis in mouse lungs by measuring mRNA levels of a marker of ferroptosis, PTSG2 (Yang et al., 2014) after oral JKE-1674 administration. JKE-1674 induced PTSG2 mRNA in lung tissue approximately 8.5-fold (Fig. 4e), similar to the level of induction by other GPX4 inhibitors (Yang et al., 2014). Treatment with JKE-1674 induced PTSG2 expression 3-fold in DUS2 KO tumors (Fig. 4f). JKE-1674 treatment did not noticeably alter mouse weight (Fig. S4a), or normalized tumor volume (Fig. S4b). However, median survival of mice receiving JKE-1647 was significantly shorter than mice receiving vehicle (Fig S4c). Among the mice receiving JKE, mice with DUS2 KO tumors had significantly increased lifespan (Fig. 4g). Together, these data indicate that either inhibition of DUS2 or combinatorial inhibition of DUS2 and induction of ferroptosis could be a promising therapeutic strategy for treatment of NSCLC patients.

**DISCUSSION**

My data indicate that high expression of a ubiquitous tRNA modifying enzyme is a specific cancer vulnerability in NSCLC cells. DUS2 is frequently over expressed in NSCLC, and patients whose tumors express high levels of DUS2 have worse outcomes(Kato et al., 2005). Using NSCLC cells depleted for DUS2, I demonstrate that DUS2 is required to support the levels of a specific family of tRNAs, tRNA CysGCA. This result highlights the outsized roles that specific tRNA substrates can play in the

biological functions of tRNA modifying enzymes (Delaunay et al., 2022; Ignatova et al., 2020, p. 6; Orellana et al., 2021; Passarelli et al., 2022). Loss of CysGCA expression in DUS2 KO cells leads to defects in translation of cysteine codons, which reduces steady state levels of many cysteine rich proteins, including metallothioneins that play key roles in regulating cellular zinc levels and responding to oxidative stress (Hurnanen et al., 1997; Sun et al., 2016; Vallee, 1995). Loss of metallothionein expression in DUS2 KO cells sensitizes the cells to ferroptosis both in vitro and in vivo.

Consistent with a role for DUS2 and tRNACysGCA in NSCLC disease severity and ferroptosis, alterations to cellular cysteine metabolism support extreme proliferation and resistance to ferroptosis in many cancers. Cancer cell lines frequently express very high levels of the cystine/glutamate antiporter xCT, and depletion of xCT triggers ferroptosis in cancer models (Badgley et al., 2020; Daher et al., 2019). Cysteine regulates ferroptosis in part through the synthesis of GSH, a critical cofactor for the lipid peroxide-detoxifying enzyme GPX4. Accordingly, knockdown of the cysteine aminoacyl tRNA synthetase (CARS) protects cells against cysteine deprivation-induced ferroptosis by inducing the transsulfuration pathway to produce more cysteine and promote GSH synthesis (Hayano et al., 2016) My results add a new layer to this model: to fend off ferroptosis, lung cancer cells require both cysteine incorporation into GSH and into cysteine rich metallothionein proteins. Inhibiting either DUS2 or the MT family could increase ferroptosis sensitivity in patients and hold therapeutic value.

## Methods

### Cell culture

A549 cells were maintained in a 50:50 mixture of DMEM:F12 medium (Gibco), supplemented with 1x penicillin/streptomycin (Gibco) and 10% FBS (Sigma). Cells were grown at 37°C with 5% CO2 and maintained at subconfluency.

### CRISPR knockout generation

DUS2 CRISPR knockout A549 cells were generated using a single-guide LentiCRISPRv2
strategy to cause deletions in the third and fourth exons of DUS2. Oligos for each guide RNA were phosphorylated and annealed and then cloned into pLentiGuide-Puro (Addgene) digested with BsmBI. Cas9/guideRNA lentiviruses were generated by transfection of pLentiGuide-Puro, psPAX2 (Addgene), and pdr8.2 (Addgene) into 293T cells. Viral supernatant was harvested, filtered and flash frozen 48 and 96 hours post transfection. For infection, 1mL of 48hr viral supernatant was placed in a 6-well dish with A549 cells at 50% confluency. At 90% confluency, the A549 cells were split in to a 10cm dish and selected for stable integrations using 1ug/mL puromycin (Sigma). After a stable puro resistant population was generated, single clones were isolated using serial

dilution and colony picking. Single cell clones were expanded, screened for lack of expression of DUS2 protein, and frozen.

**Western Blotting**

Whole cell lysates were made by pelleting A549 cells and re-suspending fresh or frozen (-80°C) pellets in RIPA buffer (50mM Tris pH 8, 150 mM NaCl, sodium deoxycholate 0.5%, sodium dodecyl sulfate 0.1%, NP-40 1%), lysed on ice for 10 min with vortexing. Lysates were clarified by centrifugation at 4°C and maximum speed (22,500 x g) for 15 min. Approximately 20ug of whole cell lysate, as determined by BCA assay, was run on a 7% Tris-Acetate Gel and transferred to nitrocellulose membranes using wet transfer. Membranes were blocked in 5% milk for 1 hour and incubated with primary antibodies overnight at 4C in 5% milk low-salt TBST (50 mM Tris pH 7.5 150 mM NaCl 0.1% Tween-20). Antibodies used for Western blot were as follows: anti-DUS2 at 1:10,000, anti-GAPDH at 1:10,000 (Sigma-Aldrich
G9545). Secondary antibody incubation was for 1 hour at room temperature using HRP conjugated goat anti-rabbit IgG at 1:3000 (Promega W4011). Washes were with high-salt TBST (50 mM Tris pH 7.5 400 mM NaCl 0.1% Tween-20)

**AlkB and AlkB D135S purification**

pET30a-AlkB and pET30a-AlkB(D135S) (Addgene) were transformed into BL21(DE3) (NEB). 1L cultures were grown to OD .55, at 37°C with shaking. IPTG (Gold Bio) and $FeSO_4$ (Sigma) were added to 1mM and 10uM final concentration. Cultures were induced for 4h at 37°C with shaking, cells were harvested with centrifugation and flash

frozen. Each 1L pellet was resuspended in 20mL fresh AlkB lysis buffer (50 mM HEPES pH8.0, 10mM Fe(II) sulfate, 300mM NaCl and 5mM imidazole). Cells were lysed by sonication and addition of lysozyme (Sigma). Lysates were clarified with a 12,000 x g spin for 30min at 4°C. Lysates were filtered through a 0.2uM filter and loaded onto a HisTrap 5mL nickel column (Cytiva). Unbound protein and RNA were removed with extensive washing with lysis buffer, and crude alkB protein was eluted from the Ni column using AlkB Lysis buffer with 250mM imidazole. AlkB protein containing fractions were pooled and desalted using a Zeba spin desalting column (Thermo). Desalted protein was purified away from bound RNA using a MonoS column (Cytiva) with a 100mM-1M NaCl gradient. AlkB protein containing fractions were pooled and concentrated using Amicon Ultra-15 10KMWCO filters (Milipore). Concentrated AlkB protein was fractionated over a HiLoad 16/60 Superdex S200 column (Cytiva). S200 fractions containing AlkB were again concentrated using Amicon Ultra-15 10KMWCO filters (Milipore), diluted to 50% glycerol, and flash frozen.

**Total RNA Isolation**

A549 cells were harvested by pelleting and resuspending fresh or frozen (-80°C) pellets in 1mL of QIAzol (Qiagen). Total RNA was harvested according to the manufacturer's protocol.

**tRNA sequencing**

Total RNA from A549 cells was resuspended in 100mM NaOAc/HOAc pH 4.8. 3μL 1M NaIO4 (50mM FC) was added and the mixture was incubated at 22°C. After 30 minutes,

6.65µL 1M glucose was added. Total RNA was then recovered by EtOH precipitation. Briefly, 10µL 3M NaOAc, 1mL EtOH were added, incubated at -20°C for 15min, and then spun at 4°C and maximum speed (22,500 x g) for 30 min. The RNA pellet was washed with 70% EtOH and spund again for 5min. The pellet was resuspended in 50µL of Na Borate pH 9.5 and incubated at 45°C for 90 minutes. Large RNAs were depleted from the total RNA with Qiagen miRNeasy spin colums using manufactures recommendations. Small RNAs were demethylated with AlkB and AlkB D135S in AlkB buffer (50 mM HEPES KOH, pH 8, 75 µM ferrous ammonium sulfate pH 5, 1 mM α-ketoglutarate, 2 mM sodium ascorbate, 50 µg/ml BSA) with with 4× molar ratio of wtAlkB and 4× molar ratio of D135S at 37°C for 100 minutes. RNA was recovered with denaturing SILANE bead cleanup. RNA was then 3′ end healed using T4 PNK (NEB) and CIP (NEB), and recovered again with denaturing SILANE bead cleanup. A 3′ adapter was ligated onto the small RNA using T4Rnl2. 5µL of RNA was incubated with 1.5µL DMSO and 0.5µL 80uM preadenylated 3′ adapter. This mixture was incubated at 65°C for 2min, and placed on ice for 1min. ligations were incubated overnight at 16°C with 3.5µL water, 2µL 10X NEB ligase buffer, 5µL 50% PEG 8000, 1µL SUPERASIN (Thermo), and 2µL RNA ligase (NEB). RNA was recovered again with denaturing SILANE bead cleanup. RNA was reverse transcribed using superscript III. 8µL of RNA was annealed to RT primer at 65°C for 5 min, and 10 min cooling to RT on benchtop. RT was performed following manufacturer's instructions. RNA was removed from cDNA by adding 1µL 1M NaOH to the RT reaction, incubating 5m 95°C and adding 1µL 1M HCl. cDNA was recovered with denaturing SILANE bead cleanup. A 5′ linker was ligated to the cDNA using T4 RNA ligase. cDNA was mixed with .8µL 80uM 5′ adapter,

and 1μL DMSO. This mixture was incubated at 75°C for 2min and placed on ice for 1min. to this was added 4.6μL water, 2μL 10X NEB RNA ligase buffer, 0.2μL 0.1M ATP, 5μL 50% PEG 8000, and 2μL RNA ligase. This mixture was incubated at RT overnight with shaking. Linker ligated cDNA was recovered with denaturing SILANE bead cleanup. Final library PCR was performed with Phusion DNA polymerase according to manufacturer's recommendation.

**tRNA rescue experiment**

T7 template DNA was constructed using PCR to fuse the T7 promoter sequence to the tRNA CysGCA sequence with CCA tail added. tRNA CysGCA RNA was prepared by run off transcription with T7 RNAP at 37°C for 8 hours followed by template removal with DNAseI (Ambion) at 37°C for 30 minutes. Full length tRNA CysGCA was purified on an 8% denaturing urea-PAGE gel, eluted overnight, precipitated with ethanol, and resuspended water. For rescue experiments, 2μg tRNACysGCA and 2μg translational reporter plasmid were co-transfected into cells using TransIT-X2 (Mirus). 48 hours after transfection, cells were harvested in 500 μL 1X passive lysis buffer (Promega) and flash frozen. Lysates were freeze thawed 2x and 75μL of lysate was used to measure firefly and renilla luciferase activity with the dual-luciferase reporter assay system (Promega) according to manufacturer's instructions.

**DUS2 rescue experiment**

Full length DUS2 was cloned into pcDNA3.1 (CMV promoter, C-terminal FLAG tag) and 2μg of DUS2 plasmid was transfected into cells using TransIT-X2 (Mirus). 48 hours after

transfection, cells were split into 6 well plates and allowed to recover for 24 hours. At 40-50% confluency, cells were treated with indicated concentrations of ferroptosis inducing compounds for 12 hours. Cells then stained with Annexin/PI as below.

**tRNAseq data analysis**

Demultiplexed reads were adapter trimmed using BBTools(Bushnell, n.d.; Bushnell et al., 2017) bbduk.sh. Adapter trimmed reads were then PCR-duplicate collapsed based on unique molecular identifier (UMI) using dedupe.sh. The UMI was then force trimmed with a second round of trimming. Adapter trimmed and duplicate collapsed reads were then aligned to a single copy of each isodecoder pseudo-genome using bbmap.sh. tRNA expression was quantified by counting the number of uniquely mapping reads that mapped to a tRNA, and differential expression analysis was performed using limma-voom(Ritchie et al., 2015). tRNAs with less than 100 uniquely mapping reads were not considered during expression analysis. tRNA charging ratio was determined using custom python scripts ratioing the number of reads terminating with CC-3′ or CCA-3′ .

**$^{35}$S Met total protein synthesis**

Equal amounts of DUS2 KO and wt cells were seeded into 6 well plates. Cells were allowed to grow to ~80% confluency, and media was switched to DMEM -Met for 20m. 10µL 100uCi/mL $^{35}$S Met was added to each well, and incubated at 37°C for 30m. To harvest, cells were washed in 1X PBS 2x, and harvested in 200µL RIPA with 1x PMSF and 1x cOmplete. Lysates were freeze thawed 2x, and spun at 4°C at 22,500 x g for 15min to pellet cellular debris. Equal amounts of whole cell lysate, as determined by

BCA assay were loaded on a 4-20% SDS-PAGE gel, dried for 2hrs and exposed overnight on a storage phosphor screen.

**Dual luciferase assay**

pCMV:codonarray:P2A:Fluc:IRES:Rluc or pCMV:metallothionein:P2A:Fluc:IRES:Rluc constructs were constructed by gibson assembly into pTwist CMV Hygro, and successful assembly was confirmed by sanger sequencing. 2µg of each plasmid was transfected into cells using TransIT-X2 (Mirus). 48 hours after transfection, cells were harvested in 1X passive lysis buffer (Promega), and flash frozen. Lysates were freeze thawed 2x, and then 75µL of lysate was used to measure firefly and renilla luciferase activity with the dual-luciferase reporter assay system (Promega) according to manufacturer's instructions.

**SILAC proteomics**

The SILAC experiment was configured as a two channel experiment: Cells were grown in either 1:1 DMEM:F12 with dialyzed FBS (Gibco) supplemented with either un-labeled Arg and Lys (Invitrogen) or $^{13}C_6$ ,$^{15}N_4$ Arg and $^{13}C_6$ ,$^{15}N_2$ Lys (Invitrogen). Cells were maintained in isotopically labeled medium for 10 doublings, and then were harvested in RIPA supplemented with 1mM PMSF and 1X HALT phosphatase/protease cocktail (Pierce). Lysates were clarified at 4C and 22,500 x g for 10 minutes. Total protein was quantified using a BCA assay, and 120µg total protein was submitted to the Yale MS & Proteomics Resource where they were processed and analyzed. Total protein samples were filtered through a 3-kDa Amicon Ultra filter, and the retentate was SpeedVac dried

and used for downstream proteomics preparation. Dried protein pellets were reduced with DTT, alkylated with iodoacetamide, enzymatically digested with trypsin, and desalted using C18 RP microspin column. High-resolution liquid chromatography mass spectrometry MS/MS data were collected on an Orbitrap Fusion mass spectrometer coupled to a NanoACQUITY UPLC. All MS/MS samples were analyzed using Mascot (Matrix Science, Mascot version 2.7.0) For peptide identification, Mascot was set up to search SwissProt assuming the digestion enzyme trypsin. Mascot was searched with a fragment ion mass tolerance of 0.020 Da and a parent ion tolerance of 10.0 PPM. Scaffold (version 4.11.1, Proteome Software)) was used to validate MS/MS based peptide and protein identifications. Peptide identifications were accepted if they could be established at greater than 95.0% probability by the Scaffold Local FDR algorithm. Protein identifications were accepted if they could be established at greater than 99.0% probability and contained at least 2 identified peptides. Protein probabilities were assigned by the Protein Prophet algorithm(Nesvizhskii et al., 2003)

**RNAseq**

Total RNA was isolated for three replicates of A549 and both DUS2 KO cell lines as described above. Stranded poly(A)+ selected mRNA-seq libraries were prepared by Genewiz and sequenced on a HiSeq X 10 with paired end 150-bp reads.

**qRT-PCR**

Total RNA was isolated as described above. For siRNA knockdown experiments, cells were seeded into 6-well plates, and transfected with siGIGFY2 or siNT siRNAs using

TransIT-X2 (Mirus) for 48hours. Total RNA was DNAse treated using TURBO DNAse (Thermo) according to manufacture instructions. One-step qRT-PCR was performed with gene specific forward and reverse primers using Luna Universal One-Step RT-qPCR (NEB) reagents on a CFX96 Real-Time PCR instrument (Bio-Rad). Fold change was calculated using the Pfaffl method(Pfaffl, 2001), with GAPDH as the housekeeping gene. For qPCR experiments from tissues and tumors, cells were disassociated, pelleted and resuspended in TRIzol (Invitrogen). RNA was then extracted following manufacturer's instructions.

**Cell death measurements by Annexin V/Propidium Iodide Staining**

Cells were counted and seeded into 6-well plates (Corning). At 40-50% confluency, cells were treated with ferroptosis inducing or inhibiting compounds (RSL3, Cayman Chemical, ML162 Cayman Chemical, Trolox, Sigma, ZVAD-FMK, Promega, $ZnCl_2$, Sigma)for 12 hours. Cells were harvested by trypsinization and centrifugation, washed once with 1X Hanks Buffered Salt Solution (HBSS), and resuspended in 1X annexin-binding buffer (Thermo) and stained with Annexin V/Propidium Iodide according to manufacturer's instructions. Cells were filtered through 70 micron filters and analyzed on a BD LSR II FACS analyzer using FITC and Propidium Iodide filter sets.

**Quantification of lipid oxidation using C11-BODIPY staining**

Cells were counted and seeded into 6-well plates (Corning). At 40-50% confluency, cells were treated with indicated concentration of ferroptosis inducing compound for 12 hours followed by treatment with 1uM C11-BODIPY for 30 minutes. Cells were then

harvested by trypsinization and centrifugation, washed once with 1X HBSS, and resuspended in 1X Dulbecco's phosphate-buffered saline (DPBS). Cells were filtered through 70 micron filters and analyzed on a BD LSR II FACS analyzer using FITC (reduced C11-BODIPY) or PE (oxidized C11-BODIPY) filter sets.

**Cellular Glutathione Concentration Measurements**

Cells were seeded into black 96 well cell culture treated plates (Corning). At 80% confluency, media was removed and cells were washed once with 1X DPBS. Glutathione levels were measured using GSH-Glo reagents (Promega) according to manufacturer instructions.

**Subcutaneous Mouse Xenografts**

All animal protocols were reviewed by the Yale University IACUC and approved under protocol 2020-20303. A549 and A549 DUS2 KO cells were washed with and resuspended in 1X PBS and combined 1:1 with Matrigel (Corning) to a concentration of 5,000,000 cells per mL. Mice were randomized before injection. 500,000 A549 cells (100 µL) were subcutaneously injected into both flanks of six female nude mice. 500,000 A549 DUS2 KO cells (100 µL) were subcutaneously injected into both flanks of six female nude mice. Mice were anesthetized with isoflurane twice weekly, during which time mice were weighed and tumor volumes were measured. Tumors were measured in two dimensions with calipers and tumor volumes were calculated with the formula $Volume = 0.5 \times L_1 \times {L_2}^2$, where $L_1 > L_2$.

Each mouse began dosing once either tumor was at least 5 mm long in at least one dimension. Mice within each group were randomized before dosing. Mice were given 10 mg/mL JKE-1674 (MedChemExpress) (10% 100 mg/mL JKE-1674 dissolved in DMSO, 90% 20%-β-cyclodextran in 1X PBS) to a concentration of 50 mg JKE-1674 per kg body weight, or vehicle solution (10% DMSO, 90% 20%-β-cyclodextran in 1X PBS) by oral gavage. Three of the six mice injected with only A549 or A549 DUS2 KO cells were dosed with JKE-1674, and the remaining mice were dosed with vehicle solution. Mice were dosed twice weekly. Survival endpoints were defined by death (either naturally or as required by veterinary technicians based on the health of each mouse), a 15% decrease in body weight, or a tumor reaching 2 cm in length in any dimension.

## Figures

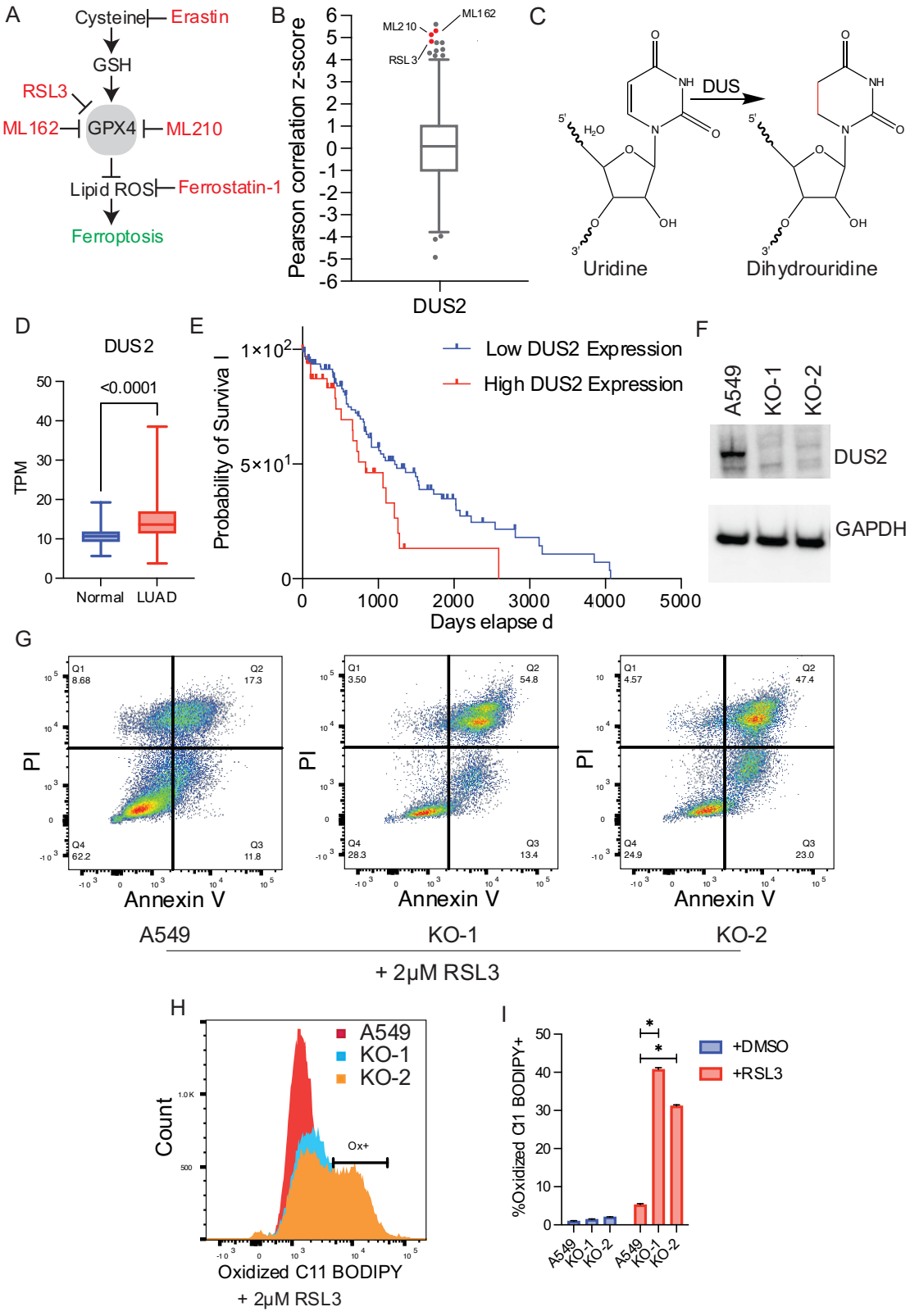
A
Cysteine
Erastin
GSH
RSL3
ML162
GPX4
ML210
Lipid ROS
Ferrostatin-1
Ferroptosis
B
Pearson correlation z-score
ML210
ML162
RSL3
DUS2
C
DUS
Uridine
Dihydrouridine
D
DUS2
<0.0001
TPM
Normal
LUAD
E
Probability of Survival
Low DUS2 Expression
High DUS2 Expression
Days elapsed
F
A549
KO-1
KO-2
DUS2
GAPDH
G
PI
Annexin V
Q1 8.68
Q2 17.3
Q4 62.2
Q3 11.8
Q1 3.50
Q2 54.8
Q4 28.3
Q3 13.4
Q1 4.57
Q2 47.4
Q4 24.9
Q3 23.0
A549
KO-1
KO-2
+ 2μM RSL3
H
Count
A549
KO-1
KO-2
Ox+
Oxidized C11 BODIPY
+ 2μM RSL3
I
%Oxidized C11 BODIPY+
+DMSO
+RSL3
A549
KO-1
KO-2

**Figure 1: DUS2 is overexpressed in lung cancer and loss of DUS2 sensitizes cells to ferroptosis**

a) Schematic of key regulators and chemical effectors of ferroptosis.
b) High DUS2 mRNA expression correlates with resistance to chemical ferroptosis inducers in a panel of 860 cancer cell lines.
c) DUS enzymes convert uridine to dihydrouridine.
d) DUS2 RNA levels are significantly higher in lung adenocarcinoma (LUAD) tumor samples compared to normal tissue (two tailed Mann-Whitney U test, CysGCA $p<.0001$).
e) High DUS2 expression predicts worse outcomes for NSCLC patients.
f) DUS2 protein expression is absent in clonal A549 DUS2 KO cells.
g) Increased cell death (Annexin V+/PI+ cells) in DUS2 KOs compared to WT A549 following treatment with 2μM RSL-3.
h) Elevated lipid ROS (C11-BODIPY staining) in DUS2 KOs compared to WT A549 following treatment with 2μM RSL3.
i) Quantification of Fig. 1h (two tailed t-test, * $p<.0001$)

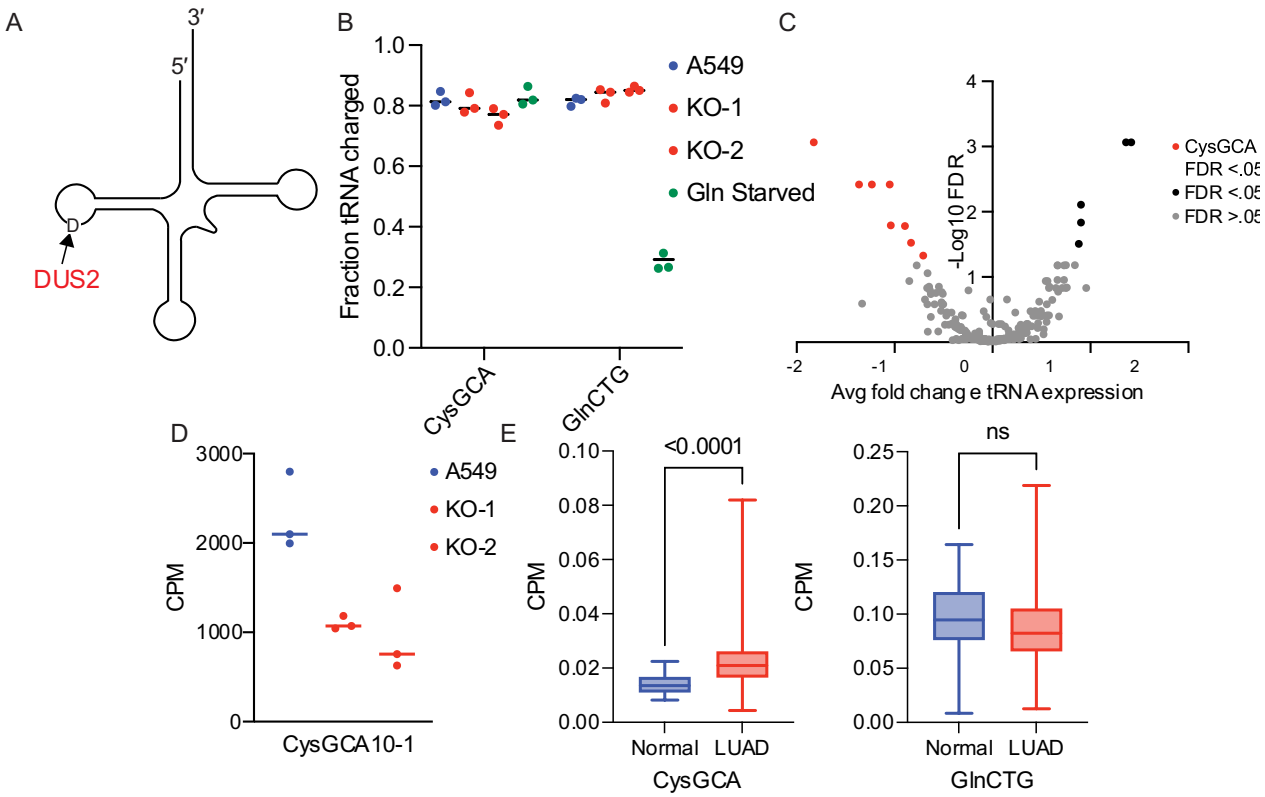
A
3′
5′
D
DUS2
B
Fraction tRNA charged
1.0
0.8
0.6
0.4
0.2
0.0
A549
KO-1
KO-2
Gln Starved
CysGCA
GlnCTG
C
-Log10 FDR
4
3
2
1
-2
-1
0
1
2
Avg fold chang e tRNA expression
CysGCA
FDR <.05
FDR <.05
FDR >.05
D
CPM
3000
2000
1000
0
A549
KO-1
KO-2
CysGCA10-1
E
CPM
0.10
0.08
0.06
0.04
0.02
0.00
<0.0001
Normal
LUAD
CysGCA
CPM
0.25
0.20
0.15
0.10
0.05
0.00
ns
Normal
LUAD
GlnCTG

**Figure 2: DUS2 is required to sustain levels of a specific tRNA, tRNACysGCA**

a) DUS2 targets position U20 in tRNA.

b) Quantification of tRNA charging levels in DUS2 WT and KO cells. tRNA charging is unaffected by loss of DUS2, whereas Gln starvation reduces tRNAGln charging levels >50%.

c) Changes in tRNA levels in DUS2 KO cells, black dots (FDR< 0.05), grey (FDR >0.05), red (tRNACysGCA with FDR< .05).

d) Example isodecoder tRNACysGCA10-1 shows ~50% lower expression in DUS2 KOs.

e) Analysis of tRNA levels in TCGA LUAD data. tRNACysGCA but not tRNAGlnCTG levels are significantly higher in tumors compared to normal tissue (two tailed Mann-Whitney U test, CysGCA p<.0001).

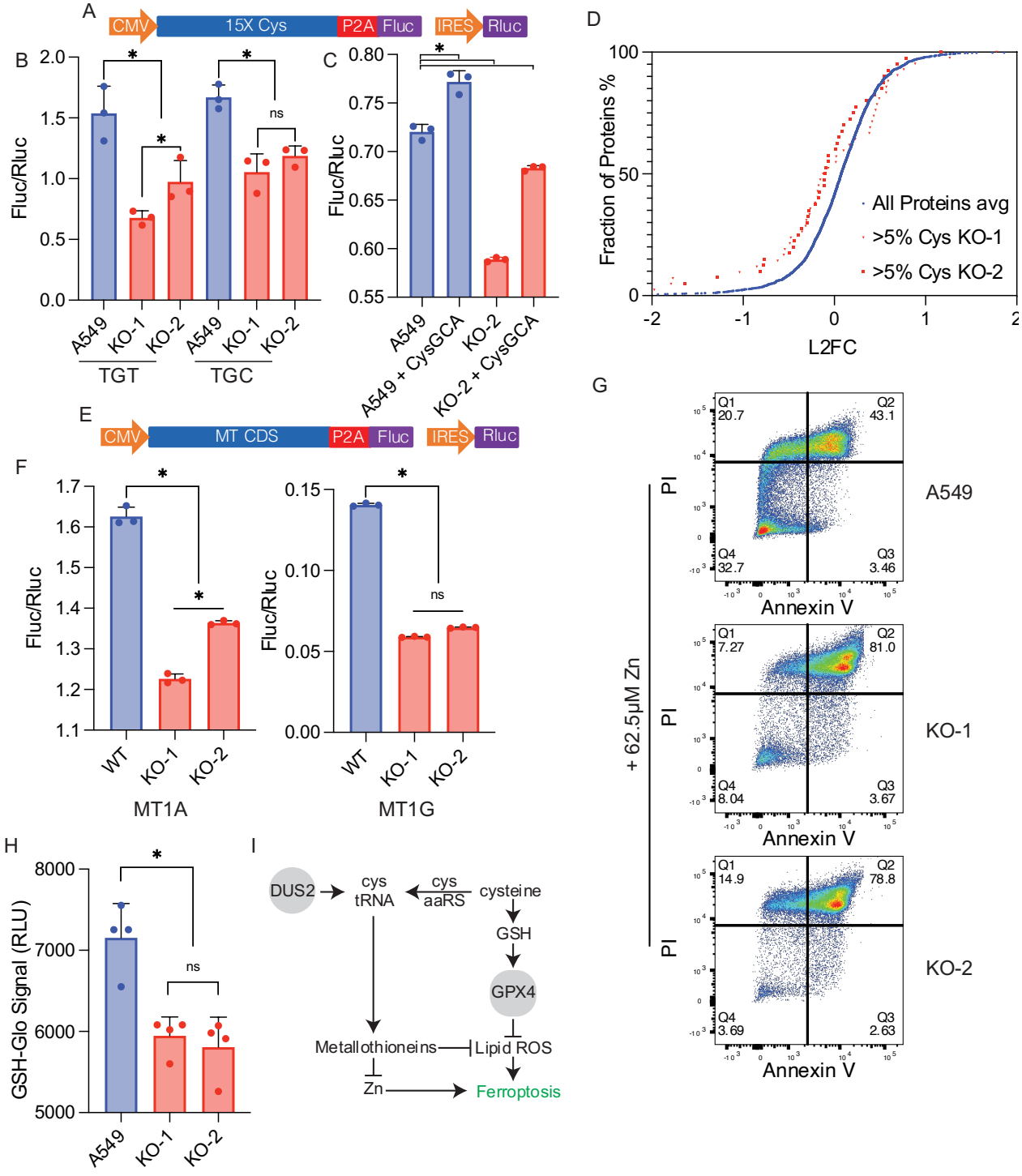
A
CMV
15X Cys
P2A
Fluc
IRES
Rluc
B
Fluc/Rluc
A549
KO-1
KO-2
TGT
TGC
ns
C
A549 + CysGCA
KO-2 + CysGCA
D
Fraction of Proteins %
L2FC
All Proteins avg
>5% Cys KO-1
>5% Cys KO-2
E
MT CDS
F
MT1A
MT1G
WT
G
PI
Annexin V
+ 62.5μM Zn
A549
KO-1
KO-2
Q1 20.7
Q2 43.1
Q4 32.7
Q3 3.46
Q1 7.27
Q2 81.0
Q4 8.04
Q3 3.67
Q1 14.9
Q2 78.8
Q4 3.69
Q3 2.63
H
GSH-Glo Signal (RLU)
I
DUS2
cys tRNA
cys aaRS
cysteine
GSH
GPX4
Metallothioneins
Lipid ROS
Zn
Ferroptosis

**Figure 3: Loss of DUS2 impairs translation of cysteine rich proteins, including metallothioneins, which leads to ferroptosis sensitivity**

a) Cysteine translation reporter
b) DUS2 KO impairs translation of TGT and TGC cysteine codons (two tailed t-test, * p<.03).
c) Rescue of TGT translation by transfection of tRNACysGCA into DUS2 KO cells (two tailed t-test, * p<.0001).
d) Proteins with high (>5%) Cys content are reduced in DUS2 KO cells. Cumulative distribution of changes in protein abundance (log2 fold change, Kolmogorov-Smirnov test, p<.05).
e) Metallothionein translation reporter
f) Metallothioneins (MT1A and MT1G) are translated less well in DUS2 KOs.
g) Increased cell death (Annexin V+/PI+ cells) in DUS2 KOs compared to WT A549 following addition of 62.5μM $ZnCl_2$.
h) DUS2 KO cells have lower levels of reduced GSH (two tailed t-test, * p<.004).
i) Model of anti-ferroptotic function of DUS2.

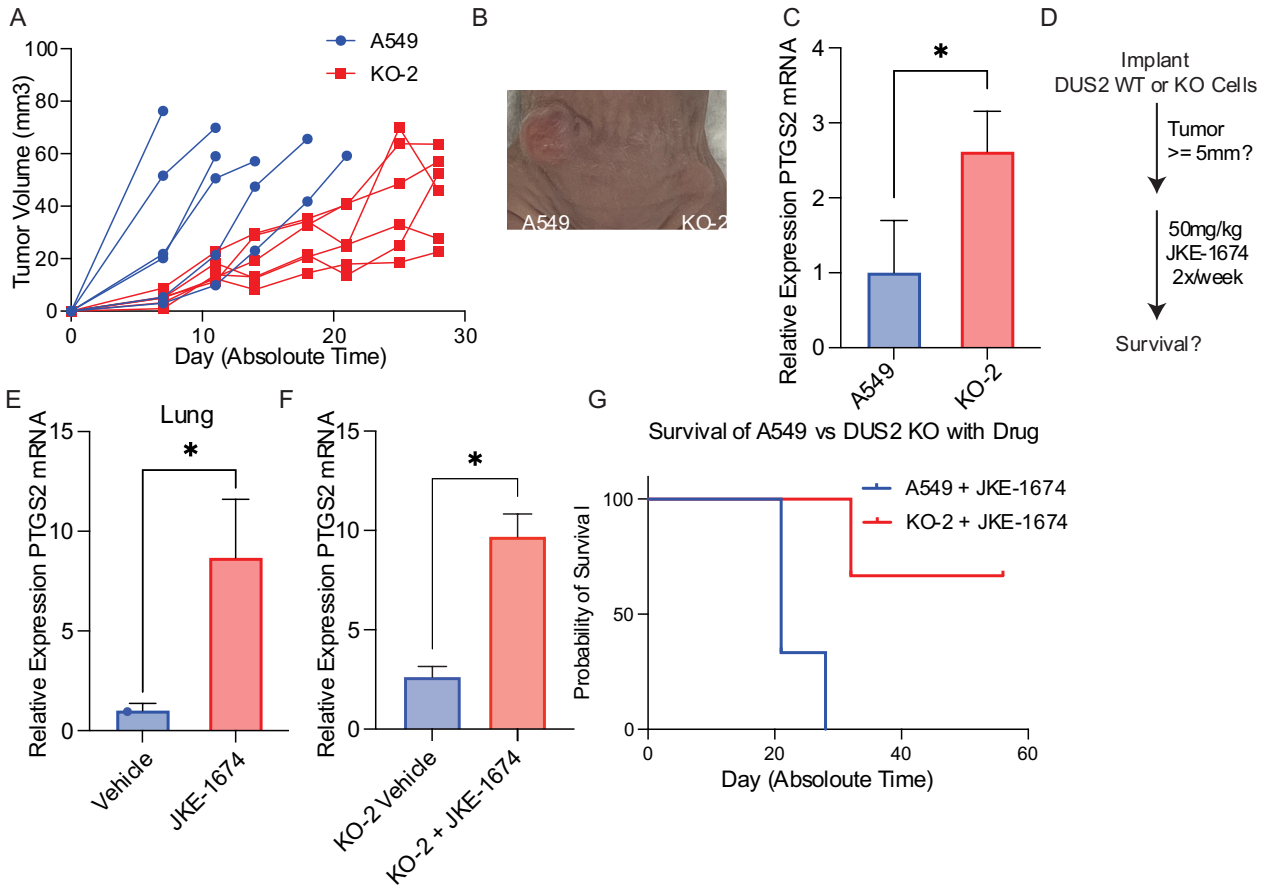
A
A549
KO-2
Tumor Volume (mm3)
Day (Absoloute Time)
B
A549
KO-2
C
Relative Expression PTGS2 mRNA
A549
KO-2
D
Implant
DUS2 WT or KO Cells
Tumor
>= 5mm?
50mg/kg
JKE-1674
2x/week
Survival?
E
Lung
Relative Expression PTGS2 mRNA
Vehicle
JKE-1674
F
Relative Expression PTGS2 mRNA
KO-2 Vehicle
KO-2 + JKE-1674
G
Survival of A549 vs DUS2 KO with Drug
A549 + JKE-1674
KO-2 + JKE-1674
Probability of Survival
Day (Absoloute Time)

**Figure 4: Combined loss of DUS2 and ferroptosis induction extends lifespan in a mouse xenograft NSCLC model**

a) A549 tumors grow faster than DUS2 KO tumors.
b) Example tumor from A549 and DUS2 KO-2
c) DUS2 KO tumors have higher expression of a marker of ferroptosis, PTGS2, than A549 cells by qRT-PCR (ANOVA, * $p<.002$).
d) Dosing scheme for xenograft experiments
e) Oral JKE-1674 treatment induces PTGS2 mRNA in mouse lungs (ANOVA, * $p<.03$).
f) JKE-1674 treatment increases PTGS2 mRNA expression in DUS2 KO tumors(ANOVA , * $p<.02$).
g) Mice implanted with DUS2 KO xenograft tumors survive longer than mice implanted with A549 tumors when treated with JKE-1674 (Mantel-Cox test * $p<.03$).

**Supplemental Information**

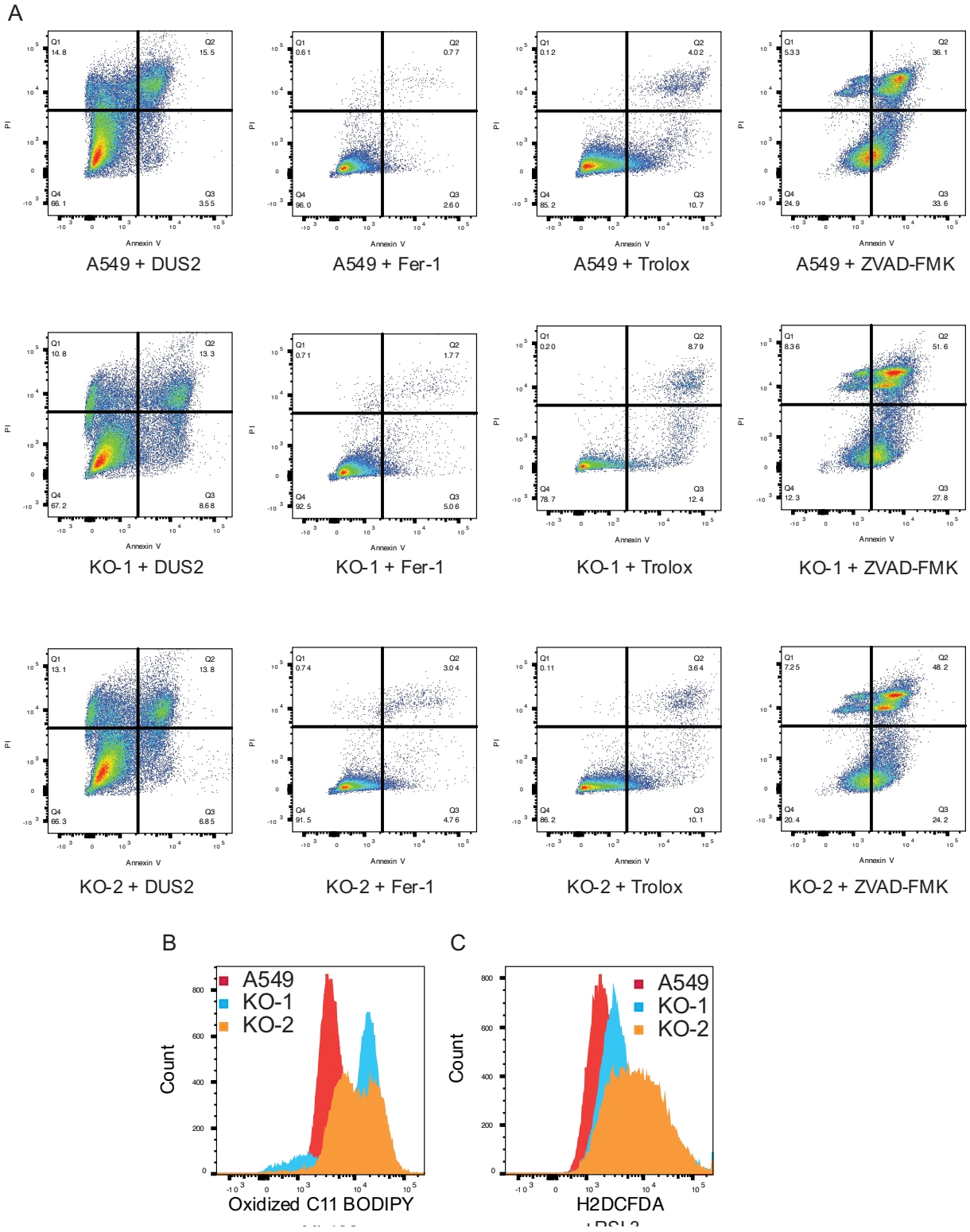
A
A549 + DUS2
A549 + Fer-1
A549 + Trolox
A549 + ZVAD-FMK
KO-1 + DUS2
KO-1 + Fer-1
KO-1 + Trolox
KO-1 + ZVAD-FMK
KO-2 + DUS2
KO-2 + Fer-1
KO-2 + Trolox
KO-2 + ZVAD-FMK
PI
Annexin V
B
C
A549
KO-1
KO-2
Count
Oxidized C11 BODIPY
H2DCFDA

**Figure S1:**

a) Fraction of dead (Annexin V+/PI+) DUS2 KO cells is reduced with pre-treated with DUS2 expression plasmid, Ferrostatin-1, Trolox but not ZVAD-FMK when treated with 2μM RSL-3.
b) DUS2 KOs have higher levels of lipid ROS measured by C11-BODIPY staining when treated with 200nM ML162.
c) DUS2 KOs have higher levels of cellular ROS measured by $H_2$DCFDA staining when treated with 2μM RSL-3.

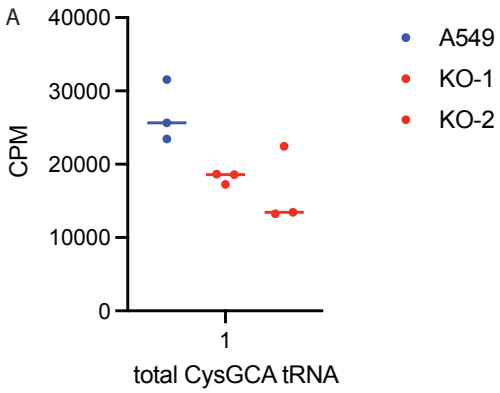
A
40000
30000
20000
10000
0
CPM
1
total CysGCA tRNA
A549
KO-1
KO-2

**Figure S2:**

a) In aggregate, the total pool of tRNACysGCA is reduced ~40% in DUS2 KO clones.

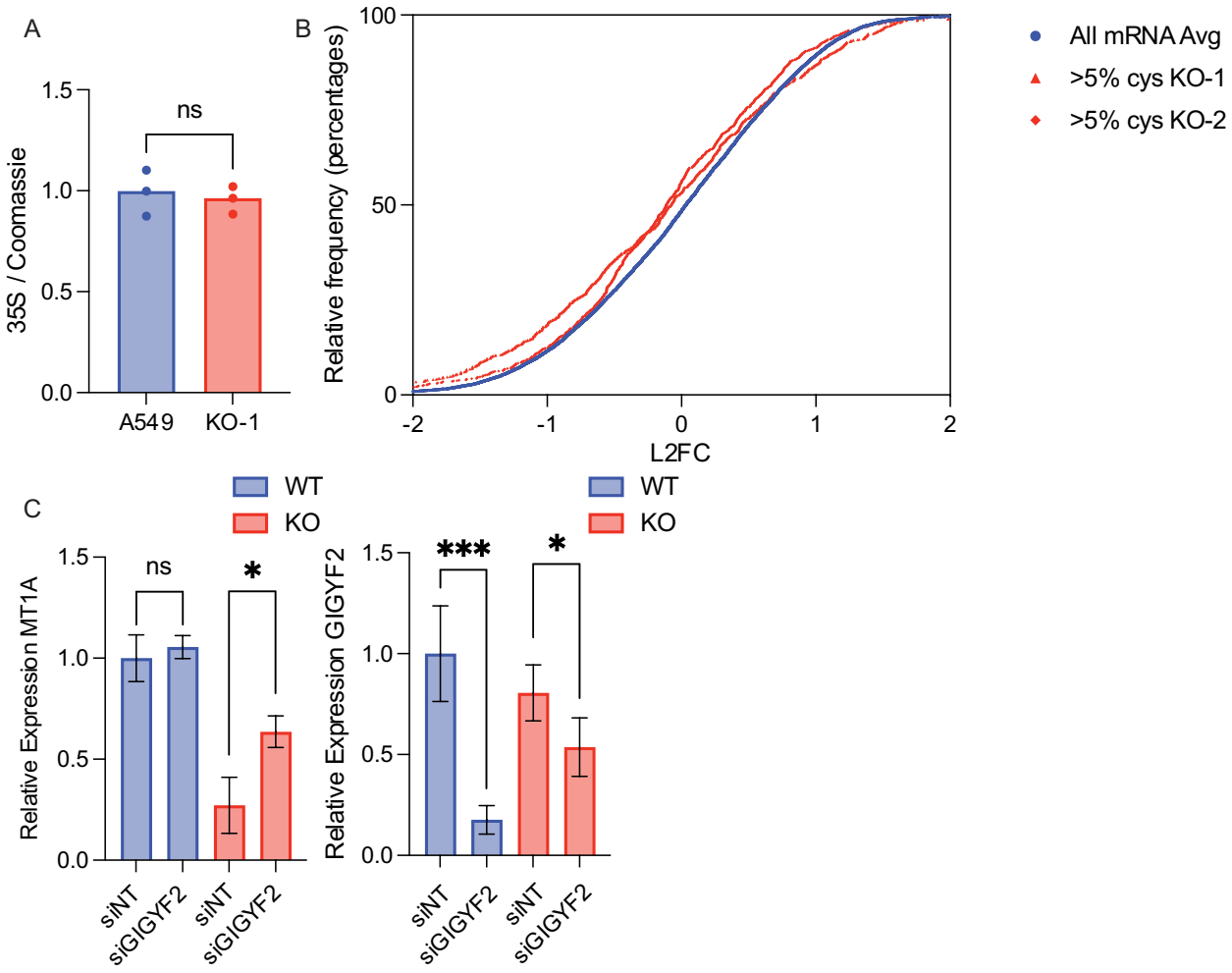
A
35S / Coomassie
1.5
1.0
0.5
0.0
ns
A549
KO-1
B
Relative frequency (percentages)
100
50
0
-2
-1
0
1
2
L2FC
All mRNA Avg
>5% cys KO-1
>5% cys KO-2
C
WT
KO
Relative Expression MT1A
ns
*
siNT
siGIGYF2
siNT
siGIGYF2
Relative Expression GIGYF2
***
*
siNT
siGIGYF2
siNT
siGIGYF2

**Figure S3:**

a) Total protein synthesis is unimpaired in DUS2 KO cells as measured by $^{35}$S-Met incorporation (two tailed t-test, * p=.67).
b) mRNAs encoding cysteine rich proteins are reduced in DUS2 KO cells consistent with RQC. Cumulative distribution of changes in mRNA abundance (log2 fold change, K-S test, p<.0001).).
c) Depletion of RQC factor GIGYF2 (siGIGYF2) rescues MT1A mRNA levels in DUS2 KO cells compared to non-targeting control (siNT) (two tailed t-test, * p<.04).

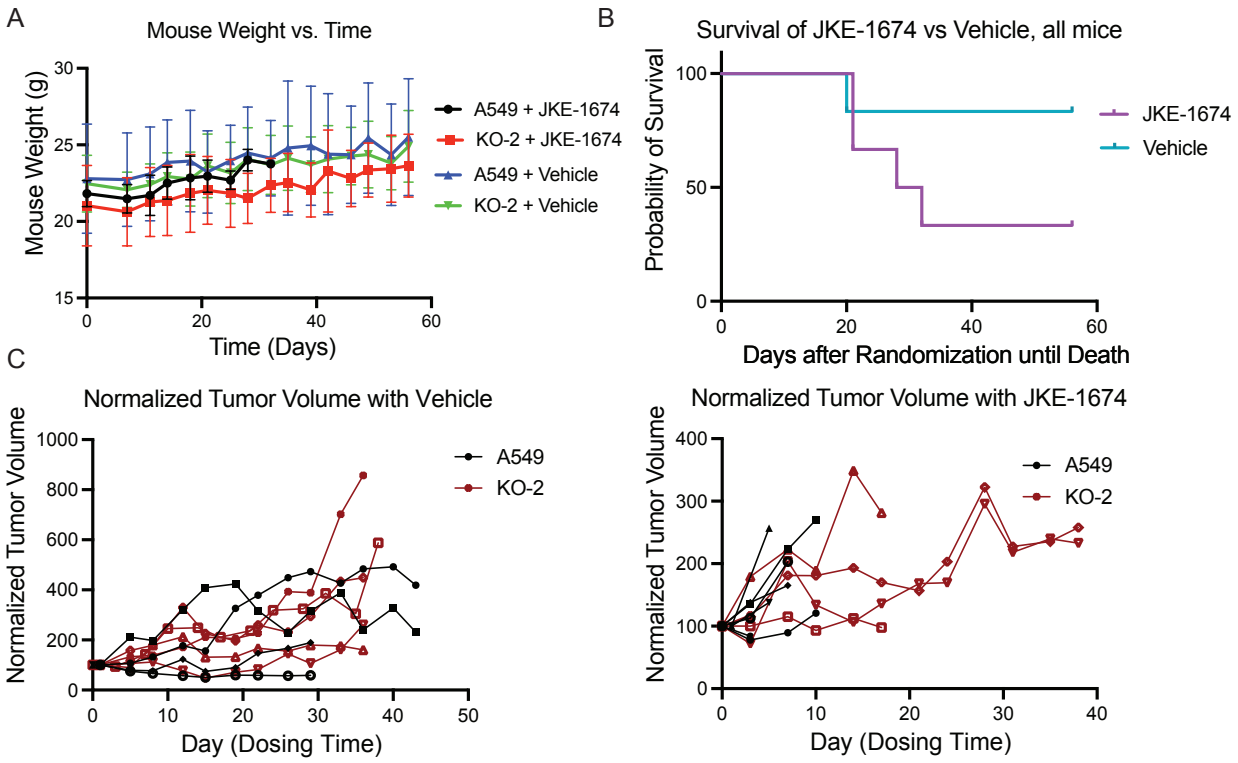
A
Mouse Weight vs. Time
Mouse Weight (g)
Time (Days)
A549 + JKE-1674
KO-2 + JKE-1674
A549 + Vehicle
KO-2 + Vehicle
B
Survival of JKE-1674 vs Vehicle, all mice
Probability of Survival
Days after Randomization until Death
JKE-1674
Vehicle
C
Normalized Tumor Volume with Vehicle
Normalized Tumor Volume
Day (Dosing Time)
A549
KO-2
Normalized Tumor Volume with JKE-1674
Normalized Tumor Volume
Day (Dosing Time)
A549
KO-2

**Figure S4:**

a) Mouse weights generally increased over time with vehicle and JKE-1674.
b) Mice receiving JKE-1674 had shorter median survival than mice receiving vehicle.
c) Normalized tumor volumes (volume at Day 0 = 100%) were similar between vehicle and JKE-1674 treatment.

**Supplemental Tables**

| | A549 %charged | KO-1 %charged | KO-2 %charged | minus-Gln %charged |
|---|---|---|---|---|
| tRNA-Ala-AGC-11-1 | 0.897 | 0.776 | 0.827 | 0.931 |
| tRNA-Ala-AGC-15-1 | 0.889 | 0.780 | 0.825 | 0.934 |
| tRNA-Ala-AGC-2-1 | 0.930 | 0.826 | 0.866 | 0.937 |
| tRNA-Ala-AGC-3-1 | 0.920 | 0.810 | 0.844 | 0.925 |
| tRNA-Ala-AGC-4-1 | 0.907 | 0.861 | 0.908 | 0.930 |
| tRNA-Ala-AGC-5-1 | 0.915 | 0.861 | 0.855 | 0.938 |
| tRNA-Ala-AGC-6-1 | 0.954 | 0.848 | 0.827 | 0.936 |
| tRNA-Ala-AGC-7-1 | 0.960 | 0.961 | 0.962 | 0.978 |
| tRNA-Ala-AGC-8-1 | 0.901 | 0.771 | 0.826 | 0.927 |
| tRNA-Ala-AGC-9-1 | 0.804 | 0.661 | 0.692 | 0.865 |
| tRNA-Ala-CGC-1-1 | 0.909 | 0.830 | 0.880 | 0.945 |
| tRNA-Ala-CGC-2-1 | 0.925 | 0.854 | 0.879 | 0.946 |
| tRNA-Ala-CGC-3-1 | 0.874 | 0.819 | 0.863 | 0.943 |
| tRNA-Ala-CGC-4-1 | 0.892 | 0.840 | 0.867 | 0.915 |
| tRNA-Ala-TGC-1-1 | 0.938 | 0.800 | 0.888 | 0.939 |
| tRNA-Ala-TGC-2-1 | 0.928 | 0.866 | 0.885 | 0.946 |
| tRNA-Ala-TGC-3-1 | 0.932 | 0.848 | 0.876 | 0.946 |
| tRNA-Ala-TGC-4-1 | 0.947 | 0.874 | 0.900 | 0.949 |
| tRNA-Ala-TGC-5-1 | 0.913 | 0.885 | 0.864 | 0.941 |
| tRNA-Ala-TGC-6-1 | 0.929 | 0.877 | 0.865 | 0.952 |
| tRNA-Arg-ACG-1-1 | 0.768 | 0.812 | 0.764 | 0.781 |
| tRNA-Arg-ACG-2-1 | 0.770 | 0.814 | 0.766 | 0.785 |
| tRNA-Arg-CCG-1-1 | 0.882 | 0.855 | 0.864 | 0.900 |
| tRNA-Arg-CCG-2-1 | 0.898 | 0.869 | 0.878 | 0.932 |
| tRNA-Arg-CCT-1-1 | 0.875 | 0.864 | 0.845 | 0.903 |
| tRNA-Arg-CCT-2-1 | 0.886 | 0.868 | 0.846 | 0.912 |
| tRNA-Arg-CCT-3-1 | 0.855 | 0.846 | 0.837 | 0.890 |
| tRNA-Arg-CCT-4-1 | 0.933 | 0.898 | 0.871 | 0.923 |
| tRNA-Arg-CCT-5-1 | 0.849 | 0.859 | 0.816 | 0.900 |
| tRNA-Arg-TCG-1-1 | 0.876 | 0.854 | 0.844 | 0.913 |
| tRNA-Arg-TCG-2-1 | 0.852 | 0.826 | 0.816 | 0.885 |
| tRNA-Arg-TCG-3-1 | 0.918 | 0.875 | 0.878 | 0.916 |
| tRNA-Arg-TCG-4-1 | 0.888 | 0.859 | 0.853 | 0.901 |
| tRNA-Arg-TCG-5-1 | 0.898 | 0.881 | 0.861 | 0.909 |
| tRNA-Arg-TCT-1-1 | 0.918 | 0.908 | 0.903 | 0.930 |

| | | | | |
|---|---|---|---|---|
| tRNA-Arg-TCT-2-1 | 0.880 | 0.865 | 0.872 | 0.898 |
| tRNA-Arg-TCT-3-1 | 0.886 | 0.878 | 0.877 | 0.900 |
| tRNA-Arg-TCT-4-1 | 0.958 | 0.919 | 0.943 | 0.953 |
| tRNA-Asn-GTT-1-1 | 0.928 | 0.855 | 0.883 | 0.959 |
| tRNA-Asn-GTT-2-1 | 0.925 | 0.875 | 0.896 | 0.956 |
| tRNA-Asn-GTT-3-1 | 0.918 | 0.872 | 0.890 | 0.955 |
| tRNA-Asn-GTT-4-1 | 0.966 | 0.908 | 0.907 | 0.964 |
| tRNA-Asn-GTT-5-1 | 0.937 | 0.867 | 0.904 | 0.969 |
| tRNA-Asn-GTT-6-1 | 0.908 | 0.860 | 0.879 | 0.962 |
| tRNA-Asp-GTC-1-1 | 0.955 | 0.899 | 0.899 | 0.974 |
| tRNA-Asp-GTC-2-1 | 0.954 | 0.902 | 0.907 | 0.974 |
| tRNA-Asp-GTC-3-1 | 0.953 | 0.900 | 0.905 | 0.972 |
| tRNA-Cys-GCA-1-1 | 0.851 | 0.768 | 0.783 | 0.783 |
| tRNA-Cys-GCA-10-1 | 0.817 | 0.880 | 0.600 | 0.696 |
| tRNA-Cys-GCA-11-1 | 0.881 | 0.817 | 0.839 | 0.847 |
| tRNA-Cys-GCA-12-1 | 0.882 | 0.684 | 0.773 | 0.816 |
| tRNA-Cys-GCA-13-1 | 0.862 | 0.838 | 0.774 | 0.736 |
| tRNA-Cys-GCA-14-1 | 0.924 | 0.930 | 0.868 | 0.871 |
| tRNA-Cys-GCA-15-1 | 0.814 | 0.806 | 0.750 | 0.710 |
| tRNA-Cys-GCA-17-1 | 0.942 | 0.901 | 0.776 | 0.817 |
| tRNA-Cys-GCA-18-1 | 0.841 | 0.778 | 0.783 | 0.774 |
| tRNA-Cys-GCA-2-1 | 0.872 | 0.819 | 0.840 | 0.844 |
| tRNA-Cys-GCA-20-1 | 0.856 | 0.828 | 0.766 | 0.737 |
| tRNA-Cys-GCA-3-1 | 0.832 | 0.732 | 0.724 | 0.755 |
| tRNA-Cys-GCA-4-1 | 0.872 | 0.809 | 0.847 | 0.843 |
| tRNA-Cys-GCA-5-1 | 0.885 | 0.814 | 0.843 | 0.844 |
| tRNA-Cys-GCA-6-1 | 0.823 | 0.763 | 0.677 | 0.716 |
| tRNA-Cys-GCA-7-1 | 0.882 | 0.819 | 0.840 | 0.845 |
| tRNA-Cys-GCA-8-1 | 0.880 | 0.833 | 0.843 | 0.849 |
| tRNA-Cys-GCA-9-1 | 0.815 | 0.771 | 0.693 | 0.713 |
| tRNA-Gln-CTG-1-1 | 0.834 | 0.812 | 0.852 | 0.222 |
| tRNA-Gln-CTG-2-1 | 0.850 | 0.824 | 0.865 | 0.226 |
| tRNA-Gln-CTG-3-1 | 0.816 | 0.801 | 0.851 | 0.199 |
| tRNA-Gln-CTG-4-1 | 0.829 | 0.802 | 0.862 | 0.200 |
| tRNA-Gln-CTG-5-1 | 0.835 | 0.848 | 0.900 | 0.289 |
| tRNA-Gln-CTG-6-1 | 0.757 | 0.766 | 0.855 | 0.462 |
| tRNA-Gln-TTG-1-1 | 0.855 | 0.830 | 0.867 | 0.287 |
| tRNA-Gln-TTG-2-1 | 0.892 | 0.865 | 0.885 | 0.169 |
| tRNA-Gln-TTG-3-1 | 0.854 | 0.828 | 0.866 | 0.288 |

| | | | | |
|---|---|---|---|---|
| tRNA-Gln-TTG-4-1 | 0.910 | 0.850 | 0.894 | 0.182 |
| tRNA-Glu-CTC-1-1 | 0.927 | 0.869 | 0.897 | 0.939 |
| tRNA-Glu-CTC-2-1 | 0.924 | 0.860 | 0.894 | 0.938 |
| tRNA-Glu-TTC-1-1 | 0.947 | 0.879 | 0.913 | 0.942 |
| tRNA-Glu-TTC-2-1 | 0.939 | 0.883 | 0.911 | 0.938 |
| tRNA-Glu-TTC-3-1 | 0.941 | 0.885 | 0.903 | 0.941 |
| tRNA-Glu-TTC-4-1 | 0.938 | 0.886 | 0.903 | 0.942 |
| tRNA-Gly-CCC-1-1 | 0.909 | 0.888 | 0.872 | 0.928 |
| tRNA-Gly-CCC-2-1 | 0.903 | 0.796 | 0.885 | 0.933 |
| tRNA-Gly-GCC-1-1 | 0.862 | 0.800 | 0.843 | 0.913 |
| tRNA-Gly-GCC-2-1 | 0.881 | 0.803 | 0.851 | 0.923 |
| tRNA-Gly-GCC-3-1 | 0.930 | 0.929 | 0.955 | 0.947 |
| tRNA-Gly-TCC-1-1 | 0.915 | 0.834 | 0.861 | 0.925 |
| tRNA-Gly-TCC-2-1 | 0.914 | 0.827 | 0.845 | 0.924 |
| tRNA-Gly-TCC-3-1 | 0.916 | 0.834 | 0.866 | 0.924 |
| tRNA-His-GTG-1-1 | 0.924 | 0.896 | 0.888 | 0.942 |
| tRNA-His-GTG-2-1 | 0.918 | 0.869 | 0.875 | 0.941 |
| tRNA-Ile-AAT-1-1 | 0.787 | 0.710 | 0.763 | 0.691 |
| tRNA-Ile-AAT-2-1 | 0.803 | 0.723 | 0.761 | 0.685 |
| tRNA-Ile-AAT-3-1 | 0.797 | 0.723 | 0.753 | 0.679 |
| tRNA-Ile-AAT-4-1 | 0.826 | 0.737 | 0.795 | 0.721 |
| tRNA-Ile-AAT-5-1 | 0.792 | 0.716 | 0.763 | 0.679 |
| tRNA-Ile-AAT-6-1 | 0.790 | 0.711 | 0.740 | 0.647 |
| tRNA-Ile-AAT-7-1 | 0.787 | 0.711 | 0.761 | 0.675 |
| tRNA-Ile-AAT-8-1 | 0.791 | 0.715 | 0.760 | 0.675 |
| tRNA-Ile-TAT-1-1 | 0.939 | 0.908 | 0.896 | 0.871 |
| tRNA-Ile-TAT-2-1 | 0.944 | 0.943 | 0.899 | 0.878 |
| tRNA-Ile-TAT-3-1 | 0.927 | 0.922 | 0.887 | 0.870 |
| tRNA-iMet-CAT-1-1 | 0.856 | 0.844 | 0.837 | 0.897 |
| tRNA-iMet-CAT-2-1 | 0.915 | 0.897 | 0.902 | 0.919 |
| tRNA-Leu-AAG-1-1 | 0.941 | 0.901 | 0.923 | 0.958 |
| tRNA-Leu-AAG-2-1 | 0.936 | 0.901 | 0.916 | 0.955 |
| tRNA-Leu-AAG-3-1 | 0.937 | 0.899 | 0.919 | 0.956 |
| tRNA-Leu-AAG-4-1 | 0.819 | 0.809 | 0.736 | 0.864 |
| tRNA-Leu-CAA-1-1 | 0.937 | 0.896 | 0.921 | 0.959 |
| tRNA-Leu-CAA-2-1 | 0.949 | 0.909 | 0.934 | 0.963 |
| tRNA-Leu-CAA-3-1 | 0.938 | 0.889 | 0.919 | 0.958 |
| tRNA-Leu-CAA-4-1 | 0.937 | 0.890 | 0.919 | 0.958 |
| tRNA-Leu-CAG-1-1 | 0.929 | 0.888 | 0.899 | 0.954 |

| | | | | |
|---|---|---|---|---|
| tRNA-Leu-CAG-2-1 | 0.932 | 0.893 | 0.897 | 0.956 |
| tRNA-Leu-TAA-1-1 | 0.926 | 0.897 | 0.916 | 0.964 |
| tRNA-Leu-TAA-2-1 | 0.943 | 0.874 | 0.976 | 0.962 |
| tRNA-Leu-TAA-3-1 | 0.955 | 0.909 | 0.919 | 0.964 |
| tRNA-Leu-TAG-1-1 | 0.940 | 0.899 | 0.923 | 0.958 |
| tRNA-Leu-TAG-2-1 | 0.934 | 0.895 | 0.915 | 0.955 |
| tRNA-Leu-TAG-3-1 | 0.923 | 0.875 | 0.863 | 0.955 |
| tRNA-Lys-CTT-1-1 | 0.963 | 0.921 | 0.928 | 0.971 |
| tRNA-Lys-CTT-2-1 | 0.966 | 0.924 | 0.938 | 0.971 |
| tRNA-Lys-CTT-3-1 | 0.972 | 0.935 | 0.944 | 0.968 |
| tRNA-Lys-CTT-4-1 | 0.967 | 0.926 | 0.933 | 0.969 |
| tRNA-Lys-CTT-5-1 | 0.979 | 0.957 | 0.971 | 0.973 |
| tRNA-Lys-TTT-2-1 | 0.953 | 0.875 | 0.907 | 0.968 |
| tRNA-Lys-TTT-3-1 | 0.961 | 0.897 | 0.904 | 0.965 |
| tRNA-Lys-TTT-4-1 | 0.946 | 0.873 | 0.905 | 0.966 |
| tRNA-Lys-TTT-5-1 | 0.963 | 0.897 | 0.901 | 0.963 |
| tRNA-Met-CAT-1-1 | 0.965 | 0.937 | 0.938 | 0.968 |
| tRNA-Met-CAT-2-1 | 0.934 | 0.870 | 0.918 | 0.961 |
| tRNA-Met-CAT-3-1 | 0.936 | 0.907 | 0.923 | 0.958 |
| tRNA-Met-CAT-4-1 | 0.940 | 0.876 | 0.916 | 0.962 |
| tRNA-Met-CAT-6-1 | 0.954 | 0.902 | 0.932 | 0.961 |
| tRNA-Phe-GAA-1-1 | 0.924 | 0.868 | 0.878 | 0.957 |
| tRNA-Phe-GAA-2-1 | 0.965 | 0.936 | 0.911 | 0.964 |
| tRNA-Phe-GAA-3-1 | 0.927 | 0.876 | 0.882 | 0.959 |
| tRNA-Pro-AGG-1-1 | 0.897 | 0.798 | 0.857 | 0.914 |
| tRNA-Pro-AGG-2-1 | 0.900 | 0.843 | 0.866 | 0.916 |
| tRNA-Pro-CGG-1-1 | 0.898 | 0.848 | 0.867 | 0.916 |
| tRNA-Pro-CGG-2-1 | 0.894 | 0.849 | 0.873 | 0.915 |
| tRNA-Pro-TGG-1-1 | 0.896 | 0.840 | 0.859 | 0.913 |
| tRNA-Pro-TGG-2-1 | 0.901 | 0.884 | 0.874 | 0.922 |
| tRNA-Pro-TGG-3-1 | 0.899 | 0.845 | 0.870 | 0.917 |
| tRNA-SeC-TCA-1-1 | 0.905 | 0.886 | 0.863 | 0.880 |
| tRNA-Ser-AGA-1-1 | 0.866 | 0.695 | 0.844 | 0.946 |
| tRNA-Ser-AGA-2-1 | 0.865 | 0.650 | 0.812 | 0.941 |
| tRNA-Ser-AGA-3-1 | 0.804 | 0.688 | 0.842 | 0.934 |
| tRNA-Ser-AGA-4-1 | 0.671 | 0.649 | 0.728 | 0.889 |
| tRNA-Ser-CGA-1-1 | 0.929 | 0.762 | 0.842 | 0.959 |
| tRNA-Ser-CGA-2-1 | 0.958 | 0.805 | 0.870 | 0.963 |
| tRNA-Ser-CGA-3-1 | 0.930 | 0.882 | 0.838 | 0.908 |

| | | | | |
|---|---|---|---|---|
| tRNA-Ser-CGA-4-1 | 0.871 | 0.720 | 0.827 | 0.950 |
| tRNA-Ser-GCT-1-1 | 0.890 | 0.747 | 0.837 | 0.947 |
| tRNA-Ser-GCT-2-1 | 0.876 | 0.706 | 0.809 | 0.947 |
| tRNA-Ser-GCT-3-1 | 0.896 | 0.724 | 0.817 | 0.950 |
| tRNA-Ser-GCT-4-1 | 0.893 | 0.713 | 0.820 | 0.949 |
| tRNA-Ser-GCT-5-1 | 0.890 | 0.760 | 0.815 | 0.945 |
| tRNA-Ser-GCT-6-1 | 0.889 | 0.700 | 0.818 | 0.950 |
| tRNA-Ser-TGA-1-1 | 0.869 | 0.680 | 0.796 | 0.946 |
| tRNA-Ser-TGA-2-1 | 0.864 | 0.660 | 0.837 | 0.948 |
| tRNA-Ser-TGA-3-1 | 0.865 | 0.649 | 0.813 | 0.941 |
| tRNA-Ser-TGA-4-1 | 0.926 | 0.651 | 0.820 | 0.960 |
| tRNA-Thr-AGT-1-1 | 0.909 | 0.735 | 0.880 | 0.963 |
| tRNA-Thr-AGT-2-1 | 0.875 | 0.723 | 0.859 | 0.963 |
| tRNA-Thr-AGT-3-1 | 0.894 | 0.718 | 0.899 | 0.961 |
| tRNA-Thr-AGT-4-1 | 0.850 | 0.683 | 0.849 | 0.963 |
| tRNA-Thr-AGT-5-1 | 0.908 | 0.735 | 0.879 | 0.963 |
| tRNA-Thr-AGT-6-1 | 0.879 | 0.732 | 0.866 | 0.963 |
| tRNA-Thr-CGT-1-1 | 0.918 | 0.729 | 0.896 | 0.955 |
| tRNA-Thr-CGT-2-1 | 0.899 | 0.752 | 0.887 | 0.961 |
| tRNA-Thr-CGT-3-1 | 0.874 | 0.719 | 0.865 | 0.964 |
| tRNA-Thr-CGT-4-1 | 0.895 | 0.752 | 0.886 | 0.959 |
| tRNA-Thr-TGT-1-1 | 0.911 | 0.800 | 0.898 | 0.971 |
| tRNA-Thr-TGT-2-1 | 0.896 | 0.794 | 0.861 | 0.957 |
| tRNA-Thr-TGT-3-1 | 0.926 | 0.768 | 0.856 | 0.955 |
| tRNA-Thr-TGT-4-1 | 0.897 | 0.801 | 0.855 | 0.960 |
| tRNA-Thr-TGT-5-1 | 0.893 | 0.802 | 0.851 | 0.960 |
| tRNA-Thr-TGT-6-1 | 0.913 | 0.759 | 0.882 | 0.959 |
| tRNA-Trp-CCA-1-1 | 0.945 | 0.906 | 0.914 | 0.966 |
| tRNA-Trp-CCA-2-1 | 0.950 | 0.904 | 0.910 | 0.966 |
| tRNA-Trp-CCA-3-1 | 0.946 | 0.904 | 0.913 | 0.966 |
| tRNA-Trp-CCA-4-1 | 0.948 | 0.910 | 0.920 | 0.970 |
| tRNA-Trp-CCA-5-1 | 0.946 | 0.900 | 0.910 | 0.965 |
| tRNA-Tyr-GTA-1-1 | 0.928 | 0.892 | 0.882 | 0.949 |
| tRNA-Tyr-GTA-2-1 | 0.923 | 0.874 | 0.886 | 0.949 |
| tRNA-Tyr-GTA-3-1 | 0.927 | 0.888 | 0.883 | 0.942 |
| tRNA-Tyr-GTA-4-1 | 0.937 | 0.893 | 0.893 | 0.970 |
| tRNA-Tyr-GTA-5-1 | 0.923 | 0.875 | 0.886 | 0.949 |
| tRNA-Tyr-GTA-6-1 | 0.928 | 0.890 | 0.883 | 0.943 |
| tRNA-Tyr-GTA-7-1 | 0.956 | 0.933 | 0.921 | 0.971 |

| | | | | |
|---|---|---|---|---|
| tRNA-Tyr-GTA-8-1 | 0.925 | 0.889 | 0.882 | 0.950 |
| tRNA-Val-AAC-1-1 | 0.963 | 0.914 | 0.929 | 0.966 |
| tRNA-Val-AAC-2-1 | 0.963 | 0.915 | 0.929 | 0.966 |
| tRNA-Val-AAC-3-1 | 0.960 | 0.909 | 0.922 | 0.963 |
| tRNA-Val-CAC-1-1 | 0.963 | 0.914 | 0.928 | 0.966 |
| tRNA-Val-CAC-3-1 | 0.958 | 0.921 | 0.936 | 0.966 |
| tRNA-Val-CAC-4-1 | 0.966 | 0.946 | 0.943 | 0.969 |
| tRNA-Val-TAC-1-1 | 0.965 | 0.927 | 0.932 | 0.971 |
| tRNA-Val-TAC-2-1 | 0.963 | 0.922 | 0.930 | 0.971 |
| tRNA-Val-TAC-4-1 | 0.983 | 0.915 | 0.907 | 0.969 |

**Table S1** Charged tRNA fractions upon DUS2 Knockout.

| #ID | L2FC KO-1 | L2FC KO-2 | FDR | AveExpr | P value |
|---|---|---|---|---|---|
| tRNA-Cys-GCA-10-1 | -1.5541464 | -2.0977973 | 0.00085937 | 6.74454054 | 7.16E-06 |
| tRNA-Gln-TTG-4-1 | 0.98231525 | 1.85211179 | 0.00085937 | 7.90882201 | 1.02E-05 |
| tRNA-Ser-CGA-4-1 | 1.39445368 | 1.33049922 | 0.00085937 | 11.4096561 | 6.58E-06 |
| tRNA-Cys-GCA-2-1 | -0.9263551 | -1.1739665 | 0.00381945 | 12.119153 | 8.21E-05 |
| tRNA-Cys-GCA-14-1 | -0.9442128 | -1.5217302 | 0.00381945 | 9.2659496 | 7.23E-05 |
| tRNA-Cys-GCA-9-1 | -1.150234 | -1.5761573 | 0.00381945 | 7.48707828 | 9.02E-05 |
| tRNA-Ser-AGA-3-1 | 0.69562143 | 1.11197502 | 0.00782033 | 10.0579964 | 0.00021552 |
| tRNA-Asn-GTT-5-1 | 0.79467269 | 1.01264262 | 0.01467142 | 10.802648 | 0.00046209 |
| tRNA-Cys-GCA-8-1 | -0.7880458 | -1.2896502 | 0.01616332 | 9.5676113 | 0.00057272 |
| tRNA-Cys-GCA-5-1 | -0.7213852 | -1.0661286 | 0.01659361 | 11.0539618 | 0.00065329 |
| tRNA-Thr-CGT-4-1 | -0.5070528 | -1.1585986 | 0.02985708 | 13.4947717 | 0.00129302 |
| tRNA-Asn-GTT-4-1 | 0.82594991 | 0.9348473 | 0.03096185 | 9.03501614 | 0.00146277 |
| tRNA-Thr-CGT-2-1 | -0.4053984 | -1.010987 | 0.0469111 | 13.3333862 | 0.00240096 |

**Table S2** tRNA abundance upon DUS2 Knockout

| Prot ID | Molecular Weight | Avg L2FC KO-1 | Avg L2FC KO-2 |
|---|---|---|---|
| KRT81 | 55 kDa | -1.7898 | -1.2802333 |
| PLSCR1 | 35 kDa | 1.776 | 1.17156667 |
| USP3 | 59 kDa | -1.0387 | 0.5472 |
| AFP | 69 kDa | -1.9745 | -2.9251 |
| SPINT2 | 28 kDa | -1.7704 | -0.81325 |
| PDLIM7 | 50 kDa | 1.18296667 | 0.19446667 |
| OCIAD2 | 17 kDa | 1.1136 | 0.08316667 |
| EHMT1 | 141 kDa | -6.4763 | -6.499 |
| ETHE1 | 28 kDa | 1.0267 | 0.9978 |
| PRAG1 | 150 kDa | 1.1234 | 1.2635 |
| SUSD2 | 90 kDa | 2.4533 | 2.09886667 |
| ZNF512 | 65 kDa | 1.2769 | 0.4356 |
| AMIGO2 | 58 kDa | 1.27545 | 0.6227 |
| IGF1R | 155 kDa | 2.0965 | 0.57645 |
| SQSTM1 | 48 kDa | -1.0069 | -1.1747 |
| FNDC3B | 133 kDa | -1.0899 | -1.25915 |
| C17orf75 | 45 kDa | -1.4596 | -0.4744 |
| CTSC | 52 kDa | 1.0355 | 0.42503333 |
| NDUFB7 | 16 kDa | 1.09546667 | 0.19135 |
| IRF2BP1 | 62 kDa | 1.0668 | 1.21493333 |
| RPP30 | 29 kDa | -1.0454 | -0.36235 |
| ACSF2 | 68 kDa | 1.23863333 | 1.10943333 |
| LSM12 | 22 kDa | -1.2253333 | -1.0747 |
| WDR43 | 75 kDa | -1.1223667 | -0.8403667 |
| CYP4F11 | 60 kDa | -2.86735 | -1.93465 |
| LDAH | 37 kDa | -2.3752 | -2.8421 |
| THEM6 | 24 kDa | -3.8271667 | 0.40246667 |
| NUDCD1 | 67 kDa | -1.5716 | -0.7280333 |
| SLC16A3 | 49 kDa | -2.15885 | -1.7532667 |
| APP | 87 kDa | 1.26155 | 1.32545 |
| RRP9 | 52 kDa | -1.3384 | -0.7308333 |
| XPOT | 110 kDa | -1.2424 | -0.1778667 |
| URB2 | 171 kDa | 1.81555 | -0.1273 |
| BCAM | 67 kDa | 1.47413333 | 0.9721 |
| ATP1B3 | 32 kDa | 1.02256667 | -0.3525333 |
| WDR12 | 48 kDa | -1.2950333 | -0.2668 |

| | | | |
|---|---|---|---|
| ATP5MF | 11 kDa | 1.0354 | -0.1676667 |
| EFL1 | 125 kDa | -1.1476 | -0.7395667 |
| EXOSC4 | 26 kDa | 1.02123333 | 0.05893333 |
| GFPT1 | 79 kDa | -1.2961 | -0.4613 |
| LRRC8A | 94 kDa | 1.3148 | 0.1971 |
| FKBP8 | 45 kDa | 1.6249 | 0.47815 |
| KYNU | 52 kDa | -1.5689333 | -0.9867667 |
| THOC5 | 79 kDa | -1.4012 | 0.3277 |
| CADM1 | 49 kDa | 1.58783333 | 0.91325 |
| CEMIP2 | 154 kDa | 1.0114 | 0.5097 |
| TUBB4B | 50 kDa | -1.0771667 | -0.40795 |
| SGPL1 | 64 kDa | 1.11443333 | 0.23133333 |
| MAP2K3 | 39 kDa | -1.96215 | -1.1521333 |
| KIF2A | 80 kDa | 1.0682 | -0.0398 |
| TCF25 | 77 kDa | 1.08726667 | -0.2291 |
| TFAM | 29 kDa | -1.7584 | -4.1011667 |
| SLC2A3 | 54 kDa | -1.9733 | -6.1787 |
| RIF1 | 274 kDa | -1.3929 | -0.1833 |
| ALKBH5 | 44 kDa | 1.9951 | 0.6878 |
| PFDN4 | 15 kDa | -1.1784667 | 0.06486667 |
| NECTIN2 | 58 kDa | 1.3831 | 0.78125 |
| CNTN1 | 113 kDa | 1.19856667 | 0.65493333 |
| MICU1 | 54 kDa | 1.0679 | 0.77165 |
| H3C1 | 15 kDa | -1.2539 | -0.0195333 |
| TNS3 | 155 kDa | 1.0573 | 0.90493333 |
| CA12 | 39 kDa | -1.2814333 | -0.9645333 |
| SKIV2L | 138 kDa | 1.12445 | 0.79465 |
| PLBD2 | 65 kDa | 1.9719 | 1.1415 |
| CPS1 | 165 kDa | -1.3043667 | 0.3106 |
| RRM2 | 45 kDa | -1.2398 | -1.5 |
| SGTA | 34 kDa | -1.2363667 | -1.2061 |
| AKR1B10 | 36 kDa | -1.3854 | -0.5225 |
| SNRPB | 25 kDa | 1.3985 | 0.9686 |
| MCCC1 | 80 kDa | -1.4729 | -1.3011 |
| PTGR1 | 36 kDa | -1.6842 | -0.6445667 |
| NNT | 114 kDa | 1.20603333 | 0.92843333 |
| HSDL2 | 45 kDa | 1.00816667 | 0.79063333 |
| RPL7L1 | 30 kDa | -1.2003333 | -0.7372667 |
| UTP15 | 58 kDa | -1.2215 | -0.5750333 |

| | | | |
|---|---|---|---|
| CD99L2 | 28 kDa | 1.08655 | 0.02246667 |
| BCKDHA | 50 kDa | 1.60175 | 0.8463 |
| SCPEP1 | 51 kDa | 1.3034 | 0.9737 |
| NIFK | 34 kDa | -1.2858 | -0.6430333 |
| NAMPT | 56 kDa | -2.2381333 | -2.1605 |
| POLR1G | 55 kDa | 1.00033333 | 0.53796667 |
| SYNPO | 99 kDa | 1.2958 | 0.084 |
| EXOC7 | 83 kDa | -1.1597 | -0.2523667 |
| DNTTIP2 | 84 kDa | -1.4769 | 0.1575 |
| MSI2 | 35 kDa | -1.658 | -0.1893 |
| MARCKS | 32 kDa | 1.34513333 | 1.03076667 |
| TP53I3 | 36 kDa | -1.3038 | -1.3242 |
| CDH2 | 100 kDa | 1.1283 | 2.30505 |
| TOP2A | 174 kDa | -1.2598 | -0.9042333 |
| EFHD2 | 27 kDa | -1.0055667 | -1.27845 |
| LAMTOR3 | 14 kDa | 1.07583333 | 0.7253 |
| TRAM1 | 43 kDa | 1.38356667 | 0.42183333 |
| BRI3BP | 28 kDa | 1.15245 | 0.98293333 |
| PLEC | 532 kDa | -1.6202667 | -0.723 |
| H3C15 | 15 kDa | -1.1819 | 0.016 |
| H3-3A | 15 kDa | -1.1810667 | 0.01036667 |
| MRPL41 | 15 kDa | 1.0069 | 0.2921 |
| BZW1 | 48 kDa | -1.0147667 | -0.9826333 |
| SMARCA2 | 181 kDa | 1.0076 | 1.0943 |
| KRT10 | 59 kDa | 1.46513333 | -0.1177 |
| MYEF2 | 64 kDa | 1.13515 | -0.6347 |
| KRT9 | 62 kDa | 3.02116667 | 2.35706667 |
| PPP1R10 | 99 kDa | 1.19253333 | 0.14995 |
| INA | 55 kDa | 1.4433 | 0.6388 |
| QKI | 38 kDa | 1.16 | 0.1739 |
| AGR2 | 20 kDa | -1.6993 | 0.6974 |
| LRRFIP2 | 82 kDa | 1.3283 | 0.438 |
| RPRD2 | 156 kDa | 1.27256667 | 0.4791 |
| TAGLN | 23 kDa | 1.06913333 | -0.4395333 |
| CHMP6 | 23 kDa | 1.32305 | 0.92745 |
| MRPS26 | 24 kDa | -1.4982667 | 0.44965 |
| KRT1 | 66 kDa | 3.2413 | 4.0934 |
| SH3KBP1 | 73 kDa | -1.3523667 | -1.5189667 |
| PGRMC2 | 24 kDa | 1.00526667 | 0.1824 |

| | | | |
|---|---|---|---|
| HDGFL2 | 74 kDa | 1.05666667 | 0.62793333 |
| PQBP1 | 30 kDa | 1.14713333 | 0.64193333 |
| UBLCP1 | 37 kDa | -1.2058 | 0.19496667 |
| RSRC2 | 51 kDa | 1.071 | 1.2747 |
| PRRC1 | 47 kDa | -1.08785 | -0.4182 |
| VIM | 54 kDa | -1.7456 | -0.9005333 |
| CALD1 | 93 kDa | 1.08156667 | 0.29933333 |
| H4C1 | 11 kDa | -1.4583 | -0.1680333 |
| H2BC5 | 14 kDa | -1.07375 | -0.2080333 |
| KRT19 | 44 kDa | -1.7206333 | -1.0152667 |

**Table S3** Protein abundance upon DUS2 Knockout

| Gene_Name | log2(FC) KO-1 | P-adj KO-1 | log2(FC) KO-1 | P-adj KO-2 |
|---|---|---|---|---|
| PEDS1-UBE2V1 | 5.09 | 9.70E-14 | 4.63 | 9.15E-15 |
| PPARGC1A | 3.19 | 8.66E-10 | 2.92 | 4.78E-09 |
| GABRQ | 2.32 | 1.47E-06 | 3.30 | 2.10E-13 |
| EDAR | 2.60 | 1.16E-05 | 2.81 | 2.60E-07 |
| PDE3A | 3.16 | 3.63E-16 | 2.09 | 4.63E-09 |
| ADAM9 | 3.12 | 7.66E-10 | 2.10 | 0.0014752 |
| TNFSF15 | 2.38 | 9.79E-13 | 2.81 | 7.03E-17 |
| PHC1P1 | 3.41 | 5.91E-06 | 1.77 | 0.01023472 |
| AC020915.4 | 3.36 | 8.31E-06 | 1.82 | 0.00913881 |
| FAT4 | 2.52 | 0.00014809 | 2.53 | 7.22E-05 |
| ABCF2-H2BE1 | 2.94 | 0.0001906 | 2.05 | 0.00469279 |
| LRIG1 | 2.96 | 5.60E-11 | 1.98 | 7.15E-06 |
| RAPGEF2 | 2.70 | 1.40E-06 | 2.22 | 1.44E-05 |
| SHISAL1 | 2.28 | 1.03E-05 | 2.57 | 1.68E-07 |
| PCDHGB5 | 2.21 | 0.0005882 | 2.46 | 2.25E-05 |
| ADH1C | 1.51 | 0.00235156 | 3.14 | 2.61E-10 |
| DDIT4L | 1.82 | 1.93E-06 | 2.79 | 1.25E-14 |
| PCDHAC1 | 2.35 | 0.00027637 | 2.26 | 0.00042178 |
| PKD2 | 2.34 | 1.96E-06 | 2.13 | 9.39E-07 |
| GLRB | 1.70 | 0.00046146 | 2.77 | 1.63E-07 |
| ITIH2 | 2.37 | 3.56E-06 | 2.08 | 1.60E-05 |
| PDK4 | 2.44 | 1.51E-19 | 2.01 | 4.80E-11 |
| TLR1 | 2.67 | 4.95E-05 | 1.76 | 0.00544087 |
| TP63 | 1.64 | 0.00053191 | 2.78 | 9.60E-13 |

| | | | | |
|---|---|---|---|---|
| ABCA12 | 2.08 | 0.00012645 | 2.33 | 9.97E-06 |
| PDCD6IP | 2.47 | 3.46E-09 | 1.91 | 2.18E-06 |
| MATR3 | 2.21 | 1.16E-06 | 2.15 | 4.33E-07 |
| OPRL1 | 2.10 | 9.01E-05 | 2.22 | 1.80E-05 |
| RAB23 | 2.77 | 2.55E-06 | 1.53 | 0.00616781 |
| FAM47E-STBD1 | 2.34 | 0.00386796 | 1.88 | 0.00919403 |
| CPE | 1.81 | 5.01E-06 | 2.38 | 4.43E-09 |
| RARRES1 | 3.08 | 2.25E-15 | 1.11 | 0.00040009 |
| ANKRD50 | 2.05 | 1.18E-06 | 2.13 | 7.41E-08 |
| PTPN13 | 1.73 | 0.00364961 | 2.43 | 8.37E-07 |
| MFAP3 | 2.29 | 3.26E-05 | 1.86 | 0.00083444 |
| FAM131B | 2.36 | 5.34E-09 | 1.75 | 3.87E-05 |
| RNF212 | 2.11 | 0.00829951 | -1.82 | 0.00220293 |
| SYTL5 | 2.18 | 0.00157941 | 1.93 | 0.00385485 |
| CCDC85A | 1.56 | 0.01336037 | 2.55 | 1.73E-05 |
| TMEM47 | 1.45 | 0.00084954 | 2.63 | 6.98E-09 |
| PRKDC | 2.31 | 6.92E-14 | 1.72 | 3.37E-06 |
| LGR4 | 3.02 | 1.19E-12 | 1.01 | 0.02929749 |
| NCOA2 | 2.29 | 1.30E-06 | 1.74 | 6.16E-05 |
| CCNG2 | 2.25 | 9.87E-07 | 1.78 | 3.87E-05 |
| FGFR2 | 1.51 | 0.00119004 | 2.50 | 3.88E-08 |
| GALNT7 | 2.31 | 4.61E-08 | 1.70 | 2.10E-05 |
| FRS2 | 1.97 | 0.00020195 | 2.03 | 4.24E-05 |
| MARCHF8 | 1.76 | 0.00029308 | 2.22 | 1.02E-07 |
| B4GALT6 | 2.00 | 2.13E-05 | 1.98 | 7.26E-05 |
| ARHGAP11A | 1.98 | 1.82E-05 | 1.98 | 2.11E-05 |
| NT5DC1 | 2.45 | 7.21E-08 | 1.48 | 0.00044748 |
| HERC3 | 1.90 | 0.00054723 | 2.02 | 4.70E-05 |
| MBOAT1 | 2.27 | 0.00018929 | 1.64 | 0.01243583 |
| AC068896.1 | 2.03 | 0.01209952 | 1.88 | 0.00944449 |
| SMAD4 | 2.12 | 1.93E-06 | 1.77 | 2.85E-05 |
| CXCL5 | 2.48 | 1.34E-08 | 1.39 | 0.00017276 |
| RDH10 | 1.99 | 7.01E-06 | 1.88 | 3.37E-09 |
| ENTPD7 | 1.75 | 0.00033132 | 2.10 | 5.88E-05 |
| BMPR1A | 2.11 | 5.45E-06 | 1.74 | 6.66E-05 |
| AOX1 | 2.41 | 2.21E-06 | 1.43 | 0.00676903 |
| AC022826.2 | 2.06 | 0.01064032 | 1.77 | 0.01611644 |
| EPB41L4A | 1.95 | 0.00015533 | 1.85 | 8.47E-05 |
| PTGS2 | 2.00 | 1.08E-07 | 1.78 | 6.95E-06 |

| | | | | |
|---|---|---|---|---|
| NPY4R2 | 1.99 | 0.00016789 | 1.78 | 7.26E-05 |
| GABRA5 | 1.89 | 7.39E-08 | 1.88 | 3.34E-11 |
| CXCL1 | 1.77 | 2.23E-05 | 1.99 | 1.01E-09 |
| HERC2P2 | 1.91 | 1.43E-05 | 1.83 | 7.23E-06 |
| DDX60 | 2.00 | 9.25E-05 | 1.71 | 0.00173779 |
| KDSR | 2.24 | 0.00026981 | 1.46 | 0.04911837 |
| TANC2 | 1.91 | 3.94E-05 | 1.78 | 4.19E-05 |
| AQP2 | 2.00 | 0.01103655 | 1.68 | 0.01988092 |
| TGFBR2 | 1.78 | 5.70E-05 | 1.89 | 3.30E-08 |
| SPIN1 | 1.91 | 7.88E-06 | 1.75 | 8.94E-06 |
| ACTR3 | 2.15 | 5.01E-08 | 1.48 | 9.37E-05 |
| WDR44 | 2.19 | 5.33E-06 | 1.44 | 0.0018751 |
| ANLN | 2.02 | 1.56E-06 | 1.61 | 2.01E-06 |
| RFTN1 | 1.05 | 0.00089351 | 2.56 | 2.80E-19 |
| MAPK1 | 1.88 | 3.95E-05 | 1.73 | 4.30E-05 |
| HIF1A | 2.14 | 8.62E-10 | 1.46 | 4.03E-05 |
| C1GALT1 | 2.28 | 3.91E-07 | 1.32 | 0.00528191 |
| PELI1 | 1.63 | 0.00072168 | 1.96 | 8.58E-06 |
| CD52 | 2.22 | 0.00045906 | 1.36 | 0.02894025 |
| FRAS1 | 1.99 | 0.00016886 | 1.58 | 0.00033629 |
| TECTA | 2.04 | 0.01270141 | 1.52 | 0.0412344 |
| ZNF365 | 1.58 | 0.02222138 | 1.98 | 0.00334685 |
| SLC7A2 | 1.96 | 4.79E-07 | 1.59 | 4.03E-05 |
| PCDHA5 | 1.68 | 0.0174196 | 1.87 | 0.00595536 |
| MOXD1 | 1.44 | 0.00403591 | 2.11 | 4.53E-05 |
| POF1B | 2.33 | 3.41E-08 | 1.22 | 0.00506172 |
| PKD1P4 | 2.13 | 0.00018805 | 1.40 | 0.00531868 |
| MEX3C | 2.21 | 0.00016597 | 1.33 | 0.01946777 |
| DNAJC6 | 2.05 | 3.97E-05 | 1.48 | 0.00315366 |
| DPYD | 1.49 | 0.00029787 | 2.04 | 1.02E-08 |
| NFKBIZ | 1.94 | 1.14E-05 | 1.58 | 0.00029272 |
| FAM230A | 2.03 | 0.00675486 | 1.50 | 0.03353584 |
| RBM12 | 1.92 | 5.91E-06 | 1.60 | 1.44E-05 |
| TP53BP2 | 2.10 | 3.59E-09 | 1.41 | 8.30E-05 |
| CKAP5 | 1.95 | 8.97E-08 | 1.55 | 3.58E-06 |
| EPHA6 | 1.63 | 0.030749 | 1.87 | 0.00843345 |
| RAB27B | 1.99 | 4.46E-05 | 1.51 | 0.0009716 |
| RGL1 | 1.85 | 1.56E-06 | 1.63 | 1.67E-05 |
| PANK3 | 1.94 | 9.18E-06 | 1.53 | 0.00016924 |

| | | | | |
|---|---|---|---|---|
| SGMS2 | 1.68 | 0.0011186 | 1.79 | 0.00055847 |
| GPR37 | 2.21 | 8.44E-06 | 1.26 | 0.02245843 |
| ZBTB39 | 2.03 | 1.17E-05 | 1.44 | 0.00304629 |
| TAF5L | 2.18 | 8.00E-07 | 1.28 | 0.0183487 |
| EFEMP1 | 1.05 | 0.00840131 | 2.41 | 2.25E-18 |
| PRDM6 | 1.57 | 0.03102303 | 1.89 | 0.00461459 |
| C3orf80 | 1.43 | 0.00081964 | 2.02 | 7.23E-06 |
| TRAM1 | 1.57 | 1.37E-05 | 1.89 | 5.40E-11 |
| SMC1A | 1.67 | 0.0002656 | 1.78 | 2.25E-05 |
| METTL14 | 1.99 | 0.00045534 | 1.45 | 0.001994 |
| SLC36A4 | 1.84 | 3.09E-05 | 1.60 | 0.00010978 |
| AKAP11 | 1.83 | 2.34E-05 | 1.61 | 0.00044338 |
| ZNF248 | 1.64 | 0.00036142 | 1.79 | 0.00015236 |
| EPHA5 | 1.50 | 0.00888385 | 1.93 | 0.00412931 |
| ADAM10 | 1.73 | 0.00027818 | 1.69 | 0.00016577 |
| SLC23A2 | 2.08 | 1.78E-07 | 1.35 | 0.00116367 |
| USP28 | 1.72 | 0.00010242 | 1.69 | 6.26E-05 |
| TM4SF20 | 1.46 | 1.15E-05 | -1.60 | 7.63E-08 |
| MUC5AC | 1.43 | 0.00025813 | -1.12 | 0.00271767 |
| PROC | 1.12 | 0.02541434 | -2.01 | 5.02E-09 |
| NPY4R | 2.12 | 8.90E-06 | 1.29 | 0.00341172 |
| LEMD3 | 1.75 | 1.51E-05 | 1.66 | 4.80E-05 |
| RB1 | 1.62 | 6.46E-05 | 1.78 | 1.88E-05 |
| AL512506.3 | 1.98 | 0.00424735 | 1.42 | 0.04710574 |
| CHI3L1 | 1.89 | 5.26E-10 | 1.50 | 5.09E-07 |
| PDZD8 | 1.85 | 2.83E-05 | 1.55 | 0.00027249 |
| GOLGA8A | 1.57 | 0.01667545 | 1.82 | 0.00268277 |
| ATP2A2 | 2.00 | 3.49E-06 | 1.38 | 0.00062602 |
| TMTC2 | 1.59 | 0.00027092 | 1.78 | 1.32E-05 |
| XPR1 | 1.89 | 4.23E-06 | 1.47 | 5.78E-05 |
| SCG2 | 1.14 | 0.01611426 | 2.23 | 8.87E-05 |
| PLCH1 | 1.73 | 1.48E-05 | 1.64 | 2.02E-05 |
| KIAA0895 | 1.73 | 0.00156298 | 1.63 | 0.00092255 |
| PAPSS2 | 1.80 | 1.29E-05 | 1.55 | 6.68E-06 |
| PSMC2 | 1.81 | 2.04E-05 | 1.52 | 0.00039665 |
| FBN2 | 2.09 | 2.06E-06 | 1.22 | 0.00269663 |
| PIGK | 1.91 | 0.00012533 | 1.37 | 0.00214594 |
| BTAF1 | 1.78 | 2.95E-05 | 1.50 | 0.00039001 |
| CNTN1 | 1.90 | 3.17E-06 | 1.38 | 0.00041699 |

| | | | | |
|---|---|---|---|---|
| SLC33A1 | 1.88 | 0.0001125 | 1.39 | 0.00719381 |
| CLPX | 1.76 | 5.21E-05 | 1.50 | 3.26E-06 |
| GPRIN3 | 2.25 | 1.62E-07 | 1.00 | 0.01565104 |
| ADAM17 | 1.87 | 8.05E-05 | 1.38 | 0.00345091 |
| CUL2 | 1.44 | 0.00060189 | 1.80 | 7.85E-07 |
| HERC1 | 1.67 | 7.35E-05 | 1.56 | 6.28E-05 |
| IKZF5 | 1.68 | 0.00136128 | 1.55 | 0.000529 |
| GNAI1 | 1.71 | 0.00012885 | 1.52 | 0.0001784 |
| PRR5L | 1.61 | 6.85E-06 | 1.61 | 1.00E-05 |
| CDON | 1.71 | 0.00045906 | 1.50 | 0.00282025 |
| SUSD6 | 1.68 | 0.00051219 | 1.54 | 0.00055847 |
| TRAF3IP3 | 1.90 | 0.00015533 | 1.32 | 0.01004266 |
| ZMYND11 | 1.66 | 2.91E-06 | 1.55 | 2.52E-06 |
| TIFA | 1.70 | 0.00091551 | 1.51 | 0.00285384 |
| PLA2G4A | 2.04 | 2.34E-05 | 1.16 | 0.00147895 |
| DOCK9 | 1.70 | 6.95E-05 | 1.50 | 9.80E-05 |
| ANO6 | 1.64 | 3.56E-06 | 1.55 | 8.94E-06 |
| MET | 1.75 | 2.89E-05 | 1.44 | 5.06E-05 |
| PCDHGB1 | 1.69 | 0.02297398 | 1.50 | 0.0385523 |
| PJA2 | 1.89 | 1.88E-08 | 1.29 | 0.00022004 |
| FNBP1L | 1.82 | 4.26E-05 | 1.36 | 0.00083952 |
| TSPAN1 | -1.18 | 0.00020628 | 1.39 | 1.45E-05 |
| PARG | 1.58 | 6.80E-05 | 1.60 | 2.93E-05 |
| PRKAR2B | 1.60 | 0.00435796 | 1.56 | 0.00169274 |
| SLC6A15 | 1.45 | 0.00809449 | 1.72 | 0.0014752 |
| PTPRG | 1.59 | 0.0018616 | 1.58 | 0.00203223 |
| OSBPL11 | 2.13 | 1.25E-06 | 1.04 | 0.01688645 |
| RNF19A | 2.05 | 3.28E-06 | 1.11 | 0.00866614 |
| AFF1 | 1.96 | 6.02E-05 | 1.19 | 0.0054431 |
| CPD | 1.96 | 2.33E-07 | 1.18 | 0.00126451 |
| ZKSCAN8 | 1.55 | 0.00148536 | 1.59 | 0.00072895 |
| HEG1 | 1.58 | 0.00148616 | 1.55 | 0.00058656 |
| ACVR1B | 2.06 | 2.25E-06 | 1.06 | 0.01462509 |
| TBCEL | 1.52 | 0.00262332 | 1.61 | 0.00181437 |
| SMARCAD1 | 1.82 | 3.46E-05 | 1.31 | 0.00268423 |
| JRKL | 1.70 | 0.00307845 | 1.42 | 0.01027377 |
| ACSL4 | 1.49 | 4.03E-05 | 1.62 | 2.85E-05 |
| ZNF217 | 1.77 | 8.10E-05 | 1.34 | 0.00027561 |
| KIRREL1 | 1.46 | 0.0007698 | 1.64 | 5.34E-05 |

| | | | | |
|---|---|---|---|---|
| TET3 | 1.71 | 0.00013829 | 1.40 | 0.00079057 |
| WWC2 | 1.61 | 0.00025052 | 1.48 | 0.00096851 |
| PRSS23 | 1.53 | 0.00011967 | 1.56 | 9.49E-07 |
| PLS1 | 1.60 | 5.01E-06 | 1.48 | 0.00154501 |
| FBXW2 | 1.60 | 0.00111717 | 1.48 | 0.00031028 |
| RIC1 | 1.71 | 0.00025576 | 1.37 | 0.0019501 |
| NSF | 1.76 | 5.39E-06 | 1.32 | 0.00063542 |
| HOOK1 | 1.37 | 0.0240106 | 1.71 | 0.00678307 |
| COL4A5 | 1.99 | 2.92E-06 | 1.09 | 0.02062202 |
| TSTD2 | 1.51 | 0.00080486 | 1.56 | 0.0003879 |
| ATP7A | 2.01 | 2.39E-05 | 1.05 | 0.01110018 |
| PDGFC | 1.00 | 0.03864907 | 2.06 | 8.94E-06 |
| CCNJ | 1.59 | 0.00403591 | 1.47 | 0.0014093 |
| AHR | 1.48 | 3.43E-05 | 1.57 | 9.82E-06 |
| FZD3 | 1.50 | 0.00267824 | 1.55 | 0.00114407 |
| IGF2R | 1.67 | 8.19E-05 | 1.37 | 0.00071188 |
| C4BPA | 1.63 | 0.00025264 | 1.42 | 0.00194575 |
| FBXO28 | 1.62 | 3.13E-05 | 1.42 | 0.00025441 |
| SPRY2 | 1.36 | 0.00105999 | 1.68 | 2.57E-05 |
| TMCC1 | 1.25 | 1.62E-05 | 1.79 | 2.53E-10 |
| MARCHF5 | 1.63 | 8.88E-05 | 1.40 | 3.98E-05 |
| CFI | 1.20 | 0.03854314 | 1.83 | 0.00244846 |
| AXIN2 | 1.46 | 0.01134396 | 1.56 | 0.0006119 |
| SERINC5 | 1.64 | 9.50E-06 | 1.38 | 0.0004731 |
| FZD6 | 1.73 | 1.14E-05 | 1.28 | 0.00148402 |
| TBC1D9 | 1.76 | 1.45E-05 | 1.25 | 0.00115667 |
| FBXO3 | 1.48 | 0.00094849 | 1.53 | 3.38E-05 |
| KIAA1109 | 1.71 | 0.0002261 | 1.29 | 0.00454364 |
| ST6GAL2 | 1.77 | 8.81E-05 | -2.04 | 4.30E-08 |
| CYTH3 | 1.52 | 0.0003096 | 1.48 | 8.35E-05 |
| GAPT | 1.88 | 0.00026015 | 1.12 | 0.03101592 |
| WDR3 | 1.50 | 0.0008012 | 1.49 | 0.00042904 |
| PHC3 | 1.43 | 0.00080382 | 1.56 | 0.00045654 |
| APP | 1.63 | 2.34E-05 | 1.36 | 3.19E-05 |
| STXBP5 | 1.50 | 0.0015078 | 1.48 | 0.00073413 |
| DNAJC10 | 1.85 | 6.02E-05 | 1.13 | 0.00412931 |
| TRRAP | 1.41 | 0.0017788 | 1.57 | 0.00013438 |
| ITGA6 | 1.75 | 1.14E-05 | 1.23 | 0.0007089 |
| EFR3A | 1.68 | 1.53E-05 | 1.30 | 0.00043173 |

| | | | | |
|---|---|---|---|---|
| FBXO34 | 1.69 | 4.35E-05 | 1.29 | 0.00031988 |
| CLASP1 | 1.75 | 7.75E-05 | 1.22 | 0.00412294 |
| RP2 | 1.84 | 3.81E-05 | 1.14 | 0.0126593 |
| NCEH1 | 1.53 | 0.00025268 | 1.44 | 1.18E-05 |
| PRDM10 | 1.54 | 0.00182089 | 1.43 | 0.00407801 |
| SEL1L | 1.66 | 3.20E-05 | 1.31 | 0.00111674 |
| FAT1 | 1.85 | 1.83E-06 | 1.12 | 0.00119182 |
| MFSD14A | 1.78 | 5.91E-06 | 1.19 | 0.00323837 |
| FAM156A | 1.68 | 6.13E-06 | 1.29 | 0.00779852 |
| ZNF300 | 1.65 | 0.01998072 | 1.32 | 0.04100114 |
| GABRB3 | 1.66 | 2.51E-06 | 1.30 | 0.0001055 |
| SOAT1 | 1.74 | 3.92E-05 | 1.22 | 0.00284784 |
| CAP2 | 1.65 | 0.00019559 | 1.31 | 0.00096489 |
| CRYBG3 | 1.70 | 0.01215739 | 1.26 | 0.04911802 |
| SLC35A5 | 1.88 | 5.13E-05 | 1.08 | 0.01712004 |
| NDST1 | 1.18 | 0.01137788 | 1.77 | 2.85E-05 |
| ZRANB1 | 1.67 | 0.0001211 | 1.27 | 0.00309807 |
| FUBP3 | 1.70 | 2.17E-05 | 1.25 | 0.00035387 |
| C18orf54 | 1.58 | 0.00174875 | 1.36 | 0.01902208 |
| TBX3 | 1.61 | 1.42E-05 | 1.31 | 4.88E-06 |
| BRMS1L | 1.55 | 0.00180447 | 1.38 | 0.0010237 |
| METAP1 | 1.62 | 0.00058526 | 1.31 | 0.00067044 |
| GSTCD | 1.43 | 0.00104144 | 1.49 | 0.00073413 |
| INTS2 | 1.91 | 4.63E-05 | 1.02 | 0.03083825 |
| AP3M1 | 1.66 | 7.04E-06 | 1.25 | 0.00016655 |
| TYROBP | 1.87 | 4.03E-05 | 1.04 | 0.03744584 |
| TXNRD1 | 1.81 | 7.88E-06 | 1.11 | 0.00230272 |
| FTO | 1.73 | 4.17E-05 | 1.18 | 0.00490646 |
| CBLL1 | 1.72 | 0.00013953 | 1.19 | 0.00404567 |
| FAM114A2 | 1.65 | 4.70E-05 | 1.26 | 0.00220293 |
| PCDHA4 | 1.65 | 0.00111092 | 1.26 | 0.0018131 |
| PLSCR4 | 1.52 | 0.00304375 | 1.38 | 0.01235687 |
| ZNF45 | 1.57 | 0.00016351 | 1.32 | 0.00417671 |
| KDM1B | 1.82 | 2.54E-05 | 1.08 | 0.01155112 |
| SPPL2A | 1.72 | 1.45E-06 | 1.17 | 0.00022726 |
| TIPARP | 1.18 | 0.00060814 | 1.71 | 3.57E-07 |
| BICRAL | 1.56 | 0.00020321 | 1.32 | 0.00235757 |
| RBBP4 | 1.53 | 1.12E-05 | 1.36 | 9.11E-05 |
| NTN4 | 1.58 | 7.02E-05 | 1.30 | 0.00092248 |

| | | | | |
|---|---|---|---|---|
| AP1G1 | 1.57 | 1.97E-05 | 1.32 | 0.00063542 |
| GLUD2 | 1.58 | 0.00298386 | 1.30 | 0.01960883 |
| SEMA3C | 1.51 | 8.10E-05 | 1.37 | 0.00092671 |
| BTBD3 | 1.53 | 0.00082613 | 1.35 | 0.00062199 |
| SLC35F2 | 1.46 | 0.00025005 | 1.41 | 0.00010685 |
| ALG10 | 1.62 | 0.00227963 | 1.25 | 0.02253047 |
| CLCN3 | 1.35 | 0.00083241 | 1.52 | 0.0001945 |
| MYOF | 1.58 | 8.96E-05 | 1.28 | 0.00077376 |
| BRPF3 | 1.73 | 6.47E-05 | 1.14 | 0.00762308 |
| PLSCR1 | 1.23 | 0.00436141 | 1.64 | 2.86E-08 |
| ARHGEF3 | 1.61 | 0.00015715 | 1.26 | 0.00455657 |
| SYBU | 1.48 | 0.00152566 | 1.38 | 0.00194575 |
| EFCAB14 | 1.59 | 0.00014121 | 1.28 | 0.00080836 |
| NNT | 1.64 | 1.56E-06 | 1.22 | 0.00091379 |
| TGFBR1 | 1.62 | 1.17E-05 | 1.24 | 0.00051945 |
| PFKFB2 | 1.45 | 0.00043821 | 1.42 | 0.00257424 |
| ADGRL3 | 1.34 | 0.00424735 | 1.51 | 0.00145243 |
| SDR42E1 | 1.66 | 0.00260051 | 1.20 | 0.03082551 |
| AHCTF1 | 1.44 | 0.00133996 | 1.41 | 0.00058179 |
| SIRT1 | 1.52 | 0.00036235 | 1.33 | 0.00096851 |
| TAF2 | 1.55 | 0.00038559 | 1.30 | 0.00203592 |
| IPO8 | 1.67 | 1.75E-05 | 1.18 | 0.00237398 |
| USP14 | 1.45 | 8.42E-06 | 1.39 | 3.87E-05 |
| EPB41L1 | 1.46 | 0.00026499 | 1.38 | 0.00011778 |
| VTA1 | 1.79 | 5.42E-08 | 1.06 | 0.0054957 |
| MTRR | 1.67 | 7.33E-05 | 1.17 | 0.00214166 |
| ACBD5 | 1.69 | 6.02E-05 | 1.15 | 0.00286589 |
| SMG8 | 1.63 | 0.00033358 | 1.21 | 0.00194381 |
| CLASP2 | 1.66 | 3.13E-05 | 1.18 | 0.0017758 |
| PFKFB3 | 1.61 | 3.01E-05 | 1.23 | 0.00127506 |
| CD109 | 1.76 | 2.50E-05 | 1.08 | 0.0054957 |
| CLINT1 | 1.67 | 1.82E-05 | 1.17 | 0.0010919 |
| WASF1 | 1.50 | 0.00067464 | 1.33 | 0.00057731 |
| ZBED4 | 1.50 | 0.0001989 | 1.33 | 0.00027546 |
| POLA1 | 1.63 | 1.48E-05 | 1.20 | 0.00211254 |
| HEATR1 | 1.50 | 3.00E-05 | 1.32 | 9.72E-05 |
| MAPK9 | 1.50 | 1.79E-05 | 1.32 | 0.00035516 |
| SOS2 | 1.53 | 0.00020908 | 1.28 | 0.00482148 |
| LRBA | 1.58 | 3.43E-05 | 1.23 | 0.00178847 |

| | | | | |
|---|---|---|---|---|
| PLB1 | 1.63 | 0.00418601 | 1.18 | 0.04775736 |
| GCNT1 | 1.45 | 0.01221969 | 1.36 | 0.01436727 |
| ACADM | 1.44 | 0.00010034 | 1.37 | 0.00204354 |
| TEAD1 | 1.55 | 0.00063748 | 1.26 | 0.00359083 |
| B3GALT5 | 1.61 | 0.00124227 | 1.19 | 0.04306656 |
| LARS2 | 1.44 | 0.00161838 | 1.36 | 0.00088111 |
| SEC24B | 1.50 | 0.00035734 | 1.30 | 0.00060736 |
| PLD5 | 1.75 | 0.0004199 | 1.05 | 0.02635239 |
| RNF44 | 1.62 | 0.00015321 | 1.17 | 0.00691969 |
| IDH3A | 1.49 | 3.62E-06 | 1.31 | 7.92E-06 |
| SMCR8 | 1.46 | 0.00259366 | 1.34 | 0.00373089 |
| RANBP6 | 1.68 | 0.00010566 | 1.11 | 0.01060503 |
| LMBR1 | 1.55 | 0.00030686 | 1.24 | 0.00017041 |
| IGSF3 | 1.59 | 0.0003833 | 1.20 | 0.00328501 |
| SCYL2 | 1.70 | 3.05E-06 | 1.08 | 0.00954928 |
| DUSP6 | 1.52 | 2.58E-05 | 1.26 | 0.00069175 |
| TMEM168 | 1.64 | 0.00027092 | 1.13 | 0.01199042 |
| UHRF1BP1 | 1.43 | 0.00029333 | 1.35 | 0.00091593 |
| SELENOT | 1.59 | 3.20E-06 | 1.19 | 0.00057008 |
| COMMD2 | 1.55 | 3.35E-05 | 1.23 | 0.0031561 |
| NCAPG2 | 1.55 | 6.34E-05 | 1.22 | 0.0001296 |
| KAT2B | 1.49 | 0.00282031 | 1.28 | 0.00719108 |
| PNMA8A | 1.11 | 0.00388099 | 1.66 | 5.09E-07 |
| GNA13 | 1.59 | 9.08E-06 | 1.18 | 0.00082805 |
| CACHD1 | 1.34 | 0.02072872 | 1.42 | 0.03818594 |
| PYGO1 | 1.31 | 0.01002733 | 1.45 | 0.00254082 |
| MMUT | 1.55 | 3.38E-05 | 1.21 | 0.0011116 |
| ERCC6L2 | 1.65 | 0.00228026 | 1.11 | 0.04882119 |
| DLD | 1.55 | 6.05E-05 | 1.21 | 0.00011434 |
| ABI1 | 1.68 | 6.50E-06 | 1.07 | 0.00325489 |
| CKAP2 | 1.53 | 1.43E-05 | 1.21 | 0.00102064 |
| GART | 1.50 | 8.98E-05 | 1.24 | 0.00047452 |
| PIGW | 1.39 | 0.00225914 | 1.35 | 0.00187787 |
| TMEM106B | 1.41 | 0.0007417 | 1.33 | 4.78E-05 |
| PEX2 | 1.72 | 0.00018805 | 1.02 | 0.01915912 |
| G3BP2 | 1.54 | 1.70E-05 | 1.20 | 0.00038912 |
| ME2 | 1.52 | 4.59E-05 | 1.21 | 0.00050941 |
| SNX30 | 1.51 | 0.0015804 | 1.22 | 0.00893719 |
| SH3RF1 | 1.39 | 0.00041479 | 1.34 | 5.34E-05 |

| | | | | |
|---|---|---|---|---|
| DTL | 1.35 | 8.77E-05 | 1.38 | 2.88E-06 |
| TNKS2 | 1.73 | 2.23E-05 | 1.00 | 0.00807901 |
| NCR3LG1 | 1.38 | 0.03012618 | 1.35 | 0.02856025 |
| ZNF436 | 1.60 | 0.00406471 | 1.12 | 0.03136327 |
| PHKA1 | 1.59 | 0.00110245 | 1.13 | 0.00358262 |
| KIFBP | 1.57 | 0.00040392 | 1.16 | 0.00120922 |
| WDR7 | 1.48 | 0.00062368 | 1.24 | 0.0047376 |
| ANKRD28 | 1.57 | 3.97E-05 | 1.15 | 0.0025499 |
| CDC6 | 1.29 | 0.0003269 | 1.43 | 8.03E-06 |
| SFMBT2 | 1.46 | 0.00381766 | 1.26 | 0.00766296 |
| HIPK1 | 1.47 | 0.00025229 | 1.24 | 0.00177417 |
| OXSR1 | 1.47 | 4.62E-05 | 1.23 | 0.00019108 |
| STARD4 | 1.08 | 0.01114616 | 1.62 | 0.0001883 |
| GATM | 1.27 | 0.00132185 | 1.44 | 0.00106969 |
| TNFRSF21 | 1.13 | 0.00184805 | 1.58 | 2.75E-07 |
| CCNT2 | 1.64 | 0.00020499 | 1.07 | 0.01491654 |
| NOTCH2 | 1.59 | 0.00040659 | 1.11 | 0.00767268 |
| FAM168B | 1.66 | 0.00012991 | 1.04 | 0.00563935 |
| TMEM184C | 1.33 | 0.00452324 | 1.38 | 0.00051338 |
| OCLN | 1.34 | 0.00215497 | 1.36 | 0.00118382 |
| SPTLC1 | 1.51 | 0.00055459 | 1.19 | 0.00178413 |
| DLAT | 1.50 | 0.00013647 | 1.20 | 0.00034203 |
| THAP10 | 1.18 | 0.01557165 | 1.52 | 0.00100021 |
| IFNGR2 | 1.48 | 0.00726889 | 1.21 | 0.01720321 |
| SLC38A2 | 1.52 | 2.66E-06 | 1.17 | 0.00038952 |
| ELOVL7 | 1.48 | 0.00026817 | 1.20 | 0.00723266 |
| C18orf25 | 1.46 | 0.00818259 | 1.22 | 0.00875286 |
| PRICKLE2 | 1.11 | 0.00040613 | 1.57 | 6.02E-06 |
| CAMSAP1 | 1.33 | 0.00015413 | 1.35 | 0.00054534 |
| MCCC2 | 1.32 | 0.00112859 | 1.36 | 3.12E-05 |
| CSGALNACT2 | 1.61 | 0.0009415 | 1.07 | 0.04058097 |
| CHST2 | 1.11 | 0.04681298 | 1.57 | 0.0060173 |
| CYP2U1 | 1.31 | 0.00633382 | 1.36 | 0.0015558 |
| MARS2 | 1.60 | 0.00375621 | 1.07 | 0.03316651 |
| SPIRE1 | 1.46 | 0.00083124 | 1.21 | 0.00402168 |
| TMEM260 | 1.43 | 0.00021068 | 1.25 | 0.00135403 |
| BUB1B | 1.29 | 0.00141029 | 1.38 | 0.00053409 |
| GASK1B | 1.09 | 0.01623353 | 1.58 | 0.00157767 |
| IFNAR1 | 1.55 | 0.00018211 | 1.11 | 0.00627779 |

| | | | | |
|---|---|---|---|---|
| PPM1D | 1.56 | 0.0005595 | 1.11 | 0.00377552 |
| SMAD2 | 1.62 | 9.08E-06 | 1.05 | 0.00140407 |
| STS | 1.28 | 0.00534586 | 1.39 | 0.00206924 |
| TSPYL4 | 1.24 | 0.00469912 | 1.42 | 0.00159806 |
| SLC18B1 | 1.40 | 0.00021685 | 1.26 | 0.00188585 |
| SOCS6 | 1.31 | 0.00027754 | 1.35 | 1.01E-05 |
| RAB2B | 1.58 | 0.00023928 | 1.08 | 0.00923454 |
| ZFP69 | 1.18 | 0.02273922 | 1.48 | 0.00528452 |
| PRKAR1A | 1.59 | 2.75E-05 | 1.07 | 0.00159806 |
| IARS1 | 1.45 | 0.00057551 | 1.20 | 0.00019108 |
| RCOR1 | 1.41 | 0.0009361 | 1.24 | 0.00129026 |
| C5orf22 | 1.55 | 0.00117524 | 1.10 | 0.00900396 |
| FIGNL1 | 1.49 | 0.0025187 | 1.16 | 0.01115616 |
| TRIM4 | 1.59 | 7.11E-05 | 1.06 | 0.00289957 |
| NEMP1 | 1.18 | 0.0045216 | 1.46 | 0.00055847 |
| KATNIP | 1.44 | 0.00026015 | 1.21 | 0.00227369 |
| PDP1 | 1.47 | 0.00240918 | 1.17 | 0.01812299 |
| MBLAC2 | 1.33 | 0.01167323 | 1.31 | 0.01071762 |
| POLR2B | 1.56 | 0.00089068 | 1.08 | 0.00085842 |
| PARM1 | 1.55 | 0.00109682 | 1.09 | 0.00475941 |
| KCTD9 | 1.49 | 0.0001145 | 1.15 | 0.00325905 |
| ATP9A | 1.11 | 0.00192422 | 1.53 | 3.34E-06 |
| FECH | 1.56 | 0.00049814 | 1.08 | 0.00321372 |
| TPD52L1 | 1.04 | 0.00790293 | 1.60 | 4.39E-08 |
| FCGR1A | 1.34 | 0.01549041 | 1.30 | 0.01457737 |
| SEC24D | 1.58 | 1.80E-05 | 1.06 | 0.00613707 |
| RHOU | 1.58 | 4.90E-06 | 1.05 | 0.00130912 |
| EIF4G2 | 1.53 | 5.99E-05 | 1.11 | 0.0002825 |
| STT3B | 1.50 | 3.28E-06 | 1.13 | 0.00026093 |
| TMEM30A | 1.34 | 0.00022275 | 1.29 | 5.65E-05 |
| UBE2G1 | 1.47 | 0.0002174 | 1.16 | 0.00116742 |
| ZNF146 | 1.39 | 0.00019431 | 1.24 | 0.00037773 |
| TRUB1 | 1.57 | 0.00016946 | 1.05 | 0.00751913 |
| TMEM19 | 1.54 | 4.14E-05 | 1.08 | 0.00255946 |
| CPEB4 | 1.31 | 0.00178684 | 1.31 | 0.00109081 |
| MAP3K21 | 1.23 | 0.00049161 | 1.39 | 2.57E-05 |
| NIPA2 | 1.30 | 0.00129765 | 1.32 | 4.80E-05 |
| TMEM87B | 1.41 | 0.00127394 | 1.21 | 0.00426629 |
| MAPK14 | 1.45 | 9.33E-05 | 1.17 | 0.00093524 |

| | | | | |
|---|---|---|---|---|
| TAF1A | 1.52 | 0.00909989 | 1.10 | 0.04982662 |
| PRSS12 | 1.58 | 0.00033433 | 1.04 | 0.03199649 |
| SDCBP | 1.43 | 2.55E-05 | 1.19 | 3.12E-05 |
| TSPAN13 | 1.39 | 0.0001223 | 1.23 | 0.0004695 |
| OGFOD1 | 1.33 | 0.00023962 | 1.28 | 0.00020589 |
| CCNT1 | 1.53 | 7.62E-05 | 1.08 | 0.00390482 |
| TGFB2 | 1.27 | 0.00061214 | 1.34 | 0.00012025 |
| HBS1L | 1.51 | 4.37E-05 | 1.10 | 0.00298325 |
| ETS2 | 1.50 | 0.00067393 | 1.11 | 0.00182942 |
| TKTL1 | 1.37 | 0.01803719 | 1.24 | 0.0240692 |
| ZNF367 | 1.38 | 0.0049699 | 1.22 | 0.01242096 |
| NBPF3 | 1.24 | 0.00304375 | 1.37 | 0.00109456 |
| OGT | 1.32 | 0.00049456 | 1.28 | 0.00023236 |
| ASB7 | 1.47 | 0.0008928 | 1.13 | 0.01568914 |
| PLS3 | 1.42 | 6.43E-05 | 1.17 | 0.00016026 |
| COL9A2 | 1.42 | 1.07E-05 | 1.18 | 0.00027249 |
| YTHDC2 | 1.47 | 0.00110544 | 1.13 | 0.00590039 |
| KIDINS220 | 1.43 | 0.00032496 | 1.16 | 0.00386691 |
| PARP4 | 1.56 | 0.00028218 | 1.04 | 0.0051961 |
| PTPN11 | 1.48 | 5.26E-05 | 1.11 | 0.00295132 |
| ST8SIA4 | 1.41 | 2.92E-05 | 1.18 | 0.00337726 |
| POGLUT3 | 1.28 | 0.00439832 | 1.31 | 0.00237398 |
| MRPL19 | 1.57 | 0.0002254 | 1.02 | 0.00545768 |
| HAVCR1 | 1.57 | 0.00056419 | 1.01 | 0.02019104 |
| UBR7 | 1.38 | 0.0002112 | 1.20 | 0.00114407 |
| ACADSB | 1.34 | 0.00018134 | 1.24 | 0.00046605 |
| NBEA | 1.28 | 0.00629997 | 1.30 | 0.01236034 |
| WDR26 | 1.41 | 9.77E-06 | 1.16 | 6.67E-05 |
| STX7 | 1.47 | 0.00267824 | 1.11 | 0.00642368 |
| DCK | 1.33 | 0.00693552 | 1.25 | 0.00183678 |
| RRN3 | 1.51 | 3.74E-05 | 1.06 | 0.00743648 |
| ABCC1 | 1.43 | 0.00014121 | 1.14 | 0.00451886 |
| MELK | 1.36 | 0.00072085 | 1.21 | 0.00157767 |
| FMC1-LUC7L2 | 1.09 | 0.049118 | 1.47 | 0.0042561 |
| GTF2H3 | 1.23 | 0.00289372 | 1.34 | 0.00083444 |
| SSX2IP | 1.38 | 0.00366284 | 1.18 | 0.01126965 |
| SRSF6 | 1.38 | 7.11E-05 | 1.18 | 0.00013686 |
| DDHD1 | 1.37 | 0.00016887 | 1.19 | 0.00323278 |
| CD14 | 1.60 | 4.83E-06 | -1.69 | 1.18E-08 |

| | | | | |
|---|---|---|---|---|
| RNFT1 | 1.41 | 0.00201683 | 1.15 | 0.01525805 |
| RNF14 | 1.47 | 0.00029697 | 1.09 | 0.0058296 |
| SLC25A40 | 1.39 | 0.00088681 | 1.17 | 0.01038525 |
| NID1 | 1.13 | 0.00057707 | 1.43 | 2.87E-05 |
| KIAA0586 | 1.51 | 6.39E-05 | 1.04 | 0.0113023 |
| FBXO30 | 1.47 | 0.0012943 | 1.08 | 0.01288654 |
| YWHAG | 1.41 | 3.77E-05 | 1.14 | 0.00016577 |
| RAB21 | 1.38 | 0.00051332 | 1.17 | 0.00707741 |
| PCNX4 | 1.39 | 5.70E-05 | 1.16 | 0.00089582 |
| OAT | 1.45 | 0.00164528 | 1.10 | 0.00231545 |
| PAPSS1 | 1.34 | 0.00050677 | 1.21 | 0.00019108 |
| PIP5K1A | 1.26 | 0.00334824 | 1.29 | 0.00071416 |
| FAN1 | 1.19 | 0.01526057 | 1.35 | 0.00324435 |
| PLAGL1 | 1.39 | 0.00180165 | 1.16 | 0.00889225 |
| VLDLR | 1.52 | 8.62E-06 | 1.03 | 0.00577121 |
| KIF23 | 1.35 | 1.76E-05 | 1.20 | 0.00011721 |
| NCOA4 | 1.40 | 0.00013533 | 1.15 | 0.0001584 |
| AGO4 | 1.38 | 0.00671558 | 1.17 | 0.02253748 |
| IRF2BP2 | 1.44 | 6.07E-05 | 1.11 | 0.00187429 |
| ZBTB6 | 1.38 | 0.01338335 | 1.16 | 0.02642548 |
| SKI | 1.44 | 0.00025961 | 1.11 | 0.00350117 |
| FAM3C | 1.17 | 0.00893692 | 1.37 | 2.24E-05 |
| HNRNPF | 1.35 | 0.00064476 | 1.18 | 0.00034515 |
| RAPGEF1 | 1.28 | 0.00276836 | 1.26 | 0.0030709 |
| MFN2 | 1.38 | 0.00105836 | 1.16 | 0.00470085 |
| ZNF862 | 1.18 | 0.01956023 | 1.35 | 0.00494126 |
| ITPRID2 | 1.35 | 0.00020628 | 1.19 | 0.0014752 |
| TPD52 | 1.38 | 0.0002938 | 1.15 | 0.0023914 |
| RACGAP1 | 1.41 | 0.00027495 | 1.13 | 0.00118382 |
| SLC19A2 | 1.21 | 0.020449 | 1.32 | 0.01684234 |
| MTMR4 | 1.26 | 0.00081383 | 1.26 | 0.0001528 |
| DMRTA2 | 1.20 | 0.01793707 | 1.33 | 0.0098189 |
| PLEKHA7 | 1.26 | 0.00588235 | 1.27 | 0.00138491 |
| USP38 | 1.31 | 0.00152753 | 1.21 | 0.00571283 |
| IMPA1 | 1.42 | 0.00083652 | 1.10 | 0.02321515 |
| UNC13B | 1.49 | 0.00034621 | 1.03 | 0.00654639 |
| CDK12 | 1.39 | 0.00012533 | 1.13 | 0.0011724 |
| GPRC5A | 1.36 | 0.00264779 | 1.16 | 0.00528124 |
| RECQL | 1.42 | 0.0005004 | 1.10 | 0.00763242 |

| | | | | |
|---|---|---|---|---|
| ROBO1 | 1.32 | 0.00228785 | 1.20 | 0.00540193 |
| TRIM68 | 1.43 | 0.0017665 | 1.09 | 0.01092548 |
| TECPR2 | 1.30 | 0.00049089 | 1.22 | 0.00392982 |
| NR1D2 | 1.39 | 0.00210038 | 1.12 | 0.01116962 |
| OSBP | 1.41 | 0.00022549 | 1.10 | 0.00071963 |
| ARNT | 1.28 | 0.01169139 | 1.24 | 0.00888684 |
| DDX3X | 1.31 | 0.00020542 | 1.21 | 0.00088758 |
| SLC39A14 | 1.33 | 0.00043927 | 1.18 | 0.00055847 |
| WWP1 | 1.36 | 0.00022251 | 1.15 | 0.00538652 |
| NLN | 1.19 | 0.00162758 | 1.32 | 0.00015791 |
| MYO5C | 1.15 | 0.00107501 | 1.36 | 9.44E-05 |
| LATS2 | 1.19 | 0.02437128 | 1.32 | 0.00398386 |
| FBXW8 | 1.20 | 0.00085924 | 1.31 | 0.00041448 |
| URB2 | 1.20 | 0.00540681 | 1.31 | 0.0018751 |
| DSC3 | 1.20 | 0.04786235 | 1.30 | 0.03629573 |
| TMED8 | 1.19 | 0.00123065 | 1.31 | 0.000529 |
| FZD8 | 1.11 | 0.0054702 | 1.39 | 0.00011343 |
| TGFA | 1.37 | 0.0073215 | 1.13 | 0.01750746 |
| RASSF2 | 1.10 | 0.00065111 | 1.39 | 2.95E-07 |
| MED23 | 1.48 | 0.00114565 | 1.01 | 0.03498725 |
| NSUN2 | 1.35 | 0.00161838 | 1.15 | 0.00055743 |
| OSMR | 1.48 | 0.00064138 | 1.01 | 0.00636921 |
| WEE1 | 1.32 | 0.0009608 | 1.17 | 0.00600694 |
| UBE3C | 1.25 | 0.00065815 | 1.24 | 0.00034515 |
| FASTKD5 | 1.47 | 0.00120667 | 1.02 | 0.00494183 |
| GPD1L | 1.42 | 0.0013494 | 1.06 | 0.00502833 |
| RABGAP1 | 1.44 | 4.93E-06 | 1.05 | 0.00126743 |
| USP10 | 1.41 | 1.42E-05 | 1.08 | 0.00126451 |
| SMARCC2 | 1.41 | 0.00021908 | 1.07 | 0.00534948 |
| ABHD17B | 1.47 | 0.00032655 | 1.01 | 0.00669817 |
| FAM168A | 1.32 | 0.00060993 | 1.16 | 0.00202362 |
| RNF38 | 1.32 | 0.00220535 | 1.16 | 0.00913685 |
| EXD2 | 1.29 | 0.00025052 | 1.19 | 0.00266723 |
| ITCH | 1.45 | 0.00021908 | 1.03 | 0.00564786 |
| SRD5A1 | 1.36 | 0.0029362 | 1.12 | 0.0060173 |
| CCDC85C | 1.36 | 0.0028305 | 1.12 | 0.01831651 |
| RNF146 | 1.34 | 0.00109236 | 1.13 | 0.01047299 |
| SH3D19 | 1.22 | 0.0017788 | 1.25 | 0.00026378 |
| KLHDC7A | 1.35 | 0.00341363 | 1.12 | 0.00500459 |

| | | | | |
|---|---|---|---|---|
| AMACR | 1.41 | 4.50E-05 | 1.07 | 0.00233802 |
| ZMIZ1 | 1.41 | 0.00061212 | 1.06 | 0.00651493 |
| TTYH3 | 1.37 | 0.0013265 | 1.10 | 0.00788763 |
| SHROOM3 | 1.19 | 0.00434842 | 1.28 | 0.00074607 |
| TOPBP1 | 1.22 | 0.00015894 | 1.24 | 0.00020656 |
| DTWD1 | 1.33 | 0.00056292 | 1.12 | 0.00544087 |
| BICC1 | 1.32 | 0.00011303 | 1.14 | 0.00073413 |
| FBXW11 | 1.22 | 0.0001145 | 1.23 | 0.0001296 |
| RNASE2 | 1.37 | 0.00110713 | 1.08 | 0.01023472 |
| TM9SF2 | 1.37 | 3.64E-05 | 1.09 | 0.00019475 |
| HORMAD1 | 1.38 | 0.0068325 | 1.08 | 0.0278183 |
| DHX32 | 1.17 | 0.00260051 | 1.28 | 0.00017498 |
| UBA6 | 1.27 | 0.02047696 | 1.18 | 0.02635401 |
| RBBP9 | 1.23 | 0.00097318 | 1.22 | 0.00025264 |
| TFRC | 1.27 | 0.00018805 | 1.18 | 0.00029571 |
| TEX2 | 1.22 | 0.00045649 | 1.23 | 0.00085243 |
| SLC25A13 | 1.32 | 0.00131801 | 1.13 | 0.00157168 |
| ARL6IP1 | 1.33 | 5.11E-07 | 1.11 | 0.0001296 |
| GZF1 | 1.31 | 0.00078553 | 1.14 | 0.00295486 |
| PRDX3 | 1.43 | 0.00391923 | 1.01 | 0.01047198 |
| ELL2 | 1.28 | 0.00024131 | 1.16 | 0.00160062 |
| PDE3B | 1.22 | 0.00604157 | 1.22 | 0.00811913 |
| KIF24 | 1.25 | 0.00513826 | 1.19 | 0.00308755 |
| DIS3 | 1.39 | 4.61E-05 | 1.05 | 0.00433172 |
| TM9SF3 | 1.41 | 0.00018788 | 1.03 | 0.00490646 |
| LIPA | 1.41 | 0.000333 | 1.03 | 0.00205993 |
| TAB2 | 1.34 | 0.00010289 | 1.10 | 0.00122803 |
| EXOC5 | 1.24 | 0.02224698 | 1.20 | 0.01850414 |
| RAB5A | 1.40 | 0.00048871 | 1.04 | 0.00272285 |
| UBA2 | 1.41 | 0.00045906 | 1.03 | 0.00189197 |
| SCAMP1 | 1.38 | 0.0002912 | 1.06 | 0.00299768 |
| RPA1 | 1.43 | 5.00E-05 | 1.01 | 0.00180546 |
| DCBLD2 | 1.06 | 0.00276004 | 1.38 | 6.33E-06 |
| RFX7 | 1.31 | 0.00174105 | 1.13 | 0.00604114 |
| ABLIM1 | 1.14 | 0.00021606 | 1.29 | 1.57E-05 |
| PPAT | 1.38 | 0.00075121 | 1.05 | 0.00937797 |
| TAF1 | 1.23 | 0.00877324 | 1.20 | 0.00650809 |
| LONRF1 | 1.34 | 0.00760416 | 1.09 | 0.03079451 |
| ADRA1D | 1.36 | 0.00010929 | 1.07 | 0.00298325 |

| | | | | |
|---|---|---|---|---|
| FAM210A | 1.22 | 0.00232796 | 1.20 | 0.00379872 |
| ADNP2 | 1.28 | 0.00071718 | 1.14 | 0.00198571 |
| ZMPSTE24 | 1.24 | 1.04E-05 | 1.18 | 0.00011992 |
| UPRT | 1.41 | 0.00525999 | 1.01 | 0.01216705 |
| SPRY4 | 1.28 | 0.00508729 | 1.14 | 0.02961204 |
| PPP1R3D | 1.33 | 0.00322928 | 1.08 | 0.01696209 |
| SLC38A1 | 1.23 | 6.90E-05 | 1.18 | 0.00018955 |
| ZNF319 | 1.38 | 0.00964617 | 1.02 | 0.03632908 |
| INCENP | 1.32 | 0.0016147 | 1.08 | 0.00588182 |
| WDFY3 | 1.29 | 0.00061318 | 1.11 | 0.00988172 |
| ZSCAN29 | 1.39 | 0.00114989 | 1.00 | 0.02525066 |
| CFL2 | 1.35 | 0.00066012 | 1.04 | 0.00198765 |
| RALGAPA2 | 1.22 | 0.00132768 | 1.17 | 0.00463959 |
| L2HGDH | 1.21 | 0.00199592 | 1.18 | 0.00264282 |
| SCN8A | 1.16 | 0.04740628 | 1.23 | 0.03514031 |
| PAXIP1 | 1.19 | 0.00168767 | 1.19 | 0.00160062 |
| GNG12 | 1.21 | 4.55E-05 | 1.18 | 0.00020656 |
| ZFP1 | 1.33 | 0.00126431 | 1.05 | 0.02188601 |
| CYB5R4 | 1.21 | 0.00713587 | 1.18 | 0.00947596 |
| SRR | 1.29 | 0.00110883 | 1.09 | 0.00136981 |
| RSU1 | 1.31 | 0.00043688 | 1.07 | 0.00183678 |
| SETD2 | 1.29 | 0.0003083 | 1.08 | 0.00241202 |
| SEPTIN8 | 1.21 | 0.00122125 | 1.16 | 0.00102798 |
| SSH1 | 1.35 | 0.00170681 | 1.02 | 0.01639318 |
| SGPP1 | 1.22 | 0.0065206 | 1.15 | 0.01155112 |
| ETV3 | 1.34 | 0.00333481 | 1.03 | 0.01193381 |
| KDM4A | 1.23 | 0.00029872 | 1.14 | 0.00038912 |
| UHRF1 | 1.05 | 0.00578067 | 1.31 | 2.20E-05 |
| RALGAPB | 1.28 | 0.00157941 | 1.09 | 0.00263413 |
| MCU | 1.33 | 0.00054415 | 1.04 | 0.0002904 |
| AP1S2 | 1.29 | 0.00015583 | 1.08 | 0.00294861 |
| FAM98B | 1.28 | 0.00042134 | 1.08 | 0.0018751 |
| DAPK1 | 1.22 | 0.00287433 | 1.15 | 0.00237398 |
| ADAR | 1.26 | 0.00056942 | 1.10 | 0.00192405 |
| ADGRA2 | 1.34 | 0.00040009 | 1.03 | 0.00742325 |
| SEC24A | 1.30 | 0.00067464 | 1.06 | 0.00526191 |
| TLCD4 | 1.33 | 0.00057234 | 1.02 | 0.01327353 |
| NFYB | 1.23 | 0.00127394 | 1.13 | 0.00646729 |
| IARS2 | 1.28 | 0.00082558 | 1.07 | 0.00052539 |

| | | | | |
|---|---|---|---|---|
| KLHL15 | 1.34 | 0.00284457 | 1.01 | 0.01609377 |
| SLC7A1 | 1.19 | 0.00151534 | 1.16 | 0.00206924 |
| POGK | 1.18 | 0.00081206 | 1.17 | 0.00124284 |
| LRRC57 | 1.34 | 0.0001987 | 1.01 | 0.01040772 |
| OCRL | 1.28 | 0.0015706 | 1.07 | 0.00464735 |
| YEATS2 | 1.26 | 0.0015946 | 1.09 | 0.00190799 |
| TRAF6 | 1.03 | 0.01514148 | 1.31 | 0.00206924 |
| QTRT2 | 1.14 | 0.00699327 | 1.20 | 0.00441594 |
| NRIP1 | 1.16 | 0.00187042 | 1.18 | 0.00098021 |
| ADSS2 | 1.33 | 0.00158541 | 1.01 | 0.00271767 |
| EID3 | 1.31 | 0.0097944 | 1.02 | 0.0327069 |
| RCBTB1 | 1.32 | 0.00104196 | 1.02 | 0.01421348 |
| TMED2 | 1.32 | 2.50E-05 | 1.01 | 0.00081208 |
| TAPT1 | 1.29 | 0.00501633 | 1.05 | 0.01702502 |
| WRN | 1.07 | 0.01798146 | 1.26 | 0.0054957 |
| MTR | 1.30 | 0.00070997 | 1.03 | 0.00942567 |
| AREL1 | 1.02 | 0.00575917 | 1.30 | 0.00011385 |
| PTPN1 | 1.20 | 0.00222889 | 1.13 | 0.00088646 |
| FBXO5 | 1.31 | 0.00024053 | 1.01 | 0.00969097 |
| CREBZF | 1.28 | 0.0021637 | 1.04 | 0.00594464 |
| NDC1 | 1.20 | 7.85E-05 | 1.12 | 0.00037383 |
| SLC49A4 | 1.29 | 0.00147329 | 1.03 | 0.01095165 |
| SNX18 | 1.11 | 0.00199434 | 1.21 | 0.00172031 |
| FAM107B | 1.26 | 1.48E-05 | 1.06 | 0.00019068 |
| CDC23 | 1.30 | 0.00018152 | 1.01 | 0.00124382 |
| MTM1 | 1.19 | 0.03778143 | 1.13 | 0.03084177 |
| ZNF740 | 1.23 | 0.00244857 | 1.08 | 0.00422168 |
| LIMD1 | 1.30 | 0.0017332 | 1.01 | 0.03127816 |
| RLF | 1.21 | 0.00017615 | 1.10 | 0.00290122 |
| DSG2 | 1.11 | 0.00166708 | 1.20 | 0.00079201 |
| GNG2 | 1.05 | 0.04021792 | 1.25 | 0.01417155 |
| LYPLA1 | 1.27 | 0.00021909 | 1.03 | 0.00253776 |
| MTARC2 | 1.09 | 0.02911926 | 1.22 | 0.00462223 |
| MBTD1 | 1.05 | 0.01459392 | 1.26 | 0.00470579 |
| VPS41 | 1.18 | 0.00652407 | 1.12 | 0.01037455 |
| SIK2 | 1.15 | 0.00148559 | 1.15 | 0.0007754 |
| LIMA1 | 1.15 | 0.00299346 | 1.14 | 0.00106969 |
| NADK2 | 1.11 | 0.00472317 | 1.19 | 0.0022159 |
| DDX20 | 1.26 | 0.00110713 | 1.04 | 0.00426973 |

| | | | | |
|---|---|---|---|---|
| LACTB2 | 1.24 | 1.15E-05 | 1.06 | 0.00086181 |
| ACTL6A | 1.22 | 0.00238413 | 1.07 | 0.00053275 |
| WDR36 | 1.26 | 0.00189872 | 1.03 | 0.00875273 |
| FAR1 | 1.20 | 0.00644082 | 1.09 | 0.00491245 |
| HGSNAT | 1.16 | 0.00177078 | 1.13 | 0.00160364 |
| SCRN1 | 1.20 | 0.00117746 | 1.08 | 0.00083952 |
| NSD2 | 1.09 | 0.00881068 | 1.19 | 0.00216473 |
| SYNGAP1 | 1.22 | 0.04688567 | 1.06 | 0.04840467 |
| SLC39A6 | 1.24 | 8.43E-05 | 1.04 | 0.00393643 |
| ACSL1 | 1.24 | 0.00168448 | 1.04 | 0.0028096 |
| MCMBP | 1.17 | 0.00058928 | 1.11 | 0.00046605 |
| NSMF | 1.25 | 0.00546195 | 1.03 | 0.0257783 |
| MORF4L1 | 1.27 | 0.00010164 | 1.00 | 0.00099697 |
| COL4A1 | 1.11 | 0.01305312 | 1.16 | 0.004328 |
| VEGFA | 1.03 | 0.01629257 | 1.24 | 0.00162316 |
| SHROOM2 | 1.03 | 0.03061974 | 1.24 | 0.03423855 |
| MMP24 | 1.07 | 0.02172795 | 1.20 | 0.00856526 |
| NDFIP2 | 1.23 | 0.00034695 | 1.04 | 0.00885672 |
| CSRNP2 | 1.15 | 0.00409248 | 1.12 | 0.00494726 |
| MAPK6 | 1.18 | 0.0008301 | 1.08 | 0.00465643 |
| UTP4 | 1.16 | 0.00190673 | 1.10 | 0.00781759 |
| VAPA | 1.27 | 9.35E-05 | 1.00 | 0.0011724 |
| PSME3 | 1.02 | 0.00663981 | 1.25 | 0.00040009 |
| GEMIN5 | 1.24 | 0.00076334 | 1.03 | 0.00225036 |
| ZBTB2 | 1.17 | 0.00871715 | 1.08 | 0.00809597 |
| SGPL1 | 1.15 | 0.002028 | 1.11 | 0.00099644 |
| KIAA1671 | 1.00 | 0.00468222 | 1.26 | 0.00089335 |
| ZNF664 | 1.21 | 0.00130524 | 1.05 | 0.00155693 |
| YPEL2 | 1.06 | 0.04776235 | 1.19 | 0.01410709 |
| CHEK1 | 1.02 | 0.00366048 | 1.23 | 0.0009859 |
| UBP1 | 1.22 | 0.00062642 | 1.02 | 0.0011144 |
| STAM | 1.17 | 0.00076366 | 1.08 | 0.00309184 |
| PPP4R1 | 1.18 | 0.00180383 | 1.06 | 0.00326864 |
| FASTKD3 | 1.21 | 0.03991144 | 1.03 | 0.02968078 |
| ARNTL2 | 1.18 | 0.00374194 | 1.06 | 0.01838159 |
| AGT | 1.18 | 0.00444571 | 1.06 | 0.0184649 |
| SEMA3A | 1.08 | 0.00758977 | 1.16 | 0.00806516 |
| CBX1 | 1.09 | 0.00152636 | 1.14 | 0.00019518 |
| TPBG | 1.18 | 0.00186045 | 1.05 | 0.00501433 |

| | | | | |
|---|---|---|---|---|
| WDR20 | 1.11 | 0.00081964 | 1.11 | 0.00228098 |
| EFL1 | 1.16 | 0.0005153 | 1.06 | 0.00028268 |
| MED17 | 1.16 | 0.0009308 | 1.06 | 0.00873124 |
| GLS | 1.07 | 0.00744331 | 1.15 | 0.00100473 |
| NEDD1 | 1.19 | 0.00448836 | 1.03 | 0.01463194 |
| PDE4B | 1.20 | 4.42E-05 | 1.01 | 0.00464966 |
| ZC3H7B | 1.18 | 0.00541397 | 1.03 | 0.00608665 |
| LAPTM5 | 1.09 | 0.00131632 | 1.12 | 0.00068926 |
| PDE12 | 1.19 | 0.00083002 | 1.03 | 0.0051834 |
| NSMAF | 1.13 | 0.0082299 | 1.08 | 0.00155238 |
| POLR1A | 1.20 | 0.00567414 | 1.01 | 0.01709113 |
| SMAD7 | 1.01 | 0.00966173 | 1.20 | 0.00120055 |
| METAP1D | 1.11 | 0.01796116 | 1.09 | 0.02346776 |
| TMPO | 1.11 | 0.00058588 | 1.09 | 0.00096813 |
| SLC30A9 | 1.19 | 0.00131915 | 1.01 | 0.01651705 |
| PIK3C2B | 1.00 | 0.02115694 | 1.19 | 0.00261919 |
| APPL2 | 1.07 | 0.00170448 | 1.12 | 0.00132059 |
| C11orf95 | 1.18 | 0.00381146 | 1.01 | 0.01408389 |
| EFR3B | 1.08 | 0.00111092 | 1.11 | 0.00157767 |
| PRKCA | 1.02 | 0.00354046 | 1.17 | 0.00060259 |
| RNF144A | 1.16 | 0.0019839 | 1.03 | 0.02159754 |
| DOK2 | 1.09 | 0.04374492 | 1.10 | 0.04974526 |
| ZDHHC9 | 1.10 | 0.00471859 | 1.08 | 0.00600236 |
| DPY19L4 | 1.16 | 0.01807882 | 1.01 | 0.02532986 |
| PTBP3 | 1.16 | 0.0015946 | 1.02 | 0.00192405 |
| SLC16A1 | 1.05 | 0.00223464 | 1.12 | 0.00101829 |
| ABHD2 | 1.10 | 0.0048178 | 1.07 | 0.00461404 |
| FRMD6 | 1.11 | 0.02864329 | 1.06 | 0.04862653 |
| XIAP | 1.13 | 5.69E-05 | 1.03 | 0.00512317 |
| POLR1C | 1.11 | 0.0167625 | 1.05 | 0.03004165 |
| GALNT10 | 1.00 | 0.00252324 | 1.15 | 0.00029616 |
| BRWD3 | 1.08 | 0.01621404 | 1.07 | 0.01886692 |
| TWNK | 1.02 | 0.0114262 | 1.12 | 0.00331258 |
| CDC27 | 1.05 | 0.00036209 | 1.10 | 0.00030264 |
| WSB1 | 1.11 | 0.00659554 | 1.03 | 0.00730177 |
| ANKS1A | 1.03 | 0.0222752 | 1.11 | 0.00364001 |
| KIF2A | 1.05 | 0.01842738 | 1.08 | 0.00541984 |
| NEURL1B | 1.07 | 0.00327133 | 1.07 | 0.00536958 |
| IGSF1 | 1.06 | 0.04115669 | 1.07 | 0.03940409 |

| | | | | |
|---|---|---|---|---|
| SUV39H2 | 1.12 | 0.01099916 | 1.01 | 0.01024976 |
| EAF1 | 1.06 | 0.00393494 | 1.06 | 0.00670324 |
| PHF2 | 1.10 | 0.01071181 | 1.02 | 0.00437511 |
| PRPS2 | 1.04 | 0.00366284 | 1.07 | 0.00147858 |
| FAM72B | 1.08 | 0.00439282 | 1.02 | 0.00700712 |
| AP3S2 | 1.05 | 0.00566222 | 1.05 | 0.00814757 |
| SPICE1 | 1.03 | 0.03959893 | 1.07 | 0.01565173 |
| RAVER2 | 1.00 | 0.01514099 | 1.10 | 0.00934246 |
| SPECC1L | 1.03 | 0.00150908 | 1.07 | 0.00075338 |
| ALDH3A2 | 1.03 | 0.00095962 | 1.06 | 0.00047214 |
| TENT4A | 1.05 | 0.01262678 | 1.04 | 0.00628854 |
| SLC22A3 | 1.00 | 0.00309431 | 1.08 | 0.00040966 |
| ZZEF1 | 1.05 | 0.00578067 | 1.03 | 0.00600004 |
| DOP1B | 1.04 | 0.03154561 | 1.04 | 0.02768165 |
| ZDHHC6 | 1.04 | 0.01098188 | 1.03 | 0.0007946 |
| SNX19 | 1.01 | 0.00370764 | 1.05 | 0.00137874 |
| AGO1 | 1.00 | 0.00583622 | 1.05 | 0.00392952 |
| TMEM192 | 1.01 | 0.00298352 | 1.04 | 0.00592642 |
| SLC9A6 | 1.03 | 0.00376319 | 1.01 | 0.00438827 |
| AGO2 | 1.02 | 0.00209749 | 1.00 | 0.00735953 |
| SNAP25 | 1.93 | 6.50E-06 | -1.16 | 0.00461936 |
| FOXS1 | -1.00 | 0.01048562 | -1.01 | 0.02092197 |
| OCEL1 | -1.03 | 0.00305529 | -1.00 | 0.00068332 |
| COPS9 | -1.02 | 0.00246808 | -1.02 | 0.00113194 |
| ELOVL6 | -1.05 | 0.00280019 | -1.00 | 0.00326864 |
| HOXD3 | -1.04 | 0.01945456 | -1.02 | 0.03484447 |
| DRAP1 | -1.04 | 0.0007926 | -1.03 | 0.00094537 |
| RSPH3 | -1.04 | 0.00583699 | -1.05 | 0.00450033 |
| RSPH9 | -1.00 | 0.02254926 | -1.09 | 0.01798782 |
| DPM3 | -1.03 | 0.00110713 | -1.08 | 0.0004519 |
| TMEM256 | -1.02 | 0.00295935 | -1.09 | 0.0010305 |
| PAM16 | -1.09 | 0.00055578 | -1.02 | 0.00100021 |
| AP1M2 | -1.07 | 0.00053574 | -1.05 | 0.0002838 |
| CCDC159 | -1.07 | 0.01970515 | -1.05 | 0.00874361 |
| CCR10 | -1.02 | 0.04344729 | -1.10 | 0.03705112 |
| POLL | -1.08 | 0.00103103 | -1.06 | 0.00021425 |
| PIN1 | -1.14 | 0.00026817 | -1.01 | 0.00067597 |
| DDX54 | -1.13 | 0.00094701 | -1.04 | 0.0019546 |
| CTR9 | -1.15 | 0.00834056 | -1.01 | 0.03225509 |

| | | | | |
|---|---|---|---|---|
| UPF3B | -1.14 | 0.00736862 | -1.02 | 0.02324195 |
| ZNF778 | -1.08 | 0.01942125 | -1.09 | 0.0171277 |
| SDF2L1 | -1.15 | 0.0010209 | -1.02 | 0.00124488 |
| WDR70 | -1.12 | 0.02644761 | -1.06 | 0.03459727 |
| ANKRD12 | -1.10 | 0.01217259 | -1.08 | 0.01284839 |
| DUSP28 | -1.02 | 0.0023424 | -1.16 | 0.000502 |
| WDR54 | -1.15 | 0.00160549 | -1.04 | 0.0008053 |
| RPS11 | -1.18 | 0.00060852 | -1.03 | 0.00164511 |
| SLC52A1 | -1.07 | 0.03190302 | -1.16 | 0.01995016 |
| EEF2 | -1.13 | 0.00104462 | -1.10 | 0.00086871 |
| WNT4 | -1.20 | 0.00838076 | -1.03 | 0.00593406 |
| NOP58 | -1.16 | 0.00714073 | -1.09 | 0.01478802 |
| KCNK6 | -1.05 | 0.0080077 | -1.20 | 0.0005184 |
| RPLP1 | -1.22 | 0.00020935 | -1.04 | 0.00090984 |
| CCDC174 | -1.18 | 0.00739976 | -1.08 | 0.01831489 |
| PCSK4 | -1.04 | 0.02043427 | -1.24 | 0.01649671 |
| FHOD1 | -1.24 | 4.46E-05 | -1.03 | 0.0006001 |
| NBL1 | -1.28 | 6.58E-05 | -1.00 | 0.00029976 |
| PPM1J | -1.20 | 0.00719364 | -1.09 | 0.02506484 |
| ABTB1 | -1.12 | 0.00096738 | -1.17 | 7.89E-05 |
| MTRNR2L11 | -1.27 | 0.00293727 | -1.02 | 0.01010276 |
| PQBP1 | -1.28 | 0.00026339 | -1.02 | 0.00166639 |
| EMILIN1 | -1.06 | 0.01961077 | -1.24 | 0.00597362 |
| AC009779.3 | -1.01 | 0.03190302 | -1.29 | 0.00855333 |
| PTRHD1 | -1.09 | 0.00124652 | -1.22 | 0.00017429 |
| ZNF791 | -1.04 | 0.00501579 | -1.27 | 0.00068471 |
| ZNF385A | -1.03 | 0.00468222 | -1.28 | 2.58E-05 |
| RPS14 | -1.26 | 0.00013897 | -1.06 | 0.00086567 |
| RPL22P1 | -1.18 | 0.00882569 | -1.14 | 0.00949726 |
| PRDX5 | -1.26 | 7.30E-05 | -1.06 | 0.00046871 |
| RPL13A | -1.28 | 0.00038954 | -1.04 | 0.00139072 |
| HSD17B8 | -1.11 | 0.00106867 | -1.21 | 0.00040426 |
| FBXL15 | -1.24 | 0.00057234 | -1.09 | 0.00112414 |
| EHBP1L1 | -1.27 | 0.00040244 | -1.06 | 0.00151746 |
| TMEM54 | -1.27 | 0.00011561 | -1.07 | 9.80E-05 |
| NME3 | -1.26 | 5.71E-05 | -1.07 | 0.00030336 |
| AKAP8L | -1.30 | 0.00014918 | -1.04 | 0.00127506 |
| DNAJC4 | -1.33 | 0.0004639 | -1.00 | 0.0025828 |
| RALA | -1.16 | 0.00507625 | -1.17 | 0.00197027 |

| | | | | |
|---|---|---|---|---|
| PRR5 | -1.26 | 0.00083124 | -1.07 | 0.00039995 |
| ARSA | -1.13 | 0.00188433 | -1.21 | 7.28E-05 |
| MOGS | -1.16 | 0.00084954 | -1.19 | 0.00066073 |
| RNFT2 | -1.26 | 0.01316983 | -1.09 | 0.02314404 |
| SLC2A11 | -1.27 | 0.00207348 | -1.09 | 0.00231744 |
| MTRNR2L1 | -1.32 | 0.0014471 | -1.04 | 0.00509702 |
| TAF3 | -1.31 | 0.00153562 | -1.05 | 0.01047775 |
| RHPN1 | -1.28 | 0.0007698 | -1.09 | 0.00084651 |
| EXOC3L1 | -1.15 | 0.04219499 | -1.21 | 0.02458122 |
| SNRPD2 | -1.36 | 0.00045043 | -1.02 | 0.00441594 |
| POLD4 | -1.09 | 0.00028874 | -1.29 | 7.23E-06 |
| TRAPPC12 | -1.19 | 0.00106251 | -1.18 | 0.00082805 |
| CHD7 | -1.21 | 0.01712386 | -1.16 | 0.0189871 |
| TGFB1I1 | -1.26 | 0.0005882 | -1.11 | 0.00021572 |
| RAB26 | -1.13 | 0.00315967 | -1.25 | 8.79E-05 |
| EIF5B | -1.10 | 0.01690975 | -1.28 | 0.00646067 |
| LRRC46 | -1.32 | 0.00142168 | -1.07 | 0.007294 |
| ZFPM1 | -1.32 | 0.0001511 | -1.07 | 0.00233229 |
| MVB12A | -1.20 | 0.0007417 | -1.19 | 4.42E-05 |
| SERGEF | -1.35 | 0.00127593 | -1.04 | 0.00980959 |
| SDSL | -1.23 | 0.00189872 | -1.17 | 0.00057107 |
| RRAS | -1.25 | 5.05E-05 | -1.14 | 7.98E-05 |
| PCED1A | -1.33 | 0.00082613 | -1.07 | 0.0018131 |
| EIF2B4 | -1.30 | 0.00022179 | -1.10 | 0.00084322 |
| CYFIP2 | -1.40 | 0.00013449 | -1.00 | 0.00549707 |
| MIB2 | -1.18 | 0.00171271 | -1.23 | 0.00018295 |
| PC | -1.13 | 0.00181202 | -1.28 | 0.0002904 |
| NDUFA3 | -1.40 | 0.00222701 | -1.00 | 0.02035504 |
| PSMG3 | -1.37 | 4.70E-05 | -1.04 | 0.00099357 |
| RABAC1 | -1.34 | 0.00019694 | -1.07 | 0.00053293 |
| KCTD14 | 1.75 | 0.00878133 | -1.40 | 0.00484629 |
| RPL3L | -1.21 | 0.00657814 | -1.20 | 0.00966738 |
| ZNF205 | -1.41 | 0.00025144 | -1.01 | 0.00392952 |
| MRNIP | -1.00 | 0.0072143 | -1.42 | 0.00367842 |
| AREG | -1.31 | 0.00064476 | -1.11 | 0.00223522 |
| THUMPD2 | -1.28 | 0.00441476 | -1.14 | 0.03380272 |
| OXLD1 | -1.37 | 0.0001125 | -1.06 | 0.00163255 |
| PMVK | -1.31 | 0.00014326 | -1.12 | 0.00022758 |
| TMSB10 | -1.18 | 0.00038843 | -1.25 | 8.47E-05 |

| | | | | |
|---|---|---|---|---|
| STX8 | -1.35 | 0.00259891 | -1.08 | 0.00528287 |
| FAM131A | -1.31 | 0.00060407 | -1.14 | 0.00264282 |
| POLE4 | -1.12 | 0.00106867 | -1.33 | 2.74E-05 |
| SLC39A4 | -1.38 | 0.0002143 | -1.07 | 0.00142598 |
| NFKBIE | -1.30 | 4.69E-05 | -1.15 | 3.97E-05 |
| C12orf45 | -1.16 | 0.00136735 | -1.30 | 0.00017289 |
| NKAPD1 | -1.37 | 0.00098959 | -1.09 | 0.01967946 |
| CENPS-CORT | -1.18 | 0.00546929 | -1.29 | 0.00220941 |
| SFTPB | -1.24 | 0.04690282 | -1.23 | 0.03705112 |
| TSPO | -1.47 | 1.36E-05 | -1.01 | 0.00061854 |
| PSPN | -1.40 | 4.97E-05 | -1.07 | 0.00440566 |
| NKAP | -1.38 | 0.00321568 | -1.10 | 0.0206723 |
| TMEM18 | -1.34 | 0.00114031 | -1.14 | 0.00228098 |
| NOP53 | -1.26 | 0.0001055 | -1.22 | 3.44E-05 |
| IRF3 | -1.44 | 0.00061214 | -1.04 | 0.00126743 |
| OBSCN | -1.01 | 0.00790293 | -1.47 | 6.28E-05 |
| CCAR1 | -1.39 | 0.00267824 | -1.09 | 0.01781119 |
| PLEKHN1 | -1.20 | 0.00275284 | -1.28 | 0.00055375 |
| LCN2 | -1.40 | 8.04E-05 | 1.40 | 2.47E-06 |
| NUDT22 | -1.45 | 0.00015849 | -1.04 | 0.00232633 |
| CTNNBL1 | -1.38 | 0.00072401 | -1.10 | 0.00822018 |
| SREK1 | -1.31 | 0.00290526 | -1.18 | 0.01419183 |
| DMAC1 | -1.33 | 0.00024053 | -1.16 | 0.00092917 |
| RASA4 | -1.18 | 0.00297531 | -1.31 | 0.00014338 |
| MED19 | -1.44 | 0.00052021 | -1.05 | 0.00425142 |
| CHKB | -1.29 | 0.00027327 | -1.21 | 0.00065958 |
| CCDC144A | -1.40 | 0.00458409 | -1.09 | 0.01608554 |
| CSF2RA | -1.17 | 0.04560669 | -1.33 | 0.00215278 |
| SIGIRR | -1.48 | 0.00033368 | -1.02 | 0.00462223 |
| CIR1 | -1.03 | 0.01890317 | -1.47 | 0.00198168 |
| IMP4 | -1.33 | 4.55E-05 | -1.18 | 6.17E-05 |
| TMUB1 | -1.47 | 0.00011574 | -1.04 | 0.00109471 |
| B3GNTL1 | -1.07 | 0.00324753 | -1.43 | 2.56E-06 |
| ARL6IP4 | -1.46 | 0.00014971 | -1.04 | 0.00364001 |
| ZNRD2 | -1.50 | 9.42E-05 | -1.01 | 0.00230465 |
| TRAPPC6A | -1.04 | 0.00139847 | -1.47 | 6.63E-07 |
| DUSP18 | -1.43 | 0.00155049 | -1.08 | 0.01688645 |
| TRIML2 | -1.43 | 0.00068556 | -1.08 | 0.01490406 |
| CDK5RAP2 | -1.13 | 0.00393494 | -1.39 | 6.77E-05 |

| | | | | |
|---|---|---|---|---|
| MAGIX | -1.49 | 5.67E-05 | -1.03 | 0.00807901 |
| AAK1 | -1.36 | 0.00659282 | -1.16 | 0.01159267 |
| MVD | -1.40 | 0.00018134 | -1.12 | 0.00014547 |
| PSMD13 | -1.46 | 1.21E-05 | -1.06 | 0.00101703 |
| MOV10 | -1.32 | 0.00137039 | -1.20 | 0.0022159 |
| GRAPL | -1.02 | 0.00511928 | -1.51 | 4.71E-05 |
| YIF1A | -1.48 | 0.00016887 | -1.04 | 0.00104681 |
| MISP3 | -1.23 | 0.00041037 | -1.30 | 9.16E-05 |
| NOL8 | -1.29 | 0.01244973 | -1.24 | 0.01405361 |
| CFAP251 | -1.20 | 0.00331352 | -1.33 | 0.00117002 |
| ETV2 | -1.46 | 0.00054448 | -1.08 | 0.00873851 |
| NDUFS6 | -1.51 | 7.30E-05 | -1.02 | 0.0041622 |
| PGF | -1.42 | 0.00033495 | -1.12 | 0.00652316 |
| EBF4 | -1.21 | 0.00974625 | -1.33 | 0.00105085 |
| SH3RF2 | -1.27 | 0.00162818 | -1.27 | 0.00072895 |
| KRT17 | -1.32 | 0.00477507 | -1.23 | 0.02133375 |
| FES | -1.18 | 0.00049092 | 1.37 | 2.10E-05 |
| GPATCH3 | -1.47 | 0.00029191 | -1.08 | 0.00101179 |
| COX5B | -1.18 | 0.00087701 | -1.37 | 2.87E-05 |
| ANXA11 | -1.50 | 6.27E-05 | -1.05 | 0.00304629 |
| CKB | -1.15 | 0.00139441 | -1.40 | 1.46E-05 |
| RBMX2 | -1.35 | 0.00210308 | -1.21 | 0.00582764 |
| MAN1B1 | -1.40 | 8.35E-05 | -1.16 | 0.00013729 |
| CCS | -1.32 | 0.0004456 | -1.24 | 4.78E-05 |
| EID2B | -1.13 | 0.00055459 | -1.43 | 1.46E-05 |
| FAM131C | -1.51 | 0.00016313 | -1.05 | 0.00258846 |
| LY6K | -1.09 | 0.04893149 | -1.47 | 0.00162214 |
| FAM174B | -1.37 | 0.0005175 | -1.19 | 0.00131604 |
| TRIM47 | -1.52 | 2.01E-06 | -1.05 | 0.00022015 |
| BLVRB | -1.08 | 0.00043968 | -1.49 | 1.37E-07 |
| CISD3 | -1.54 | 5.69E-05 | -1.04 | 0.0029109 |
| RSF1 | -1.35 | 0.00407327 | -1.22 | 0.01127336 |
| HMBS | -1.55 | 0.00321313 | -1.02 | 0.01353714 |
| KLHL18 | -1.49 | 7.54E-06 | -1.09 | 0.0010305 |
| ZCRB1 | -1.33 | 0.00448836 | -1.24 | 0.00841371 |
| SMAP1 | -1.39 | 0.00201642 | -1.18 | 0.0071308 |
| RAB11FIP2 | -1.41 | 0.00049207 | -1.17 | 0.01915912 |
| RPL8 | -1.44 | 6.14E-05 | -1.14 | 0.00034583 |
| RPS5 | -1.49 | 4.65E-05 | -1.09 | 0.00080778 |

| | | | | |
|---|---|---|---|---|
| ANKRD26 | -1.29 | 0.00652407 | -1.29 | 0.01318124 |
| LARP1B | -1.50 | 0.00134073 | -1.09 | 0.01110025 |
| CERS4 | -1.43 | 0.00038843 | -1.16 | 0.00111674 |
| SFI1 | -1.56 | 0.00077089 | -1.03 | 0.00766296 |
| REEP2 | -1.47 | 6.48E-05 | -1.12 | 0.00067884 |
| REEP6 | -1.49 | 0.00015789 | -1.10 | 0.00164284 |
| LRRC23 | -1.25 | 0.0018952 | -1.34 | 0.00011937 |
| IER5L | -1.35 | 6.08E-05 | -1.24 | 3.78E-05 |
| RP9 | -1.51 | 0.00091114 | -1.09 | 0.01239645 |
| TMEM141 | -1.43 | 6.05E-05 | -1.18 | 0.00034583 |
| BSG | -1.44 | 2.64E-05 | -1.16 | 7.04E-05 |
| PFDN5 | -1.36 | 0.00041351 | -1.24 | 0.00062748 |
| CDC34 | -1.46 | 7.35E-05 | -1.15 | 0.00038671 |
| NPW | -1.32 | 0.0017788 | -1.29 | 0.00415391 |
| PRPH | -1.61 | 1.14E-05 | -1.01 | 0.0196279 |
| ATIC | -1.28 | 0.00094333 | -1.34 | 0.00019106 |
| VPS51 | -1.47 | 0.0002643 | -1.15 | 0.00026378 |
| NDUFA11 | -1.55 | 5.02E-05 | -1.07 | 0.00142038 |
| ANKRD18A | -1.31 | 0.01733741 | -1.31 | 0.01276573 |
| TCEA2 | -1.37 | 0.00011057 | -1.25 | 7.19E-05 |
| ARL2 | -1.56 | 5.96E-05 | -1.06 | 0.00135465 |
| LAMA5 | -1.31 | 0.0001125 | -1.32 | 2.06E-05 |
| LIPE | -1.36 | 0.00053852 | -1.27 | 0.00011958 |
| ZNF296 | -1.47 | 3.14E-05 | -1.16 | 0.00023846 |
| YJEFN3 | -1.61 | 0.00073997 | -1.02 | 0.03540833 |
| NOL3 | -1.34 | 0.0009504 | -1.29 | 6.25E-05 |
| ATOX1 | -1.62 | 7.48E-05 | -1.02 | 0.00445268 |
| PDIA3P1 | -1.27 | 0.00869223 | -1.37 | 0.01531565 |
| DNLZ | -1.53 | 4.59E-05 | -1.11 | 0.00046747 |
| DOCK6 | -1.29 | 0.00166318 | -1.35 | 0.00012245 |
| ELP5 | -1.51 | 7.34E-05 | -1.13 | 0.00042178 |
| GID4 | -1.57 | 2.58E-05 | -1.07 | 0.00100473 |
| THAP4 | -1.36 | 8.81E-05 | -1.29 | 0.0001296 |
| RNF208 | -1.55 | 0.00089177 | -1.10 | 0.01782332 |
| NT5C | -1.30 | 8.73E-05 | -1.35 | 1.33E-05 |
| ZNF524 | -1.44 | 0.00019694 | -1.22 | 0.00032673 |
| HSPB1 | -1.49 | 9.33E-05 | -1.16 | 0.00035475 |
| Z97634.1 | -1.49 | 0.00200207 | -1.16 | 0.02439947 |
| STAG2 | -1.38 | 0.00234404 | -1.27 | 0.00179461 |

| | | | | |
|---|---|---|---|---|
| NAT14 | -1.53 | 8.02E-05 | -1.12 | 0.00073328 |
| UPF3A | -1.36 | 0.00060376 | -1.30 | 0.00067597 |
| C17orf49 | -1.46 | 3.49E-05 | -1.20 | 0.00016867 |
| FKBP2 | -1.53 | 0.00016307 | -1.13 | 0.00208583 |
| NDUFB11 | -1.55 | 9.82E-05 | -1.11 | 0.00116367 |
| RRP15 | -1.60 | 0.00017911 | -1.07 | 0.02099642 |
| SAXO2 | -1.24 | 0.03381847 | -1.43 | 0.01009349 |
| LAMTOR4 | -1.48 | 0.00016887 | -1.19 | 0.00069175 |
| ANKRD36C | -1.35 | 0.01832303 | -1.32 | 0.01540642 |
| DNPEP | -1.32 | 0.0002656 | -1.35 | 6.03E-06 |
| STK32C | -1.25 | 4.39E-05 | -1.43 | 5.60E-07 |
| SPHK1 | -1.51 | 8.10E-07 | -1.17 | 0.00018432 |
| RPL18 | -1.52 | 5.02E-05 | -1.16 | 0.00050075 |
| RASGRP2 | -1.35 | 0.00738795 | -1.33 | 0.00670787 |
| MAP9 | -1.37 | 0.00299645 | -1.31 | 0.00524304 |
| SPNS1 | -1.56 | 4.40E-05 | -1.12 | 0.00075876 |
| BOLA2B | -1.50 | 0.00028195 | -1.18 | 0.00243087 |
| ANTKMT | -1.52 | 3.18E-05 | -1.16 | 0.000342 |
| LSP1P4 | -1.36 | 0.0003096 | -1.33 | 5.72E-05 |
| TEN1 | -1.50 | 8.62E-05 | -1.18 | 0.00045654 |
| C11orf86 | -1.32 | 0.00015894 | -1.37 | 1.45E-05 |
| TAS1R3 | -1.28 | 0.04508299 | -1.41 | 0.0216353 |
| C19orf81 | -1.41 | 0.00014116 | -1.28 | 0.00025024 |
| RGS20 | -1.28 | 0.00082074 | -1.41 | 0.00010639 |
| WDR13 | -1.58 | 0.00014845 | -1.12 | 0.00236251 |
| FKBP8 | -1.55 | 0.00011682 | -1.15 | 0.00056083 |
| EML3 | -1.54 | 0.00019789 | -1.16 | 0.00038912 |
| BAZ1A | -1.38 | 0.00170008 | -1.33 | 0.00718042 |
| NRDE2 | -1.41 | 0.00041595 | -1.30 | 0.00120924 |
| HMGN5 | -1.45 | 0.00121789 | -1.26 | 0.00424001 |
| GPX4 | -1.51 | 3.36E-05 | -1.20 | 0.00014707 |
| TCF25 | -1.64 | 0.00011283 | -1.07 | 0.00236068 |
| NFIC | -1.71 | 0.00010164 | -1.00 | 0.00565671 |
| NDUFV1 | -1.60 | 7.34E-05 | -1.12 | 0.0007754 |
| ACSF2 | -1.40 | 0.00040464 | -1.32 | 0.00029467 |
| NUDT1 | -1.49 | 9.37E-05 | -1.23 | 0.00024768 |
| FAH | -1.60 | 3.57E-05 | -1.12 | 0.00065949 |
| UPK2 | -1.45 | 0.00221604 | -1.28 | 0.01249263 |
| UBE3A | -1.31 | 0.00966173 | -1.42 | 0.00565378 |

| | | | | |
|---|---|---|---|---|
| GLI4 | -1.35 | 0.00033692 | -1.38 | 6.32E-06 |
| CTIF | -1.58 | 0.00013532 | -1.15 | 0.00427124 |
| PSMB10 | -1.72 | 1.42E-05 | -1.02 | 0.00441692 |
| ATP2A1 | -1.68 | 0.00013358 | -1.07 | 0.01460514 |
| MYCBP2 | -1.47 | 0.0024609 | -1.28 | 0.01225616 |
| ZNF653 | -1.61 | 5.82E-06 | -1.14 | 0.00147079 |
| EIF2B5 | -1.56 | 0.00050764 | -1.20 | 0.01682656 |
| EXOSC4 | -1.67 | 3.03E-05 | -1.08 | 0.00117793 |
| CFD | -1.07 | 0.00238605 | -1.69 | 1.40E-08 |
| LIN7B | -1.36 | 0.00021606 | -1.39 | 6.14E-05 |
| GSTM1 | -1.22 | 0.01075315 | -1.53 | 0.00243864 |
| SHKBP1 | -1.52 | 0.00017587 | -1.24 | 2.70E-05 |
| RNF181 | -1.38 | 0.00022306 | -1.38 | 2.93E-05 |
| BARX1 | -1.00 | 0.00709043 | -1.76 | 3.15E-09 |
| PPDPF | -1.68 | 5.69E-05 | -1.08 | 0.00253809 |
| YIPF2 | -1.70 | 1.90E-05 | -1.06 | 0.00216861 |
| EGFL7 | -1.51 | 5.66E-05 | -1.26 | 0.0001148 |
| FAHD2B | -1.18 | 0.00026615 | -1.58 | 2.62E-08 |
| KRT86 | -1.06 | 0.00321568 | -1.71 | 2.47E-09 |
| RHCG | -1.12 | 0.01068064 | -1.65 | 6.51E-07 |
| NANOS3 | -1.71 | 0.00044111 | -1.06 | 0.03666796 |
| SPEF1 | -1.66 | 0.00060638 | -1.11 | 0.01858473 |
| SAR1A | -1.53 | 3.58E-05 | -1.24 | 0.00100473 |
| GPATCH11 | -1.32 | 0.01574051 | -1.46 | 0.00791233 |
| PTH1R | -1.53 | 0.00267824 | -1.26 | 0.01389897 |
| CCDC78 | -1.40 | 0.00409713 | -1.39 | 0.00289957 |
| MFSD3 | -1.52 | 8.53E-05 | -1.28 | 5.65E-05 |
| CNFN | -1.47 | 0.00055743 | -1.33 | 0.00027317 |
| CUTA | -1.58 | 8.21E-05 | -1.22 | 0.00024961 |
| MYG1 | -1.52 | 8.19E-05 | -1.28 | 0.00010762 |
| APRT | -1.67 | 4.59E-05 | -1.13 | 0.0011055 |
| KREMEN2 | -1.68 | 1.20E-05 | -1.13 | 0.00212523 |
| S100A1 | -1.48 | 0.00792116 | -1.32 | 0.0164959 |
| ZC3H6 | -1.60 | 0.00353214 | -1.20 | 0.03041995 |
| PAXX | -1.69 | 3.28E-05 | -1.11 | 0.00178425 |
| RALBP1 | -1.66 | 0.0001782 | -1.15 | 0.01388379 |
| AC024293.1 | -1.58 | 0.00137965 | -1.23 | 0.0249946 |
| PNPLA3 | -1.35 | 0.01047913 | -1.46 | 0.00470861 |
| ECSIT | -1.60 | 1.51E-05 | -1.21 | 0.00024699 |

| | | | | |
|---|---|---|---|---|
| MAP1LC3A | -1.55 | 2.95E-05 | -1.27 | 7.22E-05 |
| GPT | -1.42 | 0.01772896 | -1.39 | 0.0206723 |
| PPM1N | -1.29 | 0.00080486 | -1.53 | 6.30E-05 |
| ESF1 | -1.46 | 0.00077296 | -1.36 | 0.00533027 |
| WDR18 | -1.76 | 1.90E-05 | -1.06 | 0.00119916 |
| AC007342.3 | -1.48 | 0.02765847 | -1.34 | 0.04986605 |
| CEBPZ | -1.33 | 0.00088681 | -1.50 | 0.00139979 |
| MPST | -1.54 | 0.00012058 | -1.29 | 4.50E-05 |
| CCDC34 | -1.48 | 0.00258464 | -1.35 | 0.04246507 |
| EMC3-AS1 | -1.68 | 0.0002372 | -1.15 | 0.02324195 |
| MLXIPL | -1.20 | 0.00350697 | -1.63 | 9.98E-05 |
| ZNF354B | -1.64 | 0.00072871 | -1.19 | 0.00650082 |
| H2AJ | -1.55 | 2.27E-05 | -1.28 | 0.00012599 |
| CYSRT1 | -1.60 | 0.00148046 | -1.23 | 0.01221085 |
| AMDHD2 | -1.75 | 3.79E-05 | -1.09 | 0.00357597 |
| UPK3BL1 | -1.51 | 0.00055686 | -1.33 | 0.00104239 |
| RNF31 | -1.60 | 7.67E-05 | -1.24 | 0.00090887 |
| RPL9 | -1.55 | 6.33E-05 | -1.30 | 0.00063905 |
| ASL | -1.51 | 0.00032553 | -1.34 | 4.78E-05 |
| EIF3C | -1.81 | 9.76E-05 | -1.03 | 0.02188601 |
| ABCF1 | -1.66 | 0.00043968 | -1.18 | 0.00939543 |
| MAPK12 | -1.65 | 5.91E-06 | -1.20 | 0.00015452 |
| MRPL52 | -1.62 | 5.50E-05 | -1.23 | 0.00040736 |
| LSM7 | -1.72 | 6.13E-06 | -1.13 | 0.00169839 |
| VMO1 | -1.43 | 0.00165856 | -1.42 | 0.00330064 |
| PIEZO1 | -1.59 | 8.96E-05 | -1.26 | 0.00097775 |
| CHTF18 | -1.70 | 2.18E-06 | -1.16 | 0.00084435 |
| SEPTIN1 | -1.64 | 0.00015238 | -1.22 | 0.00143275 |
| UQCC2 | -1.52 | 6.24E-05 | -1.33 | 0.00016867 |
| YAF2 | -1.56 | 0.00204777 | -1.30 | 0.00776125 |
| ARPC1B | -1.72 | 2.26E-05 | -1.14 | 0.00774655 |
| GMPPA | -1.32 | 0.00040553 | -1.54 | 1.42E-07 |
| SIPA1 | -1.61 | 6.20E-05 | -1.26 | 0.00055847 |
| RPL13 | -1.58 | 4.95E-05 | -1.29 | 0.00010639 |
| TMEM91 | -1.43 | 0.00170008 | -1.44 | 0.00032115 |
| STXBP2 | -1.62 | 3.82E-05 | -1.25 | 0.0002325 |
| PTOV1 | -1.63 | 3.26E-05 | -1.25 | 0.00018832 |
| NDUFA4L2 | -1.07 | 0.02437128 | -1.80 | 6.28E-05 |
| DCTN1 | -1.51 | 7.11E-05 | -1.37 | 2.25E-05 |

| | | | | |
|---|---|---|---|---|
| FIBCD1 | -1.38 | 0.00049909 | -1.50 | 2.70E-06 |
| TDG | -1.61 | 0.00044036 | -1.28 | 0.00589972 |
| MAP2K2 | -1.73 | 6.05E-05 | -1.16 | 0.00080534 |
| KCNJ14 | -1.48 | 0.00299645 | -1.41 | 0.00129069 |
| NUDT18 | -1.45 | 0.00029933 | -1.44 | 9.80E-06 |
| MAP7D3 | -1.53 | 0.0007568 | -1.36 | 0.00146493 |
| TCIRG1 | -1.58 | 0.00010643 | -1.31 | 5.53E-05 |
| MMP17 | -1.76 | 4.63E-05 | -1.15 | 0.0010784 |
| MACROD1 | -1.43 | 0.00011595 | -1.48 | 4.42E-06 |
| ASPHD1 | -1.28 | 0.00027092 | -1.63 | 6.15E-08 |
| TTC39C | -1.11 | 0.00510664 | -1.81 | 1.40E-06 |
| LUC7L3 | -1.63 | 0.00050278 | -1.29 | 0.00611948 |
| GRIK5 | -1.44 | 0.00659215 | -1.48 | 0.01001928 |
| LCAT | -1.72 | 0.00021139 | -1.20 | 0.00549614 |
| SLC11A1 | -1.41 | 0.00713875 | -1.51 | 0.00136153 |
| TEX45 | -1.50 | 0.00366284 | -1.43 | 0.00383193 |
| ZBTB48 | -1.77 | 8.13E-05 | -1.16 | 0.00383193 |
| SYMPK | -1.72 | 1.53E-05 | -1.21 | 0.0008323 |
| CLPB | -1.47 | 7.11E-05 | -1.46 | 4.34E-06 |
| ZFHX2 | -1.59 | 9.22E-06 | -1.34 | 0.00182351 |
| PNKP | -1.60 | 0.0001108 | -1.34 | 8.55E-05 |
| MIF | -1.71 | 3.61E-05 | -1.22 | 0.00075393 |
| POLR2I | -1.74 | 4.06E-05 | -1.19 | 0.00121801 |
| AK8 | -1.67 | 5.29E-05 | -1.27 | 0.0047971 |
| NPAS1 | -1.35 | 0.00077791 | -1.58 | 1.45E-06 |
| KHK | -1.48 | 0.00012885 | -1.46 | 1.17E-05 |
| SHOC2 | -1.77 | 0.00035416 | -1.17 | 0.01086874 |
| PLPPR3 | -1.69 | 3.74E-05 | -1.26 | 0.00022182 |
| ETFB | -1.44 | 0.00022179 | -1.51 | 9.90E-06 |
| ZNF615 | -1.28 | 0.02983483 | -1.67 | 0.0034049 |
| CUL9 | -1.59 | 0.00034912 | -1.36 | 0.00062602 |
| PRPF40A | -1.30 | 0.00037242 | -1.66 | 9.20E-07 |
| DNMT1 | -1.79 | 0.0001399 | -1.17 | 0.00324925 |
| HES1 | -1.65 | 0.00016827 | -1.31 | 0.0011116 |
| ZNF581 | -1.48 | 5.67E-05 | -1.48 | 2.45E-06 |
| FAM207A | -1.69 | 4.63E-06 | -1.27 | 7.26E-05 |
| ROMO1 | -1.56 | 5.34E-05 | -1.41 | 5.56E-05 |
| CCDC25 | -1.67 | 0.00075471 | -1.30 | 0.00609314 |
| MESP1 | -1.76 | 1.51E-05 | -1.21 | 0.00045883 |

| | | | | |
|---|---|---|---|---|
| PEMT | -1.74 | 9.31E-05 | -1.23 | 0.00017942 |
| RPL13AP7 | -1.68 | 0.00083239 | -1.29 | 0.00650082 |
| BIRC7 | -1.08 | 0.01870902 | -1.90 | 1.08E-05 |
| KRT81 | -1.05 | 0.00096759 | -1.93 | 3.70E-12 |
| PHPT1 | -1.64 | 4.39E-05 | -1.35 | 0.00013561 |
| LRRC75B | -1.53 | 5.58E-05 | -1.46 | 2.51E-05 |
| BLOC1S1 | -1.57 | 7.48E-05 | -1.42 | 5.27E-05 |
| KPTN | -1.77 | 1.94E-05 | -1.22 | 5.65E-05 |
| FAM133B | -1.70 | 0.00049207 | -1.29 | 0.00960019 |
| SULT2B1 | -1.92 | 2.84E-07 | -1.07 | 0.00138491 |
| BSCL2 | -1.74 | 0.00014746 | -1.26 | 0.00206924 |
| RELB | -1.68 | 2.68E-08 | -1.32 | 2.51E-05 |
| FLNA | -1.79 | 3.58E-05 | -1.21 | 0.00214467 |
| CTU1 | -1.56 | 3.65E-05 | -1.44 | 3.36E-05 |
| SLC27A5 | -1.62 | 8.89E-05 | -1.38 | 0.00010429 |
| NENF | -1.69 | 1.58E-05 | -1.31 | 0.00013715 |
| RPL36 | -1.74 | 1.71E-05 | -1.27 | 0.00062604 |
| NOC4L | -1.79 | 1.76E-05 | -1.22 | 0.00039043 |
| ERV3-1 | -1.36 | 0.00054531 | -1.65 | 7.37E-05 |
| CCDC88B | -1.80 | 4.37E-05 | -1.21 | 0.00197769 |
| ADAMTSL3 | -1.77 | 0.00247045 | -1.24 | 0.03761963 |
| KRT83 | -1.50 | 1.43E-05 | -1.52 | 6.95E-06 |
| ALDH16A1 | -1.77 | 6.33E-05 | -1.25 | 0.00073328 |
| OAZ3 | -1.57 | 0.00145433 | -1.45 | 0.00216714 |
| ALKBH7 | -1.68 | 0.000112 | -1.34 | 0.0002842 |
| DDX49 | -1.86 | 9.50E-06 | -1.16 | 0.00210197 |
| METRN | -1.77 | 1.94E-05 | -1.25 | 0.00032854 |
| TREX1 | -1.66 | 0.00038599 | -1.36 | 0.00140766 |
| NDUFS8 | -1.82 | 2.43E-05 | -1.20 | 0.00106066 |
| ESPN | -1.60 | 0.00214975 | -1.42 | 0.01469608 |
| PTGDS | -1.32 | 0.00799742 | -1.70 | 0.00011124 |
| GALK1 | -1.72 | 3.35E-05 | -1.30 | 0.00012652 |
| ATAD3B | -1.82 | 0.00010289 | -1.21 | 0.00562594 |
| PPP2R3B | -1.46 | 4.03E-05 | -1.56 | 1.09E-06 |
| HCFC1R1 | -1.70 | 6.17E-05 | -1.32 | 0.00032783 |
| GGT1 | -1.56 | 6.34E-05 | -1.47 | 5.19E-06 |
| FDXR | -1.58 | 3.49E-05 | -1.45 | 2.71E-06 |
| POLR3G | -1.47 | 0.00053646 | -1.57 | 0.00049568 |
| EMP3 | -1.70 | 2.27E-05 | -1.34 | 3.04E-05 |

| | | | | |
|---|---|---|---|---|
| TINAGL1 | -1.52 | 0.0220529 | -1.52 | 0.02539407 |
| DDX24 | -1.87 | 0.0002656 | -1.17 | 0.01616176 |
| ABCA7 | -1.59 | 0.00024178 | -1.46 | 2.74E-05 |
| SART1 | -1.72 | 5.99E-05 | -1.33 | 0.00089043 |
| RPSAP8 | -1.81 | 0.00148073 | -1.25 | 0.01461945 |
| AC008982.1 | -1.70 | 0.00063223 | -1.35 | 0.01463194 |
| RECQL4 | -1.98 | 3.89E-06 | -1.08 | 0.00517925 |
| TRIM72 | -1.63 | 0.0012281 | -1.43 | 0.0042261 |
| MTRNR2L10 | -1.58 | 6.71E-05 | -1.48 | 0.00093689 |
| GET4 | -1.78 | 3.79E-05 | -1.29 | 0.00025441 |
| COL6A1 | -1.34 | 0.00050677 | -1.72 | 8.37E-07 |
| RNASEH2C | -1.73 | 1.19E-05 | -1.34 | 8.97E-05 |
| AURKAIP1 | -1.81 | 1.00E-05 | -1.26 | 0.00043889 |
| TMEM190 | -1.41 | 0.0223327 | -1.66 | 0.00405034 |
| C12orf57 | -1.65 | 3.42E-06 | -1.42 | 1.06E-05 |
| NUDT8 | -1.76 | 5.82E-05 | -1.32 | 0.00019106 |
| ANKRD18B | -1.68 | 0.00046943 | -1.40 | 0.0024534 |
| SLC22A18 | -1.44 | 0.00399763 | -1.64 | 5.45E-06 |
| CHCHD5 | -1.39 | 0.00013482 | -1.70 | 1.68E-07 |
| ZFAND2B | -1.68 | 1.72E-05 | -1.41 | 1.43E-05 |
| DTNB | -1.79 | 0.00020753 | -1.30 | 0.00292298 |
| SPC24 | -1.68 | 4.72E-05 | -1.41 | 1.40E-05 |
| UNC13D | -1.62 | 7.59E-09 | -1.47 | 4.78E-08 |
| PGPEP1 | -2.00 | 1.71E-05 | -1.09 | 0.00482944 |
| ASPSCR1 | -1.92 | 2.50E-05 | -1.18 | 0.00070784 |
| BRD9 | -1.93 | 4.17E-05 | -1.17 | 0.00477365 |
| GSTO2 | -1.39 | 0.0002112 | -1.71 | 1.18E-05 |
| NDUFS7 | -1.88 | 1.43E-05 | -1.23 | 0.00070176 |
| CBR3 | -1.29 | 0.00052764 | -1.82 | 9.84E-08 |
| ABCB6 | -1.36 | 0.00040244 | -1.76 | 9.90E-08 |
| MCRIP2 | -2.00 | 1.27E-05 | -1.12 | 0.00317161 |
| ARID4A | -1.64 | 5.63E-05 | -1.48 | 0.00106969 |
| ULK2 | -1.97 | 6.25E-07 | -1.16 | 0.00053594 |
| DLGAP1 | -1.75 | 0.01344155 | -1.38 | 0.04703066 |
| MRPL12 | -1.97 | 4.00E-06 | -1.16 | 0.00169489 |
| MICOS13 | -1.76 | 2.34E-05 | -1.37 | 0.00014126 |
| NDUFB7 | -1.79 | 1.37E-05 | -1.35 | 0.00024666 |
| RRP7A | -1.90 | 4.40E-06 | -1.24 | 0.00018672 |
| ERFL | -1.61 | 0.00777352 | -1.54 | 0.00829625 |

| | | | | |
|---|---|---|---|---|
| EIF4EBP1 | -1.89 | 1.06E-05 | -1.26 | 0.0005301 |
| NOSIP | -1.84 | 1.15E-05 | -1.33 | 0.00013241 |
| RNPEPL1 | -1.59 | 3.62E-05 | -1.58 | 1.10E-06 |
| ENTPD8 | -1.95 | 9.35E-05 | -1.23 | 0.03507888 |
| CDYL | -1.81 | 0.00050855 | -1.37 | 0.00534552 |
| HAGHL | -1.66 | 4.06E-05 | -1.52 | 7.09E-06 |
| REX1BD | -1.82 | 5.91E-06 | -1.37 | 0.00011102 |
| AKAP7 | -1.91 | 2.20E-05 | -1.28 | 0.01188924 |
| MRPL23 | -1.91 | 1.27E-05 | -1.28 | 0.00072744 |
| AC011448.1 | -1.73 | 8.76E-05 | -1.47 | 0.00046605 |
| POLD1 | -2.00 | 3.48E-06 | -1.19 | 0.00262052 |
| NTHL1 | -1.67 | 9.33E-05 | -1.52 | 7.38E-06 |
| GSDMD | -1.75 | 2.67E-05 | -1.46 | 4.78E-05 |
| CATIP | -1.15 | 0.03405882 | -2.06 | 7.42E-07 |
| VAX1 | -1.90 | 1.01E-05 | -1.31 | 0.00222191 |
| INHBE | -1.17 | 0.03429871 | -2.05 | 3.94E-05 |
| GLB1L3 | -1.76 | 0.00627147 | -1.46 | 0.03549699 |
| EVI5 | -1.57 | 0.00429323 | -1.65 | 5.17E-05 |
| DPP7 | -1.95 | 1.48E-05 | -1.27 | 0.00083444 |
| TSGA10 | -1.56 | 0.01712386 | -1.67 | 0.00642636 |
| METTL27 | -1.53 | 2.78E-05 | -1.71 | 2.62E-07 |
| FXYD5 | -1.92 | 1.20E-05 | -1.32 | 0.00028176 |
| INTS1 | -1.91 | 1.08E-05 | -1.33 | 0.00040312 |
| RDM1P5 | -1.93 | 9.82E-05 | -1.33 | 0.00358262 |
| ANKRD36B | -1.56 | 0.0063019 | -1.71 | 0.00319911 |
| MYOG | -1.81 | 0.02775172 | -1.45 | 0.04852796 |
| NUDT14 | -1.69 | 1.17E-05 | -1.58 | 4.08E-06 |
| AL928654.3 | -1.71 | 0.00062134 | -1.56 | 0.00073413 |
| PRSS3 | -1.58 | 2.31E-06 | -1.69 | 6.15E-08 |
| SMIM24 | -1.66 | 0.03076723 | -1.61 | 0.02715805 |
| PPIG | -1.54 | 0.00028874 | -1.73 | 0.00016026 |
| RPL24P4 | -1.74 | 0.00228139 | -1.54 | 0.01436727 |
| LMBRD2 | -2.07 | 1.07E-05 | -1.21 | 0.0195257 |
| CYBA | -1.86 | 4.76E-06 | -1.42 | 5.68E-05 |
| AK9 | -1.75 | 0.00095962 | -1.53 | 0.01028164 |
| H2AC20 | -1.75 | 2.37E-05 | -1.54 | 0.0004859 |
| KMO | -1.84 | 0.00482017 | -1.44 | 0.03084177 |
| AD000671.1 | -1.85 | 0.00044107 | -1.44 | 0.00147908 |
| TSSC4 | -1.91 | 1.42E-05 | -1.39 | 4.46E-05 |

| | | | | |
|---|---|---|---|---|
| RPS3AP20 | -1.75 | 0.0017665 | -1.55 | 0.00321372 |
| CEP164 | -2.03 | 2.04E-05 | -1.28 | 0.00229732 |
| RPS28 | -1.85 | 3.37E-05 | -1.46 | 0.00011494 |
| TNNC1 | -1.80 | 1.01E-05 | -1.51 | 7.22E-05 |
| KNOP1 | -1.99 | 6.90E-05 | -1.32 | 0.00452956 |
| GAMT | -1.93 | 1.35E-05 | -1.38 | 0.00013409 |
| HSD17B14 | -1.45 | 1.70E-05 | -1.87 | 1.61E-10 |
| CATSPER1 | -1.70 | 0.00023775 | -1.61 | 9.16E-05 |
| F12 | -1.72 | 1.14E-05 | -1.60 | 6.71E-07 |
| MAP3K6 | -1.74 | 0.00017409 | -1.58 | 9.26E-05 |
| SNX8 | -1.92 | 6.50E-06 | -1.41 | 1.28E-05 |
| INF2 | -1.88 | 4.93E-06 | -1.47 | 2.27E-05 |
| AC122718.1 | -1.81 | 0.01392804 | -1.53 | 0.03180621 |
| CCDC66 | -2.08 | 6.41E-05 | -1.26 | 0.01001609 |
| RPS9 | -1.76 | 5.33E-06 | -1.59 | 8.37E-07 |
| POTEC | -1.69 | 0.0005093 | -1.66 | 0.00237398 |
| CPSF1 | -1.88 | 3.56E-06 | -1.47 | 7.46E-05 |
| RPL18A | -1.90 | 9.83E-06 | -1.46 | 3.97E-05 |
| ELOB | -1.95 | 1.05E-05 | -1.41 | 0.00019867 |
| NAA38 | -1.78 | 3.28E-05 | -1.58 | 1.66E-05 |
| FAAP20 | -1.92 | 6.69E-06 | -1.45 | 3.35E-05 |
| CCDC167 | -1.92 | 2.36E-06 | -1.45 | 4.23E-05 |
| ADGRB1 | -1.89 | 0.00032964 | -1.48 | 0.00959623 |
| DKC1 | -2.06 | 4.40E-05 | -1.31 | 0.00516291 |
| CACNA1A | -1.94 | 6.48E-05 | -1.43 | 0.00676903 |
| PXDN | -2.01 | 7.26E-07 | -1.36 | 0.00053409 |
| IGFL1 | -2.11 | 2.50E-08 | -1.27 | 0.00548433 |
| HAMP | -1.89 | 0.00720221 | -1.48 | 0.03898641 |
| IL3RA | -1.55 | 0.00321301 | -1.83 | 6.81E-05 |
| PARD3B | -1.89 | 0.00012323 | -1.49 | 0.00338127 |
| COL6A2 | -1.54 | 1.32E-05 | -1.85 | 2.09E-09 |
| ZNF593 | -1.91 | 1.66E-05 | -1.49 | 8.05E-05 |
| ACP7 | -1.83 | 0.01789812 | -1.57 | 0.03233539 |
| POLR1G | -2.38 | 1.56E-06 | -1.03 | 0.03410363 |
| AP2S1 | -2.06 | 1.33E-05 | -1.34 | 0.00056161 |
| LRRC24 | -1.63 | 0.00077089 | -1.78 | 7.87E-06 |
| TMEM265 | -1.91 | 4.00E-06 | -1.50 | 0.0001945 |
| MYLPF | -1.95 | 0.00386173 | -1.47 | 0.0369282 |
| HES4 | -1.65 | 1.73E-06 | -1.77 | 1.63E-10 |

| | | | | |
|---|---|---|---|---|
| FAM174C | -1.93 | 8.06E-06 | -1.49 | 3.78E-05 |
| NAPRT | -1.19 | 0.01386427 | -2.23 | 5.09E-07 |
| C4orf48 | -2.10 | 5.67E-06 | -1.32 | 0.00084322 |
| FAM133CP | -1.97 | 0.0057976 | -1.46 | 0.03996255 |
| TCTEX1D4 | -1.56 | 0.03288982 | -1.87 | 0.00589119 |
| GGT5 | -1.26 | 0.02547022 | -2.18 | 2.62E-07 |
| ARHGDIG | -2.16 | 9.87E-07 | -1.27 | 0.0010961 |
| RICTOR | -1.67 | 2.50E-05 | -1.77 | 3.58E-06 |
| COL20A1 | -2.03 | 0.00185625 | -1.42 | 0.04150181 |
| ITK | -1.85 | 0.00676743 | -1.60 | 0.01453499 |
| USP9YP4 | -1.97 | 0.0158592 | -1.49 | 0.04505141 |
| SCN5A | -2.13 | 7.67E-05 | -1.33 | 0.04505141 |
| IRF7 | -2.13 | 0.00014845 | -1.33 | 0.0241807 |
| JAK3 | -1.62 | 0.00048026 | -1.86 | 3.81E-06 |
| UQCC3 | -2.08 | 4.93E-06 | -1.40 | 0.00030202 |
| MAP1S | -2.00 | 9.22E-06 | -1.48 | 0.00016655 |
| IYD | -1.92 | 0.01258222 | -1.57 | 0.03362292 |
| BCL7C | -2.02 | 1.88E-06 | -1.46 | 2.96E-05 |
| AL162231.1 | -1.96 | 6.02E-06 | -1.53 | 0.00014918 |
| CLDND2 | -1.55 | 0.00114565 | -1.94 | 2.60E-06 |
| LAMC3 | -1.56 | 0.00043968 | -1.94 | 3.28E-05 |
| SEC14L6 | -1.84 | 0.00501579 | -1.66 | 0.00581912 |
| PLXNB3 | -1.93 | 0.00032104 | -1.57 | 0.01200646 |
| CX3CL1 | -2.08 | 0.00016582 | -1.43 | 0.01947393 |
| EDN2 | -1.64 | 0.00067436 | -1.90 | 0.00013509 |
| NELFE | -1.81 | 4.27E-05 | -1.73 | 7.95E-06 |
| CHRNA1 | -2.14 | 0.00849262 | -1.41 | 0.04673231 |
| INAFM1 | -1.84 | 4.59E-05 | -1.71 | 1.90E-06 |
| GPR85 | -1.99 | 3.35E-05 | -1.56 | 0.00556287 |
| IGFBP6 | -2.13 | 5.64E-07 | -1.43 | 5.65E-05 |
| MAFB | -1.88 | 0.00171423 | -1.68 | 0.00928085 |
| GSTM2 | -1.45 | 0.0003096 | -2.12 | 1.69E-08 |
| RPS3AP21 | -1.87 | 0.00444613 | -1.69 | 0.00915765 |
| PNPLA6 | -2.04 | 1.05E-05 | -1.54 | 5.06E-05 |
| PERM1 | -1.90 | 6.41E-05 | -1.68 | 0.00021455 |
| EMILIN3 | -1.57 | 0.02841554 | -2.02 | 0.00164872 |
| NRIP3 | -2.00 | 0.00097943 | -1.59 | 0.0054957 |
| UPF2 | -1.95 | 2.41E-05 | -1.64 | 0.00055394 |
| WNT10A | -1.67 | 0.04531907 | -1.92 | 0.00841339 |

| | | | | |
|---|---|---|---|---|
| FUOM | -2.06 | 1.16E-06 | -1.53 | 2.40E-05 |
| UBBP1 | -2.08 | 0.00744331 | -1.51 | 0.0418692 |
| DEFB1 | -1.56 | 0.01750255 | -2.04 | 0.000463 |
| NMT1 | -2.10 | 8.37E-06 | -1.51 | 0.00026439 |
| RPL21P6 | -2.20 | 0.00660947 | -1.41 | 0.04646864 |
| STARD10 | -2.11 | 9.87E-07 | -1.50 | 5.13E-06 |
| TPGS1 | -1.88 | 4.04E-06 | -1.74 | 7.04E-07 |
| APOE | -1.69 | 1.05E-05 | -1.93 | 2.23E-08 |
| AARD | -2.14 | 0.00252799 | -1.49 | 0.03755117 |
| AC006509.1 | -2.25 | 5.33E-06 | -1.39 | 0.01353714 |
| MICALL2 | -2.01 | 3.62E-06 | -1.63 | 7.24E-06 |
| WFIKKN1 | -2.22 | 0.00035173 | -1.43 | 0.03917975 |
| TBL3 | -2.05 | 3.06E-06 | -1.60 | 6.52E-06 |
| GCHFR | -1.79 | 8.37E-06 | -1.87 | 5.31E-09 |
| CRPPA | -2.18 | 0.00053574 | -1.47 | 0.01343216 |
| CDKL1 | -1.97 | 0.00077699 | -1.70 | 0.00172031 |
| RPS26P6 | -1.93 | 0.0018952 | -1.74 | 0.00738244 |
| CAMK2B | -2.30 | 1.51E-05 | -1.37 | 0.02984981 |
| MZT2B | -1.89 | 1.28E-05 | -1.78 | 8.37E-07 |
| RHO | -1.90 | 0.01141181 | -1.77 | 0.01072607 |
| ZP3 | -2.08 | 3.46E-06 | -1.59 | 4.92E-06 |
| PTAFR | -1.71 | 0.00073315 | -1.98 | 7.73E-05 |
| NRTN | -1.89 | 1.54E-05 | -1.79 | 3.74E-05 |
| MMP2 | -1.90 | 5.40E-05 | -1.79 | 2.40E-05 |
| HLA-B | -1.91 | 0.00581257 | -1.79 | 0.0106439 |
| TRAPPC5 | -2.12 | 1.00E-05 | -1.58 | 6.14E-05 |
| TMEM160 | -2.20 | 1.83E-06 | -1.50 | 0.00010057 |
| HSP90AB3P | -1.96 | 0.00111717 | -1.74 | 0.00812551 |
| MYL5 | -1.86 | 2.26E-05 | -1.84 | 9.20E-07 |
| NECAB2 | -1.35 | 0.00184751 | -2.36 | 7.13E-10 |
| ANKRD30BL | -1.92 | 6.55E-05 | -1.81 | 7.09E-06 |
| CCDC85B | -2.26 | 6.91E-07 | -1.50 | 9.58E-05 |
| DEK | -2.24 | 7.79E-05 | -1.52 | 0.03464549 |
| DRD4 | -1.80 | 0.01774075 | -1.96 | 0.00503114 |
| DYNC1I2 | -1.89 | 0.00018862 | -1.88 | 5.63E-05 |
| ARGFXP2 | -2.23 | 0.00423103 | -1.55 | 0.03737092 |
| GC | -1.90 | 0.00968831 | -1.88 | 0.00788367 |
| ZNF350 | -2.02 | 0.00032253 | -1.78 | 0.00231915 |
| NRXN1 | -2.14 | 0.00767395 | -1.65 | 0.02508925 |

| | | | | |
|---|---|---|---|---|
| HSP90AB2P | -2.07 | 0.00178786 | -1.74 | 0.00855456 |
| CCDC7 | -2.28 | 0.00019594 | -1.54 | 0.0079118 |
| SYCE1L | -1.92 | 6.41E-05 | -1.90 | 5.76E-06 |
| FMO1 | -2.29 | 0.00377387 | -1.54 | 0.03618248 |
| PSG2 | -2.10 | 0.00732259 | -1.74 | 0.01776956 |
| TRPV2 | -1.85 | 0.00013482 | -1.99 | 3.12E-05 |
| NEB | -2.15 | 0.00062368 | -1.69 | 0.01029443 |
| ZBTB8B | -2.27 | 0.00082937 | -1.57 | 0.01915912 |
| PDE6B | -2.12 | 0.00300062 | -1.73 | 0.01608554 |
| ASGR1 | -1.40 | 0.02155015 | -2.46 | 5.92E-07 |
| NOS1 | -1.66 | 0.01280625 | -2.20 | 0.0006692 |
| TTN | -2.10 | 1.56E-06 | -1.76 | 0.00210705 |
| CADM2 | -2.13 | 0.00877324 | -1.75 | 0.01439883 |
| SRGAP1 | -2.23 | 0.00264214 | -1.65 | 0.01915912 |
| FXYD1 | -1.82 | 0.005202 | -2.07 | 0.00106277 |
| BRD4 | -2.34 | 1.43E-06 | -1.56 | 0.00030433 |
| MSLN | -2.45 | 4.91E-08 | -1.45 | 0.00055431 |
| GADD45GIP1 | -2.25 | 1.43E-06 | -1.66 | 2.85E-05 |
| ITFG2 | -2.49 | 3.32E-06 | -1.43 | 0.03877799 |
| PLCXD2 | -1.94 | 2.33E-05 | -2.00 | 1.21E-06 |
| AP5Z1 | -2.22 | 8.90E-06 | -1.74 | 0.00011721 |
| ZNF236 | -2.32 | 1.80E-05 | -1.65 | 0.00120922 |
| BAZ2A | -2.26 | 2.50E-06 | -1.72 | 7.07E-05 |
| RRAD | -1.93 | 0.00019356 | -2.06 | 8.02E-05 |
| AEBP1 | -1.94 | 0.01004379 | -2.06 | 0.00378874 |
| HES2 | -1.69 | 0.0015946 | -2.31 | 5.72E-07 |
| AC008716.1 | -2.46 | 0.00215497 | -1.56 | 0.03171685 |
| FTH1P15 | -1.91 | 0.00035416 | -2.11 | 0.00010429 |
| EEF1D | -2.24 | 1.43E-06 | -1.82 | 3.81E-06 |
| POLRMT | -2.31 | 1.11E-06 | -1.76 | 5.19E-06 |
| RPSAP53 | -2.24 | 0.00370723 | -1.83 | 0.01199042 |
| ANGPTL4 | -1.52 | 6.41E-05 | -2.56 | 6.36E-20 |
| PI3 | -2.22 | 8.19E-05 | -1.89 | 0.00029929 |
| TMEM238 | -2.19 | 1.63E-06 | -1.92 | 4.78E-08 |
| PTPRN | -2.08 | 0.0097944 | -2.06 | 0.00437675 |
| LAMB2 | -2.18 | 1.94E-06 | -1.97 | 4.96E-07 |
| APOA1 | -2.19 | 0.00030569 | -1.95 | 0.00106969 |
| HS3ST6 | -1.76 | 4.27E-05 | -2.40 | 3.58E-11 |
| ODF3B | -1.53 | 0.00142567 | -2.64 | 1.33E-13 |

| | | | | |
|---|---|---|---|---|
| CRIP1 | -2.19 | 1.56E-06 | -1.99 | 1.14E-07 |
| TNNI3 | -2.06 | 1.93E-06 | -2.14 | 3.89E-09 |
| AC011479.1 | -2.85 | 6.09E-07 | -1.35 | 0.03299447 |
| CD248 | -2.53 | 0.00153504 | -1.67 | 0.02134742 |
| SOX11 | -2.41 | 0.00064138 | -1.82 | 0.01011535 |
| NACA4P | -2.26 | 0.0015946 | -1.98 | 0.00491245 |
| LIMS2 | -2.46 | 1.34E-08 | -1.79 | 2.31E-05 |
| CYP2C8 | -2.39 | 0.00233094 | -1.86 | 0.01077761 |
| AC010422.3 | -2.37 | 0.00139167 | -1.91 | 0.00630115 |
| ANGPTL2 | -2.61 | 0.00099253 | -1.68 | 0.02061561 |
| MICU3 | -2.62 | 5.82E-06 | -1.67 | 0.00496582 |
| KLRD1 | -2.25 | 3.91E-07 | -2.05 | 0.0008019 |
| SDK2 | -2.38 | 6.90E-05 | -1.95 | 0.00048401 |
| ACAP1 | -2.23 | 4.75E-07 | -2.12 | 1.37E-07 |
| CDH11 | -2.70 | 0.00058729 | -1.66 | 0.02281378 |
| ATP6V0D2 | -2.23 | 0.00472865 | -2.14 | 0.00313245 |
| GPAT2 | -1.92 | 0.01943894 | -2.45 | 0.00056083 |
| AMZ1 | -2.57 | 0.00061214 | -1.80 | 0.01400799 |
| AP3D1 | -1.95 | 0.01774849 | -2.43 | 3.81E-06 |
| SGCA | -1.77 | 0.00094789 | -2.62 | 4.10E-10 |
| AL357055.1 | -2.58 | 0.00097943 | -1.83 | 0.01225616 |
| MYO7B | -1.86 | 0.00916776 | -2.56 | 1.74E-05 |
| EIF4A1P6 | -2.45 | 0.00241206 | -1.98 | 0.00600236 |
| HSPA5P1 | -2.92 | 2.11E-05 | -1.52 | 0.04199296 |
| EEF1A1P7 | -2.74 | 0.00044107 | -1.69 | 0.02064007 |
| TFPT | -2.58 | 1.63E-06 | -1.85 | 0.00015952 |
| IFITM3P9 | -2.46 | 0.0021798 | -1.99 | 0.00601801 |
| IL34 | -2.01 | 0.00126773 | -2.46 | 2.88E-05 |
| CA8 | -1.17 | 0.02740475 | -3.33 | 8.91E-20 |
| AC079414.2 | -2.80 | 0.00032104 | -1.71 | 0.02039993 |
| RPSAP23 | -2.76 | 4.59E-05 | -1.75 | 0.01722299 |
| SNCG | -1.75 | 1.43E-06 | -2.77 | 1.45E-21 |
| PABPC3 | -2.72 | 0.00046365 | -1.81 | 0.01299636 |
| CST2 | -1.75 | 0.0049814 | -2.82 | 8.83E-08 |
| SERPINC1 | -2.30 | 0.00106528 | -2.30 | 0.00051946 |
| AL158071.1 | -2.60 | 0.00090206 | -2.02 | 0.00552301 |
| PAH | -2.76 | 3.44E-05 | -1.87 | 0.00692161 |
| STMN2 | -3.22 | 5.01E-05 | -1.41 | 0.0455291 |
| ACTN2 | -2.78 | 0.00046365 | -1.86 | 0.01016578 |

| | | | | |
|---|---|---|---|---|
| CD37 | -2.65 | 4.15E-06 | -2.01 | 3.94E-05 |
| AC022018.1 | -2.90 | 0.00013482 | -1.79 | 0.01426688 |
| TRPS1 | -2.51 | 1.95E-06 | -2.18 | 0.00098898 |
| PHF1 | -2.61 | 2.96E-05 | -2.08 | 0.0008854 |
| DPPA4 | -2.34 | 0.00387372 | -2.37 | 0.00051018 |
| KCNJ3 | -2.77 | 3.73E-06 | -1.94 | 0.00261235 |
| ACTG1P21 | -2.68 | 0.00072794 | -2.03 | 0.00501433 |
| ASS1P6 | -2.80 | 0.0002656 | -1.94 | 0.00771565 |
| NECTIN4 | -1.88 | 0.00877324 | -2.88 | 6.51E-07 |
| RPSAP31 | -2.94 | 1.58E-05 | -1.87 | 0.01027377 |
| TYMP | -1.66 | 0.00032139 | -3.15 | 6.33E-21 |
| HBB | -2.53 | 0.00014782 | -2.28 | 0.0004401 |
| RASL10B | -2.49 | 0.00150908 | -2.35 | 0.00091593 |
| ZFP91-CNTF | -3.16 | 7.30E-05 | -1.68 | 0.01981231 |
| DCN | -2.80 | 0.00010263 | -2.06 | 0.00454544 |
| KLF15 | -3.62 | 2.17E-21 | -1.26 | 0.00031175 |
| PRRG3 | -2.67 | 3.91E-07 | -2.23 | 2.93E-05 |
| PPIAP8 | -2.82 | 0.00035416 | -2.09 | 0.00392055 |
| RPS4XP21 | -3.20 | 3.77E-05 | -1.72 | 0.01775731 |
| RGN | -3.14 | 5.43E-05 | -1.79 | 0.01396396 |
| KPNA5 | -3.05 | 5.40E-07 | -1.89 | 0.00101703 |
| HLA-V | -2.76 | 5.91E-06 | -2.20 | 0.00027974 |
| EEF1A1P17 | -3.03 | 2.08E-05 | -1.93 | 0.00802309 |
| HBQ1 | -2.84 | 1.83E-10 | -2.15 | 1.92E-08 |
| SCN9A | -2.27 | 6.33E-05 | -2.74 | 2.86E-08 |
| A2MP1 | -2.88 | 4.39E-05 | -2.13 | 0.00226271 |
| KLHL41 | -3.07 | 6.05E-05 | -2.00 | 0.00577121 |
| ALB | -2.61 | 0.0003522 | -2.50 | 0.00027974 |
| GSTM5 | -2.53 | 0.00012036 | -2.59 | 4.25E-05 |
| NCAM1 | -3.07 | 1.98E-06 | -2.10 | 0.00321372 |
| FGF23 | -3.22 | 2.83E-10 | -1.96 | 0.00518667 |
| EVA1B | -2.20 | 5.70E-09 | -3.02 | 1.06E-24 |
| CDA | -1.44 | 8.59E-06 | -3.83 | 1.16E-48 |
| ZNF347 | -2.36 | 1.78E-05 | -2.93 | 5.43E-08 |
| LBHD2 | -1.65 | 0.04159628 | -3.64 | 3.41E-08 |
| RPSAP48 | -2.90 | 0.00010929 | -2.39 | 0.00067044 |
| RSPO3 | -1.78 | 7.26E-05 | -3.52 | 6.00E-23 |
| TUBB8 | -3.03 | 0.00010008 | -2.27 | 0.00163674 |
| FTH1P16 | -2.88 | 7.26E-07 | -2.47 | 8.87E-05 |

| | | | | |
|---|---|---|---|---|
| BHLHE41 | -3.08 | 8.91E-06 | -2.35 | 0.00089335 |
| GAPDHP44 | -3.24 | 5.29E-07 | -2.19 | 0.00169839 |
| INHBA | -3.19 | 1.48E-05 | -2.25 | 0.00167834 |
| NCLP2 | -3.38 | 1.12E-05 | -2.06 | 0.00446719 |
| AP003467.2 | -3.27 | 2.20E-05 | -2.19 | 0.00245785 |
| CTSK | -3.70 | 1.29E-29 | -1.76 | 0.01693203 |
| DLC1 | -1.82 | 0.02427011 | -3.66 | 3.94E-10 |
| LY6D | -2.01 | 0.00243432 | -3.48 | 2.65E-12 |
| C5orf63 | -3.11 | 3.55E-11 | -2.44 | 2.32E-09 |
| CST1 | -2.42 | 4.00E-11 | -3.22 | 2.74E-23 |
| AC097658.1 | -3.12 | 5.40E-07 | -2.54 | 0.00016406 |
| FAM83A | -2.47 | 1.37E-06 | -3.21 | 4.34E-15 |
| PTX3 | -3.22 | 6.64E-07 | -2.47 | 0.00038952 |
| ZNF90 | -2.82 | 0.00036142 | -2.93 | 1.46E-05 |
| LDLRAD2 | -3.27 | 6.16E-08 | -2.56 | 1.33E-07 |
| SNORC | -2.62 | 2.83E-08 | -3.21 | 1.03E-19 |
| CPS1 | -2.63 | 8.15E-08 | -3.33 | 7.99E-32 |
| PDGFRB | -2.95 | 4.40E-05 | -3.01 | 3.81E-06 |
| GUCY2D | -3.31 | 1.73E-05 | -2.88 | 3.48E-05 |
| AL049629.2 | -3.93 | 4.59E-14 | -2.47 | 0.00037737 |
| KLK10 | -4.84 | 2.69E-30 | -1.57 | 0.01064864 |
| HTRA3 | -2.00 | 0.00066035 | -4.46 | 1.82E-32 |
| A1BG | -2.21 | 5.45E-09 | -4.31 | 1.80E-44 |
| IGF1 | -3.60 | 2.09E-07 | -2.96 | 8.76E-06 |
| SPARC | -3.28 | 5.44E-17 | -3.35 | 8.29E-16 |
| HHIPL2 | -1.32 | 0.02578796 | -5.41 | 3.34E-54 |
| PKNOX2 | -3.14 | 7.62E-07 | -3.67 | 3.01E-12 |
| GPM6A | -3.95 | 2.23E-09 | -2.90 | 1.38E-05 |
| CSAG1 | -3.96 | 1.06E-12 | -3.05 | 2.04E-07 |
| COL3A1 | -3.85 | 6.07E-13 | -3.42 | 6.87E-11 |
| RPL10L | -4.39 | 1.50E-09 | -2.97 | 2.31E-05 |
| COX5BP1 | -4.20 | 3.46E-09 | -3.17 | 3.34E-06 |
| DNAAF1 | -5.19 | 5.43E-20 | -4.23 | 1.11E-15 |
| GP1BB | -6.99 | 2.69E-30 | -6.41 | 4.36E-34 |

**Table S4** Protein abundance upon DUS2 Knockout

# Postlude

While the above chapters provide both a tool (Chapter 1) to study the location and function of D in RNA, and reveal (Chapter 2) a mechanism by which DUS2 contributes to NSCLC disease severity, they raise many additional questions, including:

1. What are the functional consequences of mRNA and snoRNA modification by DUS?
2. Why is tRNA CysGCA specifically sensitive to DUS2 levels?

Below, I will discuss some of the data relevant to these questions and suggest future experiments to begin to answer them:

**What are the functional consequences of mRNA and snoRNA modification by DUS?**

D-seq in yeast revealed hundreds of novel D sites in yeast mRNA and snoRNAs. Several of the novel mRNA and snoRNA D sites are in conserved RNA structures. This structural conservation, combined with the known role that D plays in stabilizing to the correct folding of the tRNA D-loop, suggests that D might play a role in the folding of functional RNA structures.

To investigate the functions D might have in RNA folding, I collaborated with a graduate student in Karla Neugeubauer's group, Leonard Schärfen. First, to directly test the impact of D on RNA folding, we generated a library of mutagenized MS2 RNA hairpins. As MS2 hairpin RNA is known to fold into a stable, well behaved structure (Helgstrand et al., 2002), we generated MS2 variants with only a single U or D in each hairpin, and tested the impact of D at each position in the structure using high-throughput chemical

probing with DMS. Consistent with previous reports (Dyubankova et al., 2015) that D can alter the folding of small RNA structures, we observed changes in the folding of some of our MS2 variants in the presence of D.

To determine if D impacts RNA folding in vivo, and to dissect the specific impacts of D on RNA structure from possible indirect effects downstream of DUS knockout (KO) in cells, Leonard Schärfen and I performed transcriptome wide DMS-MaPseq on in vitro re-folded RNA from wild type and DUS KO yeast strains. Our in vitro DMS-MaPseq data revealed hundreds of regions of RNA with differential DMS reactivity between wild type and DUS KO. Many of the differentially DMS reactive sites are adjacent to Ds in H/ACA box snoRNAs, indicating that D may play a role in snoRNA structure and function. To test if D impacts H/ACA box snoRNA function, I performed quantitative pseudouridine profiling using eRBS-MaP (Khoddami et al., 2019, Christian Fagre, unpublished method) on ribosomal RNA from wild type and DUS KO yeast. I am currently waiting for sequencing results from this experiment.

Beyond the snoRNA Ds, Leonard and I also detect differentially DMS reactive sites in multiple mRNAs. Several of the mRNAs with differentially reactive regions encode for aminoacyl tRNA synthetases (aaRS). In yeast, several aaRS mRNAs are known to contain folded RNA domains that are structurally similar to tRNAs (Levi and Arava, 2019). These structures are known be bound by aaRS proteins and are thought to play a role in aaRS autoregulation. It is tempting to speculate that the tRNA-like domains in these aaRS mRNAs are DUS substrates and exhibit differential DMS reactivity because they lack D in the DUS KO. In the future, determining if these mRNAs contain D (I lack coverage to inspect them in the D-seq dataset), and if D-deficient strains have defects

in autoregulation of the aaRS, could illuminate a function for mRNA D in gene regulation.

**Why is CysGCA specifically sensitive to DUS2 levels?**

A major question remaining from the DUS2 NSCLC experiments is why tRNA cysGCA is specifically sensitive to DUS2 expression. The selective reduction in tRNA cysGCA levels in the DUS2 knockout could arise either from a tRNA synthesis defect (e.g. a failure to process and produce mature tRNA cysGCA) or alternatively, instability and decay of the mature tRNA cysGCA.

Loss of several different tRNA body modifications in yeast is known to trigger rapid tRNA decay (RTD) of only a specific subset of tRNAs (Alexandrov et al., 2006; Tasak and Phizicky, 2022; Zoysa and Phizicky, 2020). Though I do not detect evidence for accumulation of tRNA cysGCA precursors in the DUS2 KO cells, this does not conclusively rule out a defect in tRNA synthesis and processing. Several experiments could help here. First, perturbing the human orthologs of the RTD machinery (primarily the 5′–3′ exonucleases Rat1 and Xrn1 (Chernyakov et al., 2008)) and testing to see if that rescued the defect in tRNA cysGCA levels in the DUS2 KO cells would demonstrate that mature tRNA cysGCA is an RTD substrate and provide evidence for the mature tRNA decay model. Alternatively, a metabolic labeling TimeLase-seq (Schofield et al., 2018) style experiment on tRNAs from DUS2 WT and KO would measure tRNA half-lives and rule in or out the mature tRNA decay model.

## Concluding Remarks

In addition to the work I present in Chapter 2, several recent studies have investigated the links between specific tRNA-modifying enzymes and certain cancers (Goodarzi et al., 2016; Orellana et al., 2021; Passarelli et al., 2022). While each of these studies focused a link from a specific tRNA modifying enzyme to a specific cancer, my re-analysis of a large tumor sequencing data set from the Cancer Genome Atlas (TCGA) suggests these are only the tip of the iceberg. My reanalysis of TCGA data connects high expression of dozens of tRNA-modifying enzymes to worse patient outcomes in more than 15 cancer types.

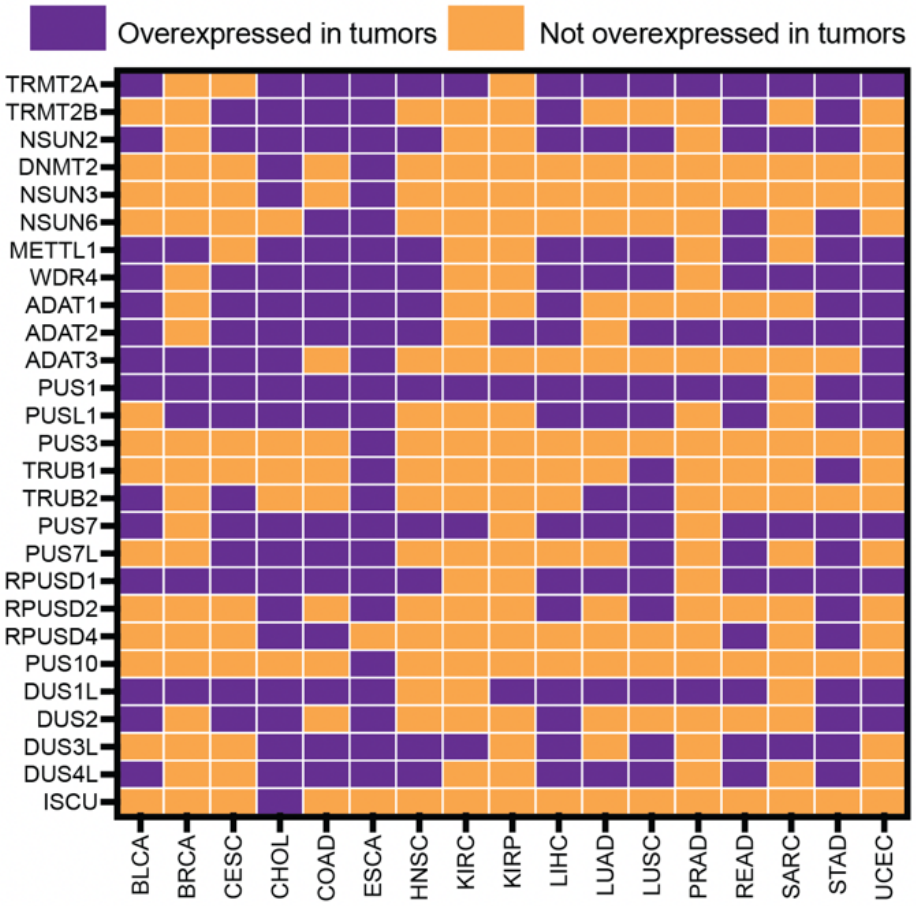


**Figure 1: Specific tRNA modifying enzymes are overexpressed in certain cancers**

For the majority of these disease-associated tRNA-modifying enzymes, we lack a mechanistic explanation for how their dysregulation drives disease progression and pathology. I believe this is fertile ground for future investigation, and I eagerly await future work to untangle these links.

## References


Alexandrov A, Chernyakov I, Gu W, Hiley SL, Hughes TR, Grayhack EJ, Phizicky EM. 2006. Rapid tRNA Decay Can Result from Lack of Nonessential Modifications. *Molecular Cell* **21**:87–96. doi:10.1016/j.molcel.2005.10.036

Alvarez SW, Sviderskiy VO, Terzi EM, Papagiannakopoulos T, Moreira AL, Adams S, Sabatini DM, Birsoy K, Possemato R. 2017. NFS1 undergoes positive selection in lung tumours and protects cells from ferroptosis. *Nature* **551**:639–643. doi:10.1038/nature24637

Badgley MA, Kremer DM, Maurer HC, DelGiorno KE, Lee H-J, Purohit V, Sagalovskiy IR, Ma A, Kapilian J, Firl CEM, Decker AR, Sastra SA, Palermo CF, Andrade LR, Sajjakulnukit P, Zhang L, Tolstyka ZP, Hirschhorn T, Lamb C, Liu T, Gu W, Seeley ES, Stone E, Georgiou G, Manor U, Iuga A, Wahl GM, Stockwell BR, Lyssiotis CA, Olive KP. 2020. "Cysteine depletion induces pancreatic tumor ferroptosis in mice." *Science* **368**:85–89. doi:10.1126/science.aaw9872

Basu A, Bodycombe NE, Cheah JH, Price EV, Liu K, Schaefer GI, Ebright RY, Stewart ML, Ito D, Wang S, Bracha AL, Liefeld T, Wawer M, Gilbert JC, Wilson AJ, Stransky N, Kryukov GV, Dancik V, Barretina J, Garraway LA, Hon CS-Y, Munoz B, Bittker JA, Stockwell BR, Khabele D, Stern AM, Clemons PA, Shamji AF, Schreiber SL. 2013. An interactive resource to identify cancer genetic and lineage dependencies targeted by small molecules. *Cell* **154**:1151–1161. doi:10.1016/j.cell.2013.08.003

Batt RD, Martin JK, Ploeser JMcT, Murray J. 1954. Chemistry of the Dihydropyrimidines. Ultraviolet Spectra and Alkaline Decomposition1a. *J Am Chem Soc* **76**:3663–3665. doi:10.1021/ja01643a018

Bebber CM, Thomas ES, Stroh J, Chen Z, Androulidaki A, Schmitt A, Höhne MN, Stüker L, de Pádua Alves C, Khonsari A, Dammert MA, Parmaksiz F, Tumbrink HL, Beleggia F, Sos ML, Riemer J, George J, Brodesser S, Thomas RK, Reinhardt HC, von Karstedt S. 2021. Ferroptosis response segregates small cell lung cancer (SCLC) neuroendocrine subtypes. *Nat Commun* **12**:2048. doi:10.1038/s41467-021-22336-4

Beckmann BM, Horos R, Fischer B, Castello A, Eichelbaum K, Alleaume A-M, Schwarzl T, Curk T, Foehr S, Huber W, Krijgsveld J, Hentze MW. 2015. The RNA-binding proteomes from yeast to man harbour conserved enigmRBPs. *Nature Communications* **6**:10127. doi:10.1038/ncomms10127

Behm-Ansmant I, Helm M, Motorin Y. 2011. Use of Specific Chemical Reagents for Detection of Modified Nucleotides in RNA. *Journal of Nucleic Acids* **2011**. doi:10.4061/2011/408053

Beroukhim R, Mermel CH, Porter D, Wei G, Raychaudhuri S, Donovan J, Barretina J, Boehm JS, Dobson J, Urashima M, Mc Henry KT, Pinchback RM, Ligon AH, Cho Y-J, Haery L, Greulich H, Reich M, Winckler W, Lawrence MS, Weir BA, Tanaka KE, Chiang DY, Bass AJ, Loo A, Hoffman C, Prensner J, Liefeld T, Gao Q, Yecies D, Signoretti S, Maher E, Kaye FJ, Sasaki H, Tepper JE, Fletcher JA, Tabernero J, Baselga J, Tsao M-S, Demichelis F, Rubin MA, Janne PA, Daly MJ, Nucera C, Levine RL, Ebert BL, Gabriel S, Rustgi AK, Antonescu CR, Ladanyi M,

Letai A, Garraway LA, Loda M, Beer DG, True LD, Okamoto A, Pomeroy SL, Singer S, Golub TR, Lander ES, Getz G, Sellers WR, Meyerson M. 2010. The landscape of somatic copy-number alteration across human cancers. *Nature* **463**:899–905. doi:10.1038/nature08822

Bushnell B. n.d. BBMap. *SourceForge*. https://sourceforge.net/projects/bbmap/

Bushnell B, Rood J, Singer E. 2017. BBMerge – Accurate paired shotgun read merging via overlap. *PLOS ONE* **12**:e0185056. doi:10.1371/journal.pone.0185056

Carlile TM, Rojas-Duran MF, Gilbert WV. 2015. Pseudo-Seq: Genome-Wide Detection of Pseudouridine Modifications in RNA. *Meth Enzymol* **560**:219–245. doi:10.1016/bs.mie.2015.03.011

Cerutti P, Kondo Y, Landis WR, Witkop B. 1968. Photoreduction of uridine and reduction of dihydrouridine with sodium borohydride. *J Am Chem Soc* **90**:771–775. doi:10.1021/ja01005a039

Cerutti P, Miller N. 1967. Selective reduction of yeast transfer ribonucleic acid with sodium borohydride. *Journal of Molecular Biology* **26**:55–66. doi:10.1016/0022-2836(67)90260-4

Chen P-H, Wu J, Xu Y, Ding C-KC, Mestre AA, Lin C-C, Yang W-H, Chi J-T. 2021. Zinc transporter ZIP7 is a novel determinant of ferroptosis. *Cell Death Dis* **12**:198. doi:10.1038/s41419-021-03482-5

Chernyakov I, Whipple JM, Kotelawala L, Grayhack EJ, Phizicky EM. 2008. Degradation of several hypomodified mature tRNA species in Saccharomyces cerevisiae is mediated by Met22 and the 5′–3′ exonucleases Rat1 and Xrn1. *Genes Dev* **22**:1369–1380. doi:10.1101/gad.1654308

Cozen AE, Quartley E, Holmes AD, Hrabeta-Robinson E, Phizicky EM, Lowe TM. 2015. ARM-seq: AlkB-facilitated RNA methylation sequencing reveals a complex landscape of modified tRNA fragments. *Nature Methods* **12**:879–884. doi:10.1038/nmeth.3508

Creighton CJ, Christopher J. Ricketts, Ramaprasad Srinivasan, Spellman PT, Linehan WM. 2016. Comprehensive Molecular Characterization of Papillary Renal-Cell Carcinoma. *New England Journal of Medicine* **374**:135–145. doi:10.1056/NEJMoa1505917

Creighton CJ, Morgan M, Gunaratne PH, Wheeler DA, Gibbs RA, Gordon Robertson A, Chu A, Beroukhim R, Cibulskis K, Signoretti S, Vandin Hsin-Ta Wu F, Raphael BJ, Verhaak RGW, Tamboli P, Torres-Garcia W, Akbani R, Weinstein JN, Reuter V, Hsieh JJ, Rose Brannon A, Ari Hakimi A, Jacobsen A, Ciriello G, Reva B, Ricketts CJ, Marston Linehan W, Stuart JM, Kimryn Rathmell W, Shen H, Laird PW, Muzny D, Davis C, Morgan M, Xi L, Chang K, Kakkar N, Treviño LR, Benton S, Reid JG, Morton D, Doddapaneni H, Han Y, Lewis L, Dinh H, Kovar C, Zhu Y, Santibanez J, Wang M, Hale W, Kalra D, Creighton CJ, Wheeler DA, Gibbs RA, Getz G, Cibulskis K, Lawrence MS, Sougnez C, Carter SL, Sivachenko A, Lichtenstein L, Stewart C, Voet D, Fisher S, Gabriel SB, Lander E, Beroukhim R, Schumacher SE, Tabak B, Saksena G, Onofrio RC, Carter SL, Cherniack AD, Gentry J, Ardlie K, Sougnez C, Getz G, Gabriel SB, Meyerson M, Gordon Robertson A, Chu A, Chun H-JE, Mungall AJ, Sipahimalani P, Stoll D, Ally A, Balasundaram M, Butterfield YSN, Carlsen R, Carter C, Chuah E, Coope RJN, Dhalla N, Gorski S, Guin R, Hirst C, Hirst M, Holt RA, Lebovitz C, Lee D, Li HI,

Mayo M, Moore RA, Pleasance E, Plettner P, Schein JE, Shafiei A, Slobodan JR, Tam A, Thiessen N, Varhol RJ, Wye N, Zhao Y, Birol I, Jones SJM, Marra MA, Auman JT, Tan D, Jones CD, Hoadley KA, Mieczkowski PA, Mose LE, Jefferys SR, Topal MD, Liquori C, Turman YJ, Shi Y, Waring S, Buda E, Walsh J, Wu J, Bodenheimer T, Hoyle AP, Simons JV, Soloway MG, Balu S, Parker JS, Neil Hayes D, Perou CM, Kucherlapati R, Park P, Shen H, Triche Jr T, Weisenberger DJ, Lai PH, Bootwalla MS, Maglinte DT, Mahurkar S, Berman BP, Van Den Berg DJ, Cope L, Baylin SB, Laird PW, Creighton CJ, Wheeler DA, Getz G, Noble MS, DiCara D, Zhang H, Cho J, Heiman DI, Gehlenborg N, Voet D, Mallard W, Lin P, Frazer S, Stojanov P, Liu Y, Zhou L, Kim J, Lawrence MS, Chin L, Vandin F, Wu H-T, Raphael BJ, Benz C, Yau C, Reynolds SM, Shmulevich I, Verhaak RGW, Torres-Garcia W, Vegesna R, Kim H, Zhang W, Cogdell D, Jonasch E, Ding Z, Lu Y, Akbani R, Zhang N, Unruh AK, Casasent TD, Wakefield C, Tsavachidou D, Chin L, Mills GB, Weinstein JN, Jacobsen A, Rose Brannon A, Ciriello G, Schultz N, Ari Hakimi A, Reva B, Antipin Y, Gao J, Cerami E, Gross B, Arman Aksoy B, Sinha R, Weinhold N, Onur Sumer S, Taylor BS, Shen R, Ostrovnaya I, Hsieh JJ, Berger MF, Ladanyi M, Sander C, Fei SS, Stout A, Spellman PT, Rubin DL, Liu TT, Stuart JM, Ng S, Paull EO, Carlin D, Goldstein T, Waltman P, Ellrott K, Zhu J, Haussler D, Gunaratne PH, Xiao W, Shelton C, Gardner J, Penny R, Sherman M, Mallery D, Morris S, Paulauskis J, Burnett K, Shelton T, Signoretti S, Kaelin WG, Choueiri T, Atkins MB, Penny R, Burnett K, Mallery D, Curley E, Tickoo S, Reuter V, Kimryn Rathmell W, Thorne L, Boice L, Huang M, Fisher JC, Marston Linehan W, Vocke CD, Peterson J, Worrell R, Merino MJ, The Cancer Genome

Atlas Research Network, Analysis working group: Baylor College of Medicine, BC Cancer Agency, Broad Institute, Brigham & Women's Hospital, Brown University, The University of Texas MD Anderson Cancer Center, Memorial Sloan-Kettering Cancer Center, National Cancer Institute, University of California Santa Cruz, University of North Carolina CH, University of Southern California, Genome sequencing centres: Baylor College of Medicine, Genome characterization centres: Broad Institute, Harvard Medical School, University of Southern California & Johns Hopkins University, Genome data analysis: Baylor College of Medicine, Buck Institute for Research on Aging, Institute for Systems Biology, Oregon Health & Science University, Stanford University, University of Houston, Biospecimen core resource: International Genomics Consortium, Tissue source sites: Brigham & Women's Hospital, Dana-Farber Cancer Institute, Georgetown University, International Genomics Consortium, University of North Carolina at Chapel Hill. 2013. Comprehensive molecular characterization of clear cell renal cell carcinoma. *Nature* **499**:43–49. doi:10.1038/nature12222

Daher B, Parks SK, Durivault J, Cormerais Y, Baidarjad H, Tambutte E, Pouysségur J, Vučetić M. 2019. Genetic ablation of the cystine transporter xCT in PDAC cells inhibits mTORC1, growth, survival, and tumor formation via nutrient and oxidative stresses. *Cancer research* **79**:3877–3890.

Dai Q, Zheng G, Schwartz MH, Clark WC, Pan T. 2017. Selective Enzymatic Demethylation of N2 ,N2 -Dimethylguanosine in RNA and Its Application in High-Throughput tRNA Sequencing. *Angew Chem Int Ed Engl* **56**:5017–5020. doi:10.1002/anie.201700537

Dalluge JJ, Hashizume T, Sopchik AE, McCloskey JA, Davis DR. 1996. Conformational flexibility in RNA: the role of dihydrouridine. *Nucleic Acids Res* **24**:1073–1079.

Delaunay S, Pascual G, Feng B, Klann K, Behm M, Hotz-Wagenblatt A, Richter K, Zaoui K, Herpel E, Münch C, Dietmann S, Hess J, Benitah SA, Frye M. 2022. Mitochondrial RNA modifications shape metabolic plasticity in metastasis. *Nature* 1–11. doi:10.1038/s41586-022-04898-5

Dixon SJ, Lemberg KM, Lamprecht MR, Skouta R, Zaitsev EM, Gleason CE, Patel DN, Bauer AJ, Cantley AM, Yang WS, Morrison B, Stockwell BR. 2012. Ferroptosis: An Iron-Dependent Form of Nonapoptotic Cell Death. *Cell* **149**:1060–1072. doi:10.1016/j.cell.2012.03.042

Dixon SJ, Stockwell BR. 2019. The Hallmarks of Ferroptosis. *Annu Rev Cancer Biol* **3**:35–54. doi:10.1146/annurev-cancerbio-030518-055844

Drummen GPC, van Liebergen LCM, Op den Kamp JAF, Post JA. 2002. C11-BODIPY581/591, an oxidation-sensitive fluorescent lipid peroxidation probe: (micro)spectroscopic characterization and validation of methodology. *Free Radical Biology and Medicine* **33**:473–490. doi:10.1016/S0891-5849(02)00848-1

Dyubankova N, Sochacka E, Kraszewska K, Nawrot B, Herdewijn P, Lescrinier E. 2015. Contribution of dihydrouridine in folding of the D-arm in tRNA. *Org Biomol Chem* **13**:4960–4966. doi:10.1039/c5ob00164a

Eaton JK, Furst L, Ruberto RA, Moosmayer D, Hilpmann A, Ryan MJ, Zimmermann K, Cai LL, Niehues M, Badock V, Kramm A, Chen S, Hillig RC, Clemons PA, Gradl S, Montagnon C, Lazarski KE, Christian S, Bajrami B, Neuhaus R, Eheim AL, Viswanathan VS, Schreiber SL. 2020. Selective covalent targeting of GPX4 using

masked nitrile-oxide electrophiles. *Nat Chem Biol* **16**:497–506. doi:10.1038/s41589-020-0501-5

Eaton JK, Ruberto RA, Kramm A, Viswanathan VS, Schreiber SL. 2019. Diacylfuroxans Are Masked Nitrile Oxides That Inhibit GPX4 Covalently. *J Am Chem Soc* **141**:20407–20415. doi:10.1021/jacs.9b10769

Ellis SR, Morales MJ, Li JM, Hopper AK, Martin NC. 1986. Isolation and characterization of the TRM1 locus, a gene essential for the N2,N2-dimethylguanosine modification of both mitochondrial and cytoplasmic tRNA in Saccharomyces cerevisiae. *J Biol Chem* **261**:9703–9709.

Emerson J, Sundaralingam M. 1980. Structure of the potassium salt of the modified nucleotide dihydrouridine 3'-monophosphate hemihydrate: correlation between the base pucker and sugar pucker and models for metal interactions with ribonucleic acid loops. *Acta Crystallographica Section B: Structural Crystallography and Crystal Chemistry* **36**:537–543. doi:10.1107/S0567740880003780

Eyler DE, Franco MK, Batool Z, Wu MZ, Dubuke ML, Dobosz-Bartoszek M, Jones JD, Polikanov YS, Roy B, Koutmou KS. 2019. Pseudouridinylation of mRNA coding sequences alters translation. *PNAS* **116**:23068–23074. doi:10.1073/pnas.1821754116

Finet O, Yague-Sanz C, Krüger LK, Tran P, Migeot V, Louski M, Nevers A, Rougemaille M, Sun J, Ernst FGM, Wacheul L, Wery M, Morillon A, Dedon P, Lafontaine DLJ, Hermand D. 2021. Transcription-wide mapping of dihydrouridine reveals that

mRNA dihydrouridylation is required for meiotic chromosome segregation. *Molecular Cell*. doi:10.1016/j.molcel.2021.11.003

Goodarzi H, Nguyen HCB, Zhang S, Dill BD, Molina H, Tavazoie SF. 2016. Modulated Expression of Specific tRNAs Drives Gene Expression and Cancer Progression. *Cell* **165**:1416–1427. doi:10.1016/j.cell.2016.05.046

Hadian K, Stockwell BR. 2021. A roadmap to creating ferroptosis-based medicines. *Nat Chem Biol* **17**:1113–1116. doi:10.1038/s41589-021-00853-z

Hanahan D, Weinberg RA. 2000. The Hallmarks of Cancer. *Cell* **100**:57–70. doi:10.1016/S0092-8674(00)81683-9

Hayano M, Yang WS, Corn CK, Pagano NC, Stockwell BR. 2016. Loss of cysteinyl-tRNA synthetase (CARS) induces the transsulfuration pathway and inhibits ferroptosis induced by cystine deprivation. *Cell Death Differ* **23**:270–278. doi:10.1038/cdd.2015.93

Helgstrand C, Grahn E, Moss T, Stonehouse NJ, Tars K, Stockley PG, Liljas L. 2002. Investigating the structural basis of purine specificity in the structures of MS2 coat protein RNA translational operator hairpins. *Nucleic Acids Res* **30**:2678–2685.

Hickey KL, Dickson K, Cogan JZ, Replogle JM, Schoof M, D'Orazio KN, Sinha NK, Hussmann JA, Jost M, Frost A, Green R, Weissman JS, Kostova KK. 2020. GIGYF2 and 4EHP Inhibit Translation Initiation of Defective Messenger RNAs to Assist Ribosome-Associated Quality Control. *Molecular Cell* **79**:950-962.e6. doi:10.1016/j.molcel.2020.07.007

Homann OR, Johnson AD. 2010. MochiView: versatile software for genome browsing and DNA motif analysis. *BMC Biol* **8**:49. doi:10.1186/1741-7007-8-49

Hurnanen D, Chan HM, Kubow S. 1997. The Protective Effect of Metallothionein Against Lipid Peroxidation Caused by Retinoic Acid in Human Breast Cancer Cells **283**:9.

Ignatova VV, Kaiser S, Ho JSY, Bing X, Stolz P, Tan YX, Lee CL, Gay FPH, Lastres PR, Gerlini R, Rathkolb B, Aguilar-Pimentel A, Sanz-Moreno A, Klein-Rodewald T, Calzada-Wack J, Ibragimov E, Valenta M, Lukauskas S, Pavesi A, Marschall S, Leuchtenberger S, Fuchs H, Gailus-Durner V, de Angelis MH, Bultmann S, Rando OJ, Guccione E, Kellner SM, Schneider R. 2020. METTL6 is a tRNA m3C methyltransferase that regulates pluripotency and tumor cell growth. *Science Advances* **6**:eaaz4551. doi:10.1126/sciadv.aaz4551

Juszkiewicz S, Chandrasekaran V, Lin Z, Kraatz S, Ramakrishnan V, Hegde RS. 2018. ZNF598 Is a Quality Control Sensor of Collided Ribosomes. *Molecular Cell* **72**:469-481.e7. doi:10.1016/j.molcel.2018.08.037

Kato T, Daigo Y, Hayama S, Ishikawa N, Yamabuki T, Ito T, Miyamoto M, Kondo S, Nakamura Y. 2005. A novel human tRNA-dihydrouridine synthase involved in pulmonary carcinogenesis. *Cancer Res* **65**:5638–5646. doi:10.1158/0008-5472.CAN-05-0600

Kaur J, Raj M, Cooperman BS. 2011. Fluorescent labeling of tRNA dihydrouridine residues: Mechanism and distribution. *RNA* **17**:1393–1400. doi:10.1261/rna.2670811

Khanna M, Wu H, Johansson C, Caizergues-Ferrer M, Feigon J. 2006. Structural study of the H/ACA snoRNP components Nop10p and the 3′ hairpin of U65 snoRNA. *RNA* **12**:40–52. doi:10.1261/rna.2221606

Khoddami V, Yerra A, Mosbruger TL, Fleming AM, Burrows CJ, Cairns BR. 2019. Transcriptome-wide profiling of multiple RNA modifications simultaneously at single-base resolution. *Proc Natl Acad Sci U S A* **116**:6784–6789. doi:10.1073/pnas.1817334116

Kligun E, Mandel-Gutfreund Y. 2015. The role of RNA conformation in RNA-protein recognition. *RNA Biology* **12**:720–727. doi:10.1080/15476286.2015.1040977

Kowalak JA, Bruenger E, McCloskey JA. 1995. Posttranscriptional Modification of the Central Loop of Domain V in Escherichia coli 23 S Ribosomal RNA (∗). *Journal of Biological Chemistry* **270**:17758–17764. doi:10.1074/jbc.270.30.17758

Krężel A, Maret W. 2017. The Functions of Metamorphic Metallothioneins in Zinc and Copper Metabolism. *Int J Mol Sci* **18**:1237. doi:10.3390/ijms18061237

Kuchino Y, Borek E. 1978. Tumour-specific phenylalanine tRNA contains two supernumerary methylated bases. *Nature* **271**:126–129. doi:10.1038/271126a0

Kuhlman B, Dantas G, Ireton GC, Varani G, Stoddard BL, Baker D. 2003. Design of a novel globular protein fold with atomic-level accuracy. *Science* **302**:1364–1368. doi:10.1126/science.1089427

Kwok CK, Tang Y, Assmann SM, Bevilacqua PC. 2015. The RNA structurome: transcriptome-wide structure probing with next-generation sequencing. *Trends Biochem Sci* **40**:221–232. doi:10.1016/j.tibs.2015.02.005

Levi O, Arava Y. 2019. mRNA association by aminoacyl tRNA synthetase occurs at a putative anticodon mimic and autoregulates translation in response to tRNA levels. *PLoS Biol* **17**:e3000274. doi:10.1371/journal.pbio.3000274

Leys C, Ley C, Klein O, Bernard P, Licata L. 2013. Detecting outliers: Do not use standard deviation around the mean, use absolute deviation around the median. *Journal of Experimental Social Psychology* **49**:764–766. doi:10.1016/j.jesp.2013.03.013

Lu Z, Chang HY. 2016. Decoding the RNA structurome. *Current Opinion in Structural Biology*, Folding and binding • Nucleic acids-protein complexes **36**:142–148. doi:10.1016/j.sbi.2016.01.007

Magrath DI, Shaw DC. 1967. The occurrence and source of β-alanine in alkaline hydrolysates of sRNA: A sensitive method for the detection and assay of 5,6-dihydrouracil residues in RNA. *Biochemical and Biophysical Research Communications* **26**:32–37. doi:10.1016/0006-291X(67)90248-3

McIntyre W, Netzband R, Bonenfant G, Biegel JM, Miller C, Fuchs G, Henderson E, Arra M, Canki M, Fabris D, Pager CT. 2018. Positive-sense RNA viruses reveal the complexity and dynamics of the cellular and viral epitranscriptomes during infection. *Nucleic Acids Research* **46**:5776–5791. doi:10.1093/nar/gky029

Mitchell SF, Jain S, She M, Parker R. 2013. Global analysis of yeast mRNPs. *Nat Struct Mol Biol* **20**:127–133. doi:10.1038/nsmb.2468

Miura T, Muraoka S, Ogiso T. 1997. Antioxidant activity of metallothionein compared with reduced glutathione. *Life Sciences* **60**:301–309. doi:10.1016/S0024-3205(97)00156-2

Nesvizhskii AI, Keller A, Kolker E, Aebersold R. 2003. A statistical model for identifying proteins by tandem mass spectrometry. *Anal Chem* **75**:4646–4658. doi:10.1021/ac0341261

Network TCGAR, Weinstein JN, Collisson EA, Mills GB, Shaw KRM, Ozenberger BA, Ellrott K, Shmulevich I, Sander C, Stuart JM. 2013. The Cancer Genome Atlas Pan-Cancer analysis project. *Nature Genetics*. doi:10.1038/ng.2764

Ng KP, Hillmer AM, Chuah CTH, Juan WC, Ko TK, Teo ASM, Ariyaratne PN, Takahashi N, Sawada K, Fei Y, Soh S, Lee WH, Huang JWJ, Allen JC, Woo XY, Nagarajan N, Kumar V, Thalamuthu A, Poh WT, Ang AL, Mya HT, How GF, Yang LY, Koh LP, Chowbay B, Chang C-T, Nadarajan VS, Chng WJ, Than H, Lim LC, Goh YT, Zhang S, Poh D, Tan P, Seet J-E, Ang M-K, Chau N-M, Ng Q-S, Tan DSW, Soda M, Isobe K, Nöthen MM, Wong TY, Shahab A, Ruan X, Cacheux-Rataboul V, Sung W-K, Tan EH, Yatabe Y, Mano H, Soo RA, Chin TM, Lim W-T, Ruan Y, Ong ST. 2012. A common BIM deletion polymorphism mediates intrinsic resistance and inferior responses to tyrosine kinase inhibitors in cancer. *Nat Med* **18**:521–528. doi:10.1038/nm.2713

Orct T, Lazarus M, Ljubojević M, Sekovanić A, Sabolić I, Blanuša M. 2015. Metallothionein, essential elements and lipid peroxidation in mercury-exposed suckling rats pretreated with selenium. *Biometals* **28**:701–712. doi:10.1007/s10534-015-9859-3

Orellana EA, Liu Q, Yankova E, Pirouz M, De Braekeleer E, Zhang W, Lim J, Aspris D, Sendinc E, Garyfallos DA, Gu M, Ali R, Gutierrez A, Mikutis S, Bernardes GJL, Fischer ES, Bradley A, Vassiliou GS, Slack FJ, Tzelepis K, Gregory RI. 2021.

METTL1-mediated m7G modification of Arg-TCT tRNA drives oncogenic transformation. *Molecular Cell* **81**:3323-3338.e14. doi:10.1016/j.molcel.2021.06.031

Pan D, Qin H, Cooperman BS. 2009. Synthesis and functional activity of tRNAs labeled with fluorescent hydrazides in the D-loop. *RNA* **15**:346–354. doi:10.1261/rna.1257509

Passarelli MC, Pinzaru AM, Asgharian H, Liberti MV, Heissel S, Molina H, Goodarzi H, Tavazoie SF. 2022. Leucyl-tRNA synthetase is a tumour suppressor in breast cancer and regulates codon-dependent translation dynamics. *Nat Cell Biol* **24**:307–315. doi:10.1038/s41556-022-00856-5

Pfaffl MW. 2001. A new mathematical model for relative quantification in real-time RT–PCR. *Nucleic Acids Res* **29**:e45.

Quinlan AR, Hall IM. 2010. BEDTools: a flexible suite of utilities for comparing genomic features. *Bioinformatics* **26**:841–842. doi:10.1093/bioinformatics/btq033

Rees MG, Seashore-Ludlow B, Cheah JH, Adams DJ, Price EV, Gill S, Javaid S, Coletti ME, Jones VL, Bodycombe NE, Soule CK, Alexander B, Li A, Montgomery P, Kotz JD, Hon CS-Y, Munoz B, Liefeld T, Dančík V, Haber DA, Clish CB, Bittker JA, Palmer M, Wagner BK, Clemons PA, Shamji AF, Schreiber SL. 2016. Correlating chemical sensitivity and basal gene expression reveals mechanism of action. *Nat Chem Biol* **12**:109–116. doi:10.1038/nchembio.1986

Ritchie ME, Phipson B, Wu D, Hu Y, Law CW, Shi W, Smyth GK. 2015. limma powers differential expression analyses for RNA-sequencing and microarray studies. *Nucleic Acids Research* **43**:e47. doi:10.1093/nar/gkv007

Roundtree IA, Evans ME, Pan T, He C. 2017. Dynamic RNA modifications in gene expression regulation. *Cell* **169**:1187–1200. doi:10.1016/j.cell.2017.05.045

Rouskin S, Zubradt M, Washietl S, Kellis M, Weissman JS. 2014. Genome-wide probing of RNA structure reveals active unfolding of mRNA structures in vivo. *Nature* **505**:701–705. doi:10.1038/nature12894

Ryu H-H, Jung S, Jung T-Y, Moon K-S, Kim I-Y, Jeong Y-I, Jin S-G, Pei J, Wen M, Jang W-Y. 2012. Role of metallothionein 1E in the migration and invasion of human glioma cell lines. *International Journal of Oncology* **41**:1305–1313. doi:10.3892/ijo.2012.1570

Schofield JA, Duffy EE, Kiefer L, Sullivan MC, Simon MD. 2018. TimeLapse-seq: adding a temporal dimension to RNA sequencing through nucleoside recoding. *Nat Methods* **15**:221–225. doi:10.1038/nmeth.4582

Schwarz MA, Lazo JS, Yalowich JC, Reynolds I, Kagan VE, Tyurin V, Kim YM, Watkins SC, Pitt BR. 1994. Cytoplasmic metallothionein overexpression protects NIH 3T3 cells from tert-butyl hydroperoxide toxicity. *Journal of Biological Chemistry* **269**:15238–15243. doi:10.1016/S0021-9258(17)36597-3

Seashore-Ludlow B, Rees MG, Cheah JH, Cokol M, Price EV, Coletti ME, Jones V, Bodycombe NE, Soule CK, Gould J, Alexander B, Li A, Montgomery P, Wawer MJ, Kuru N, Kotz JD, Hon CS-Y, Munoz B, Liefeld T, Dančík V, Bittker JA, Palmer M, Bradner JE, Shamji AF, Clemons PA, Schreiber SL. 2015. Harnessing Connectivity in a Large-Scale Small-Molecule Sensitivity Dataset. *Cancer Discov* **5**:1210–1223. doi:10.1158/2159-8290.CD-15-0235

Sipa K, Sochacka E, Kazmierczak-Baranska J, Maszewska M, Janicka M, Nowak G, Nawrot B. 2007. Effect of base modifications on structure, thermodynamic stability, and gene silencing activity of short interfering RNA. *RNA* **13**:1301–1316. doi:10.1261/rna.538907

Smola MJ, Rice GM, Busan S, Siegfried NA, Weeks KM. 2015. Selective 2′-hydroxyl acylation analyzed by primer extension and mutational profiling (SHAPE-MaP) for direct, versatile, and accurate RNA structure analysis. *Nat Protoc* **10**:1643–1669. doi:10.1038/nprot.2015.103

Sun X, Niu X, Chen R, He W, Chen D, Kang R, Tang D. 2016. Metallothionein-1G Facilitates Sorafenib Resistance through Inhibition of Ferroptosis. *Hepatology* **64**:488–500. doi:10.1002/hep.28574

Sutherland DEK, Willans MJ, Stillman MJ. 2012. Single domain metallothioneins: supermetalation of human MT 1a. *J Am Chem Soc* **134**:3290–3299. doi:10.1021/ja211767m

Tasak M, Phizicky EM. 2022. Initiator tRNA lacking 1-methyladenosine is targeted by the rapid tRNA decay pathway in evolutionarily distant yeast species. *PLOS Genetics* **18**:e1010215. doi:10.1371/journal.pgen.1010215

Thornalley PJ, Vašák M. 1985. Possible role for metallothionein in protection against radiation-induced oxidative stress. Kinetics and mechanism of its reaction with superoxide and hydroxyl radicals. *Biochimica et Biophysica Acta (BBA) - Protein Structure and Molecular Enzymology* **827**:36–44. doi:10.1016/0167-4838(85)90098-6

Vallee BL. 1995. The function of metallothionein. *Neurochemistry International* **27**:23–33. doi:10.1016/0197-0186(94)00165-Q

Watkins NJ, Dickmanns A, Lührmann R. 2002. Conserved stem II of the box C/D motif is essential for nucleolar localization and is required, along with the 15.5K protein, for the hierarchical assembly of the box C/D snoRNP. *Mol Cell Biol* **22**:8342–8352. doi:10.1128/mcb.22.23.8342-8352.2002

Westhof E, Dumas P, Moras D. 1988. Restrained refinement of two crystalline forms of yeast aspartic acid and phenylalanine transfer RNA crystals. *Acta crystallographica Section A, Foundations of crystallography* **44 ( Pt 2)**:112–23.

White SA, Hoeger M, Schweppe JJ, Shillingford A, Shipilov V, Zarutskie J. 2004. Internal loop mutations in the ribosomal protein L30 binding site of the yeast L30 RNA transcript. *RNA* **10**:369–377. doi:10.1261/rna.2159504

Wiernicki B, Dubois H, Tyurina YY, Hassannia B, Bayir H, Kagan VE, Vandenabeele P, Wullaert A, Vanden Berghe T. 2020. Excessive phospholipid peroxidation distinguishes ferroptosis from other cell death modes including pyroptosis. *Cell Death Dis* **11**:1–11. doi:10.1038/s41419-020-03118-0

Wintermeyer W, Zachau HG. 1979. Fluorescent Derivatives of Yeast tRNAPhe. *European Journal of Biochemistry* **98**:465–475. doi:10.1111/j.1432-1033.1979.tb13207.x

Wohlhieter CA, Richards AL, Uddin F, Hulton CH, Quintanal-Villalonga À, Martin A, de Stanchina E, Bhanot U, Asher M, Shah NS, Hayatt O, Buonocore DJ, Rekhtman N, Shen R, Arbour KC, Donoghue M, Poirier JT, Sen T, Rudin CM. 2020. Concurrent Mutations in STK11 and KEAP1 Promote Ferroptosis Protection and

SCD1 Dependence in Lung Cancer. *Cell Reports* **33**:108444. doi:10.1016/j.celrep.2020.108444

Xing F, Hiley SL, Hughes TR, Phizicky EM. 2004. The Specificities of Four Yeast Dihydrouridine Synthases for Cytoplasmic tRNAs. *J Biol Chem* **279**:17850–17860. doi:10.1074/jbc.M401221200

Xing F, Martzen MR, Phizicky EM. 2002. A conserved family of Saccharomyces cerevisiae synthases effects dihydrouridine modification of tRNA. *RNA* **8**:370–381.

Xiong R, He R, Liu B, Jiang W, Wang B, Li N, Geng Q. 2021. Ferroptosis: A New Promising Target for Lung Cancer Therapy. *Oxidative Medicine and Cellular Longevity* **2021**:e8457521. doi:10.1155/2021/8457521

Yang WS, SriRamaratnam R, Welsch ME, Shimada K, Skouta R, Viswanathan VS, Cheah JH, Clemons PA, Shamji AF, Clish CB, Brown LM, Girotti AW, Cornish VW, Schreiber SL, Stockwell BR. 2014. Regulation of ferroptotic cancer cell death by GPX4. *Cell* **156**:317–331. doi:10.1016/j.cell.2013.12.010

You HJ, Lee KJ, Jeong HG. 2002. Overexpression of human metallothionein-III prevents hydrogen peroxide-induced oxidative stress in human fibroblasts. *FEBS Lett* **521**:175–179. doi:10.1016/s0014-5793(02)02870-3

Zheng G, Qin Y, Clark WC, Dai Q, Yi C, He C, Lambowitz AM, Pan T. 2015. Efficient and quantitative high-throughput transfer RNA sequencing. *Nat Methods* **12**:835–837. doi:10.1038/nmeth.3478

Zoysa TD, Phizicky EM. 2020. Hypomodified tRNA in evolutionarily distant yeasts can trigger rapid tRNA decay to activate the general amino acid control response, but

with different consequences. *PLOS Genetics* **16**:e1008893. doi:10.1371/journal.pgen.1008893

Zubradt M, Gupta P, Persad S, Lambowitz AM, Weissman JS, Rouskin S. 2017. DMS-MaPseq for genome-wide or targeted RNA structure probing in vivo. *Nat Methods* **14**:75–82. doi:10.1038/nmeth.4057